

DUDLEY KNOX LIBRARY
NAVAL POSTGRADUATE SCHOOL
MONTEREY CA 93943-5101

Approved for public release; distribution is unlimited.

NATURAL CONVECTION IMMERSION COOLING OF AN ARRAY OF
VERTICALLY
ORIENTED HEATED PROTRUSIONS IN AN ENCLOSURE FILLED WITH A
DIELECTRIC LIQUID: EFFECTS OF ENCLOSURE WIDTH, PRANDTL
NUMBER
AND COMPONENT ORIENTATION

by

Scott T. Matthews
Lieutenant, United States Navy
B.S., Pennsylvania State University

Submitted in partial fulfillment of the
requirements for the degree of

MASTER OF SCIENCE IN MECHANICAL ENGINEERING

from the

NAVAL POSTGRADUATE SCHOOL
December 1991

classified

ity classification of this page

REPORT DOCUMENTATION PAGE

Report Security Classification Unclassified		1b Restrictive Markings	
Security Classification Authority		3 Distribution Availability of Report Approved for public release; distribution is unlimited.	
Declassification Downgrading Schedule			
Performing Organization Report Number(s)		5 Monitoring Organization Report Number(s)	
Name of Performing Organization Naval Postgraduate School	6b Office Symbol (if applicable) 52	7a Name of Monitoring Organization Naval Postgraduate School	
Address (city, state, and ZIP code) Monterey, CA 93943-5000		7b Address (city, state, and ZIP code) Monterey, CA 93943-5000	
Name of Funding Sponsoring Organization	8b Office Symbol (if applicable)	9 Procurement Instrument Identification Number	
Address (city, state, and ZIP code)		10 Source of Funding Numbers	
		Program Element No	Project No
		Task No	Work Unit Accession No

Title (include security classification) **NATURAL CONVECTION IMMERSION COOLING OF AN ARRAY OF VERTICALLY ORIENTED HEATED PROTRUSIONS IN AN ENCLOSURE FILLED WITH A DIELECTRIC LIQUID: EFFECTS OF ENCLOSURE WIDTH, PRANDTL NUMBER AND COMPONENT ORIENTATION**

Personal Author(s) **Scott T. Matthews**

Type of Report Master's Thesis	13b Time Covered From To	14 Date of Report (year, month, day) December 1991	15 Page Count 97
--	--	--	----------------------------

Supplementary Notation The views expressed in this thesis are those of the author and do not reflect the official policy or position of the Department of Defense or the U.S. Government.

Cosati Codes			18 Subject Terms (continue on reverse if necessary and identify by block number) natural convection, immersion cooling, electronic components
d	Group	Subgroup	

Abstract (continue on reverse if necessary and identify by block number)

The natural convection heat transfer characteristics of a 3x3 array of vertically oriented heated protrusions, immersed in dielectric liquid, were investigated. Aluminum blocks, 24mm x 8mm x 6mm, were used to simulate 20 pin dual in-line packages. Surface temperature measurements of the components were made by imbedding copper-constantan thermocouples on the surface of each component face. A constant heat flux was provided to each component using an Inconel foil heating element. Power supplied to each component varied from 0.115W to 2.90W. The aluminum blocks were mounted on a plexiglass substrate to form a 3x3 array of simulated electronic components. The circuit board containing the components was placed in a rectangular, plexiglass enclosure with inner dimensions: L = 203.2mm H = 152.0mm W = 82.6mm, and wall thickness of 25.4mm. The upper boundary was maintained at 10°C, while all other exterior surfaces were insulated. The chamber width, measured from the surface of the circuit board to the opposite, inner wall of the enclosure, was varied from 42mm to 7mm by inserting plexiglass spacers into the enclosure. Two dielectric liquids, FC-75 and FC-43, were used as working fluids.

Non-dimensional data from this study was combined with the data obtained by Aytar (1991) for a horizontal component orientation, to develop an empirical correlation which predicts the Nusselt number as a function of Rayleigh number and Prandtl number, component orientation and chamber width. This correlation was found to be accurate to within 11% of the original curve fit data. Heat transfer in FC-75 was found to occur mainly by convection arising from buoyancy forces, regardless of chamber width. Heat transfer in FC-43 was found to occur mainly by molecular diffusion for chamber widths of 1mm or greater, and by convection at a chamber width of 7mm. The maximum uncertainty in the Nusselt and Rayleigh numbers was 2.5%, based on a zeroth order uncertainty analysis, and occurred at the lowest power level, where the maximum uncertainty in the temperature measurements resided.

Distribution Availability of Abstract Unclassified unlimited <input type="checkbox"/> same as report <input type="checkbox"/> DTIC users	21 Abstract Security Classification Unclassified	
Name of Responsible Individual D.Kelleher	22b Telephone (include Area code) (408) 646-2035	22c Office Symbol 54Ss

FORM 1473,84 MAR

83 APR edition may be used until exhausted
All other editions are obsolete

security classification of this page

NAVAL POSTGRADUATE SCHOOL

Monterey , California



THESIS

NATURAL CONVECTION IMMERSION COOLING
OF AN ARRAY OF VERTICALLY
ORIENTED HEATED PROTRUSIONS IN AN EN-
CLOSURE FILLED WITH A
DIELECTRIC LIQUID: EFFECTS OF ENCLOSURE
WIDTH, PRANDTL NUMBER
AND COMPONENT ORIENTATION

by

Scott T. Matthews

December 1991

Thesis Advisor

M.D.Kelleher

Approved for public release: Distribution is unlimited

ABSTRACT

The natural convection heat transfer characteristics of a 3x3 array of vertically oriented heated protrusions, immersed in a dielectric liquid, were investigated. Aluminum blocks, 24mm x 8mm x 6mm, were used to simulate 20 pin dual in-line packages. Surface temperature measurements of the components were made by imbedding copper-constantan thermocouples below the surface of each component face. A constant heat flux was provided to each component using an Inconel foil heating element. Power supplied to each component varied from 0.115W to 2.90W. The aluminum blocks were mounted on a plexiglass substrate to form a 3x3 array of simulated electronic components. The circuit board containing the components was placed in a rectangular, plexiglass enclosure with inner dimensions: $L = 203.2\text{mm}$ $H = 152.0\text{mm}$ $W = 82.6\text{mm}$, and a wall thickness of 25.4mm. The upper boundary was maintained at 10°C , while all other exterior surfaces were insulated. The chamber width, measured from the surface of the circuit board to the opposite, inner wall of the enclosure, was varied from 42mm to 7mm by inserting plexiglass spacers into the enclosure. Two dielectric liquids, FC-75 and FC-43, were used as working fluids.

Non-dimensional data from this study was combined with the data obtained by Aytar (1991) for a horizontal component orientation, to develop an empirical correlation which predicts the Nusselt number as a function of Rayleigh number, Prandtl number, component orientation and chamber width. This correlation was found to be accurate to within 11% of the original curve fit data. Heat transfer in FC-75 was found to occur mainly by convection arising from buoyancy forces, regardless of chamber width. Heat transfer in FC-43 was found to occur mainly by molecular diffusion for chamber widths of 11mm or greater, and by convection at a chamber width of 7mm. The maximum uncertainty in the Nusselt and Rayleigh numbers was 2.5%, based on a zeroth order uncertainty analysis, and occurred at the lowest power level, where the maximum uncertainty in the temperature measurements resided.

10513
M 3826
C.1

TABLE OF CONTENTS

I. INTRODUCTION	1
A. PROBLEM STATEMENT	1
B. LITERATURE REVIEW	1
C. OBJECTIVES	5
II. EXPERIMENTAL APPARATUS	6
A. TEST CHAMBER	6
B. HEAT EXCHANGER	6
C. SIMULATED ELECTRONIC COMPONENTS	7
D. HEATING ELEMENTS	7
E. CIRCUIT BOARD	7
F. SYSTEM HARDWARE	8
III. EXPERIMENTAL PROCEDURE AND DATA ANALYSIS	15
A. SYSTEM PREPARATION	15
B. EXPERIMENTAL PROCEDURE	15
C. DATA ACQUISITION	16
IV. DATA ANALYSIS	17
V. RESULTS	22
A. GENERAL	22
B. DIMENSIONAL RESULTS	22
C. NON-DIMENSIONAL RESULTS	24
1. FC-75	24
a. Effect of Rayleigh Number	25
b. Effect of Chamber Width	26
2. FC-43	26
a. Effect of Rayleigh Number	27
b. Effect of Chamber Width	27
3. Effect of Component Orientation	28

4. Effect of Prandtl Number	29
5. Uncertainty Analysis	30

VI. CONCLUSIONS	77
-----------------------	----

VII. RECOMMENDATIONS	79
----------------------------	----

APPENDIX A. UNCERTAINTY ANALYSIS	80
--	----

REFERENCES	83
------------------	----

INITIAL DISTRIBUTION LIST	85
---------------------------------	----

LIST OF FIGURES

Figure 1.	Top View of the Test Chamber and Circuit Board with Vertically Oriented Components.	9
Figure 2.	Plexiglass Enclosure with the Water Chilled Heat Exchanger Mounted in Place.	10
Figure 3.	Aluminum Blocks and Thermocouple Wells.	11
Figure 4.	Aluminum Block Mounted with Copper-Constantan Thermocouples and an Inconel Foil Heating Element.	12
Figure 5.	Front and Plan View of Circuit Board and Vertically Oriented Components.	13
Figure 6.	Circuit Board with Vertically Oriented Components.	14
Figure 7.	Average Array Temperature as a function of Net Power and Chamber Width for FC-75.	31
Figure 8.	Average Array Temperature as a function of Net Power and Chamber Width for FC-43.	32
Figure 9.	Nu_1 vs Ra_f for a Vertical Component Orientation, FC-75 and all Chamber Widths.	33
Figure 10.	Nu_1 vs Ra_f for a Vertical Component Orientation, FC-75 and a 42mm Chamber Width using Array Averaged Values.	34
Figure 11.	Nu_1 vs Ra_f for a Vertical Component Orientation, FC-75 and a 30mm Chamber Width using Array Averaged Values.	35
Figure 12.	Nu_1 vs Ra_f for a Vertical Component Orientation, FC-75 and an 18mm Chamber Width using Array Averaged Values.	36
Figure 13.	Nu_1 vs Ra_f for a Vertical Component Orientation, FC-75 and an 11mm Chamber Width using Array Averaged Values.	37
Figure 14.	Nu_1 vs Ra_f for a Vertical Component Orientation, FC-75 and a 7mm Chamber Width using Array Averaged Values.	38
Figure 15.	Nu_1 vs Ra_f for a Vertical Component Orientation, FC-75 and a 42mm Chamber Width using Bottom Row Averaged Values.	39
Figure 16.	Nu_1 vs Ra_f for a Vertical Component Orientation, FC-75 and a 42mm Chamber Width using Middle Row Averaged Values.	40

Figure 17. Nu_1 vs Ra_f for a Vertical Component Orientation, FC-75 and a 42mm Chamber Width using Top Row Averaged Values. 41

Figure 18. Nu_1 vs Ra_f for a Vertical Component Orientation, FC-75 and a 30mm Chamber Width using Bottom Row Averaged Values. 42

Figure 19. Nu_1 vs Ra_f for a Vertical Component Orientation, FC-75 and a 30mm Chamber Width using Middle Row Averaged Values. 43

Figure 20. Nu_1 vs Ra_f for a Vertical Component Orientation, FC-75 and a 30mm Chamber Width using Top Row Averaged Values. 44

Figure 21. Nu_1 vs Ra_f for a Vertical Component Orientation, FC-75 and an 18mm Chamber Width using Bottom Row Averaged Values. 45

Figure 22. Nu_1 vs Ra_f for a Vertical Component Orientation, FC-75 and an 18mm Chamber Width using Middle Row Averaged Values. 46

Figure 23. Nu_1 vs Ra_f for a Vertical Component Orientation, FC-75 and an 18mm Chamber Width using Top Row Averaged Values. 47

Figure 24. Nu_1 vs Ra_f for a Vertical Component Orientation, FC-75 and an 11mm Chamber Width using Bottom Row Averaged Values. 48

Figure 25. Nu_1 vs Ra_f for a Vertical Component Orientation, FC-75 and an 11mm Chamber Width using Middle Row Averaged Values. 49

Figure 26. Nu_1 vs Ra_f for a Vertical Component Orientation, FC-75 and an 11mm Chamber Width using Top Row Averaged Values. 50

Figure 27. Nu_1 vs Ra_f for a Vertical Component Orientation, FC-75 and a 7mm Chamber Width using Bottom Row Averaged Values. 51

Figure 28. Nu_1 vs Ra_f for a Vertical Component Orientation, FC-75 and a 7mm Chamber Width using Middle Row Averaged Values. 52

Figure 29. Nu_1 vs Ra_f for a Vertical Component Orientation, FC-75 and a 7mm Chamber Width using Top Row Averaged Values. 53

Figure 30. Nu_1 vs X for a Vertical Component Orientation and both Dielectric Liquids. 54

Figure 31. Nu_1 vs Ra_f for a Vertical Component Orientation, FC-43 and all Chamber Widths. 55

Figure 32. Nu_1 vs Ra_f for a Vertical Component Orientation, FC-43 and a 42mm Chamber Width using Array Averaged Values. 56

Figure 33. Nu_1 vs Ra_f for a Vertical Component Orientation, FC-43 and a 30mm Chamber Width using Array Averaged Values. 57

Figure 34. Nu_1 vs Ra_f for a Vertical Component Orientation, FC-43 and an 18mm Chamber Width using Array Averaged Values. 58

Figure 35. Nu_1 vs Ra_f for a Vertical Component Orientation, FC-43 and an 11mm Chamber Width using Array Averaged Values. 59

Figure 36. Nu_1 vs Ra_f for a Vertical Component Orientation, FC-43 and a 7mm Chamber Width using Array Averaged Values. 60

Figure 37. Nu_1 vs Ra_f for a Vertical Component Orientation, FC-43 and a 42mm Chamber Width using Bottom Row Averaged Values. 61

Figure 38. Nu_1 vs Ra_f for a Vertical Component Orientation, FC-43 and a 42mm Chamber Width using Middle Row Averaged Values. 62

Figure 39. Nu_1 vs Ra_f for a Vertical Component Orientation, FC-43 and a 42mm Chamber Width using Top Row Averaged Values. 63

Figure 40. Nu_1 vs Ra_f for a Vertical Component Orientation, FC-43 and a 30mm Chamber Width using Bottom Row Averaged Values. 64

Figure 41. Nu_1 vs Ra_f for a Vertical Component Orientation, FC-43 and a 30mm Chamber Width using Middle Row Averaged Values. 65

Figure 42. Nu_1 vs Ra_f for a Vertical Component Orientation, FC-43 and a 30mm Chamber Width using Top Row Averaged Values. 66

Figure 43. Nu_1 vs Ra_f for a Vertical Component Orientation, FC-43 and an 18mm Chamber Width using Bottom Row Averaged Values. 67

Figure 44. Nu_1 vs Ra_f for a Vertical Component Orientation, FC-43 and an 18mm Chamber Width using Middle Row Averaged Values. 68

Figure 45. Nu_1 vs Ra_f for a Vertical Component Orientation, FC-43 and an 18mm Chamber Width using Top Row Averaged Values. 69

Figure 46. Nu_1 vs Ra_f for a Vertical Component Orientation, FC-43 and an 11mm Chamber Width using Bottom Row Averaged Values. 70

Figure 47. Nu_1 vs Ra_f for a Vertical Component Orientation, FC-43 and an 11mm Chamber Width using Middle Row Averaged Values. 71

Figure 48. Nu_1 vs Ra_f for a Vertical Component Orientation, FC-43 and an 11mm Chamber Width using Top Row Averaged Values. 72

Figure 49. Nu_1 vs Ra_f for a Vertical Component Orientation, FC-43 and a 7mm Chamber Width using Bottom Row Averaged Values. 73

Figure 50. Nu_1 vs Ra_f for a Vertical Component Orientation, FC-43 and a 7mm Chamber Width using Middle Row Averaged Values. 74

Figure 51. Nu_1 vs Ra_1 for a Vertical Component Orientation, FC-43 and a 7mm Chamber Width using Top Row Averaged Values. 75

Figure 52. Nu_1 vs Pr_{avg} and Non-Dimensional Chamber Width for a Vertical Component Orientation. 76

NOMENCLATURE

Symbol	Description	Units
A	Area	m^2
A_{total}	Total wetted surface area	m^2
C_p	Specific heat	$\frac{J}{kg^\circ C}$
δ	Uncertainty	various
emf	Thermocouple voltage	volt
g	Gravitational acceleration	$\frac{m}{s^2}$
Gr	Grashof number	dimensionless
h	Average heat transfer coefficient	$\frac{W}{m^2^\circ C}$
k_f	Liquid thermal conductivity	$\frac{W}{m^\circ C}$
k_p	Plexiglass thermal conductivity	$\frac{W}{m^\circ C}$
L	Component length in the vertical direction	m
Nu_1	Nusselt number	dimensionless
Pr	Prandtl number	dimensionless
Power	Power supplied to a heating element	Watts
Q_{loss}	Heat loss through the plexiglass substrate	Watts
Q_{net}	Net power dissipated by a component	Watts
R_c	Total thermal resistance of the substrate	$\frac{^\circ C}{W}$
R_p	Electrical resistance of a precision resistor	Ω
Ra_f	Flux based Rayleigh number	dimensionless
Ra_t	Temperature based Rayleigh number	dimensionless
T	Temperature	$^\circ C$
T_{avg}	Average component temperature	$^\circ C$
T_b	back surface temperature	$^\circ C$
T_{film}	Film temperature	$^\circ C$
T_{sink}	Average heat exchanger temperature	$^\circ C$
Volt	Input voltage from the DC power supply	volts
X	Non-dimensional chamber width	dimensionless

W	Chamber width	mm
α	Thermal diffusivity	$\frac{m^2}{s}$
β	Thermal expansion coefficient	$\frac{1}{^\circ K}$
ρ	Density	$\frac{kg}{m^3}$
ν	Kinematic viscosity	$\frac{m^2}{s}$

I. INTRODUCTION

A. PROBLEM STATEMENT

As today's circuit technology moves beyond Very Large Scale Integration (VLSI), increases in the number of devices per chip, package densities per module, and power densities at both the chip and module level have made it difficult to maintain adequate operating temperatures (Incopera, 1990). As junction temperature increases, microelectronic chip failure increases exponentially (Park and Bergles, 1987). Conversely, for every 20°C drop in junction temperature, chip failure rates are reduced by 50% (Oktay, 1986). Forced air cooling and indirect liquid cooling appear to be inadequate. More emphasis is therefore being placed on direct immersion cooling using dielectric liquids. This may involve natural, forced or mixed convection processes, and can occur in a single phase as well as pool or forced boiling convection modes (Incopera, 1990).

Natural convection direct immersion cooling using dielectric liquids offers a high power dissipation capability, while providing high reliability with little or no noise (Liu, 1987). With the many possible applications of packaging electronic components within an enclosure, few studies have been conducted using discrete, protruding heat sources immersed in a dielectric liquid (Incopera, 1988). Studying an array of protruding heat sources of uniform size and simple geometric orientation may provide valuable insight and prediction capabilities for the complex geometric arrangements and size variations often encountered in circuit technology today.

B. LITERATURE REVIEW

Park and Bergles (1987) conducted natural convection heat transfer experiments involving both flush and protruding, thin foil heaters mounted on a vertical wall within an insulated enclosure. Using water and R-113 as working fluids, the experiment consisted of three different cases:

- A single flush mounted heater
- An array of flush mounted heaters (in-line and staggered)
- An array of protruding heaters

For the single flush mounted heaters, two different heights (5mm and 10mm) with variations in width from 2mm to 70mm were investigated. The height and width of the flush mounted heaters were limited to 5mm when they were arranged in an array. The

protruding heaters were 4.9mm in the vertical direction, 5.3mm wide and extended 1.1mm from the substrate surface. The experimental results showed that for a single flush mounted heater:

- The heat transfer coefficient increases as the heater width decreases. A 5mm x 5mm test section displayed a heat transfer coefficient 80 to 100 times larger than the widest section (70mm). A similar effect was observed for a 9.86mm x 5mm test section.
- The width effect was much less pronounced for water than for R-113.
- The heat transfer coefficients obtained for the widest test section were 20% larger than those predicted by the Fujii and Fujii correlation (Fujii and Fujii, 1976), which is based on boundary layer solutions for a vertical plate with constant heat flux.

For an array of in-line or staggered flush mounted heaters, where the distance between them was varied, the results showed that:

- The top heater had a substantially lower heat transfer coefficient than the bottom heater.
- The heat transfer coefficient for the top heater increased as the distance between the heaters increased up to a value of $G/H = 3.5$, where H is the height of the heater and G the distance between them. For values of G/H greater than 3.5, the heat transfer coefficient ratio remained constant.
- For staggered flush mounted heaters, the heat transfer coefficient increased as the transverse distance between the heaters increased at small G/H . The opposite effect occurred at large G/H .

For a single protruding heater, the heat transfer coefficient was found to be 14% larger than the flush mounted value, and 120% larger than the predicted values using the Fujii and Fujii correlation. Heat transfer coefficients for the top heater in an array were higher than the bottom and increased as the distance between them increased. This was in contrast to the result obtained for flush mounted heaters.

Kelleher et al. (1987) conducted an experimental investigation of natural convection in a water filled, rectangular enclosure with a single heated protrusion on a vertical wall. All vertical exterior surfaces were insulated and assumed adiabatic. The upper and lower horizontal boundaries were maintained at an isothermal sink temperature, T_c . The heated protrusion had the following dimensions: $H = 25.4\text{mm}$ $W = 203.0\text{mm}$ and protruded 12.8mm from the surface of the wall. The enclosure was constructed such that the heated protrusion could be set at 3 different elevations within the enclosure. Experimental runs were conducted in the Rayleigh number range: $.99 \times 10^6 < Ra < 8 \times 10^6$. A flow visualization study was also carried out. The experimental results showed that:

- For a given Rayleigh number, Nusselt number decreased as the height of the heater within the enclosure increased.
- Flow visualization revealed a dual celled flow which consisted of a buoyancy driven upper cell and a shear driven lower cell. The motion of the lower cell arises due to the viscous drag of the upper cell. The majority of fluid motion takes place in the upper cell and accounts for the most of the convective heat transfer.

Lee et al. (1987) conducted a numerical simulation of laminar natural convection in a water-filled rectangular enclosure, using a single heated protrusion on a vertical wall. This was a companion paper to the research done by Kelleher et al. (1987). A 2-dimensional, full variable-property, finite difference method calculation was used to simulate the experimental conditions investigated by Kelleher et al. (1987). The numerical solution to the governing conservation equations revealed the following:

- At high Rayleigh numbers, there is reasonable agreement between the experimental and numerical data for the Nusselt number.
- At low Rayleigh numbers, the numerical solution predicts values of the Nusselt number as much as 50% higher than those observed experimentally.
- In contrast to the experimental results of Kelleher et al. (1987), the numerical solution showed that the Nusselt number increased as the elevation of the heater within the enclosure was increased.
- Flow visualization showed that the flow is concentrated in the region above the heater. The region below the heater was essentially stratified. Flow in the upper region was buoyancy driven, while the region below the heater was shear driven by the buoyant flow above.

Chen and Kuo (1988) studied the natural convective heat transfer from 10mm x 20mm x 150mm block-like heat generating modules. A numerical study was first conducted using a laminar, 2-dimensional, constant property finite-difference scheme. Results were provided for a Rayleigh number range of: $10^2 < Ra < 10^5$ at $Pr=0.7$. The numerical results were corroborated experimentally by measuring temperatures with a laser holographic interferometer. The results indicate that:

- Heat transfer on the upstream side of the heated surface is in general higher than the downstream side.
- The heat transfer coefficient for the upper heater is affected by the flow generated by the lower heater. This effect increases as the Rayleigh number increases.

Keyhani et al. (1991) conducted experiments to determine the effect of aspect ratio on the natural convection in an enclosure with 5 protruding heat sources. The enclosure had inner dimensions: $H=171.35\text{mm}$ $L=141.0\text{mm}$ $W=139.7\text{mm}$, and was constructed of 25.4mm thick plexiglass. The upper horizontal boundary of the enclosure was main-

tained at a constant temperature. The width of the enclosure was varied from 13.5mm to 55mm by inserting a movable, vertical plate into the enclosure. The protruding heaters were 15mm in the vertical direction, and extended 9mm from the surface of the phenolite wall on which they were mounted. The protruding heaters were mounted such that identical rows of protruding heaters and flush unheated sections were obtained. Using ethylene glycol as a working fluid, experimental runs were carried out for power inputs of 2W to 13 W per heated section, for 6 enclosure widths. The Prandtl number for ethylene glycol varied from 62 to 110. Flow visualization experiments were also conducted to investigate the flow structure. A correlation which relates the local Nusselt number to the local modified Rayleigh number and aspect ratio ($\frac{H}{W}$) was reported:

$$Nu_y = 0.296(Ra_y^*)^{0.223} \left(\frac{H}{W} \right)^{-0.53}$$

where $Ra_y^* = Ra_y Nu$. This correlation is independent of the number of heaters in the array, enclosure width to protrusion heater height ratio, and vertical height location of the heaters. The conditions for which this conclusion is valid are outlined in Keyhani et al. (1991). The averaged deviation of this correlation from the experimental data was reported as 4.5%.

The experimental study reported in this thesis is a direct continuation of the work conducted by Aytar (1991), who investigated the heat transfer characteristics of a 3x3 array of horizontally oriented components. Frequent references are made to Aytar's (1991) research throughout this study, since most facets of his study have been repeated herein.

Aluminum blocks 24mm x 8mm x 6mm, each simulating a 20 pin dual-inline package, were mounted to a plexiglass substrate to produce a 3x3 array of vertically oriented simulated electronic components (Figure 5 and Figure 6). The resulting circuit board was affixed in a rectangular plexiglass enclosure and immersed in a dielectric liquid. The enclosure had inner dimensions of: H = 152.0mm L = 203.2mm W = 82.6mm, and was constructed of 25.4mm thick plexiglass (Figure 1). A constant heat flux was supplied to each of the 9 components using an Inconel foil resistive heating element connected in parallel to a 0-100 0.5A DC power supply. Power supplied to the heating elements varied from 0.115W to 2.90W per element. The effect of chamber width was investigated at the following values: 42, 30, 18, 11 and 7mm. The upper horizontal boundary of the enclosure was maintained at 10°C using a circulating chilled water heat exchanger. All other exterior surfaces were insulated. The distance from the front center face of the

different thicknesses. Temperature measurements at the component faces, the rear plane of the circuit board, and the heat exchanger boundary, were made using copper-constantan thermocouples. The thermocouples were tack welded in small wells below the aluminum block surface to minimize any contact resistance (Figure 3 and Figure 4). An HP3497A data acquisition system, controlled by an HP9826 microcomputer, was used to collect the raw temperature data after the system achieved steady state. Steady state conditions were assumed when surface temperature fluctuations were less than 1°C in 10 minutes for FC-75 and 0.4°C for FC-43. These criterion were based on steady state surface temperature fluctuation measurements made by Aytar (1991) for a horizontal component orientation.

C. OBJECTIVES

The objectives of this work were:

1. Manufacture a 3x3 array of vertically oriented simulated electronic components.
2. Collect data for the vertical component orientation by varying the power level supplied to the heating elements and the width of the enclosure using FC-75 and FC-43 as working fluids.
3. Reduce the data into both dimensional and non-dimensional heat transfer parameters for the chamber widths and power levels investigated.
4. Develop an empirical correlation which predicts the heat transfer characteristics of the array, taking into account the effects of Rayleigh number, Prandtl number, chamber width and component orientation.
5. Make comparisons between the vertical component orientation and the horizontal component orientation, using both dimensional and non-dimensional data.
6. Based on the findings of this study, make recommendations for future research.

II. EXPERIMENTAL APPARATUS

A. TEST CHAMBER

During the course of this experimental study, 2 test chambers were used. Each was constructed of plexiglass with inner dimensions: $L = 203.2\text{mm}$ $W = 82.6\text{mm}$ $H = 152.0\text{mm}$, and a 12mm thick bottom boundary (Figure 1). The first chamber had a wall thickness of 12.7mm, and was used to obtain data for FC-75 at chamber widths of 42, 30, 18 and 11mm. During these experimental runs the chamber experienced brittle fractures at numerous points along its boundary, particularly at the corners. This resulted in the chamber having to be discarded. A photograph of the first enclosure, with the chilled water heat exchanger mounted in place, is presented in Figure 2 to provide some general insight into the enclosure's detail. A second chamber was constructed with the following modifications:

- The wall thickness was increased to 25.4mm
- The lower steel tubing, which served as a fill and removal point for the dielectric liquid, was moved slightly forward of the circuit board surface, to provide an unobstructed flow path for the dielectric.
- The upper steel tubing, which cannot be seen in Figure 2, was removed since it no longer served any useful purpose. It was previously used as an air removal point in a past enclosure design.
- Threaded studs were permanently set within the chamber walls in order to lessen the wear on the threads within the plexiglass walls themselves. The heat exchanger was then fastened to the chamber using washers and nuts.

A top view of the second chamber with the circuit board and vertically mounted components are shown in Figure 1. The experimental runs carried out for FC-75 using the initial chamber were also completed using the second chamber.

B. HEAT EXCHANGER

The upper horizontal boundary of the chamber was maintained at 10°C using a water-cooled channel type heat exchanger. The shell was constructed of plexiglass and contained a 3mm thick aluminum plate, which provided a nearly uniform temperature surface between the dielectric liquid and the cooling water. A detailed drawing and description of the heat exchanger and its construction was given by Torres (1988). Prior to this study, the aluminum plate contained 2 rows of 3 symmetrically placed thermocouples. An additional row of thermocouples, as recommended by Aytar (1991),

was added to the aluminum plate to provide a better measurement of the average upper boundary temperature at the various chamber widths. Flow through the channels, as well as the inlet water temperature, was adjusted from the refrigerated circulating bath unit.

C. SIMULATED ELECTRONIC COMPONENTS

Rectangular aluminum blocks 24mm x 8mm x 6mm were used to simulate 20 pin dual-in-line packages. Prefabricated copper-constantan thermocouples were used to measure the surface temperature of the components. A detailed drawing of the aluminum blocks and the thermocouple wells is shown in Figure 3 (after Benedict, 1988). The thermocouples were mounted to the aluminum blocks in accordance with the procedure described by Aytar (1991). A photograph of a finished component is provided in Figure 4.

D. HEATING ELEMENTS

Inconel foil resistive heating elements were used to provide a constant heat flux to the back surface of the components, via a 0-100V 0-5A DC power supply. The heaters were mounted to the plexiglass substrate in accordance with the procedure described by Aytar (1991). The resistance of each heating element was approximately 11Ω . Each heating element was connected in series with a $2\Omega \pm 2.5\%$ precision resistor. The 9 heater-precision resistor series elements were then connected in a parallel combination with the DC power supply. By measuring the voltage drop across each component for a given power supply voltage, the current, and therefore the power provided to each component, was determined.

E. CIRCUIT BOARD

The aluminum blocks were mounted to a plexiglass substrate with their largest vertical dimension (24mm) oriented in the direction of the gravitational vector, to produce a 3x3 array of simulated electronic components. The substrate was 152.0mm in the vertical direction, 203.2mm wide and 12mm thick. Side walls were added to the back of the circuit board to provide stability when it was inserted into the test chamber. The dimensions of the side walls were such that when the board was inserted into the chamber without a spacer, the distance from the surface of the board containing the components, to the inner surface of the chamber, was 42mm. A small groove was made in the upper right hand corner of the board to allow air to pass from the front of the chamber to the back, where it could then be vented to the atmosphere as the chamber was filled.

A front and plan view of the circuit board with the vertically mounted components are shown in Figure 5. A photo of the finished circuit board is shown in Figure 6.

F. SYSTEM HARDWARE

All thermocouples and heating elements were connected to an HP3497A data acquisition system, which was controlled by an HP9826 microcomputer. The channel numbering scheme was the same as used by Aytar (1991), and is repeated below:

- Channels 0 through 53: Component surface temperatures
- Channels 54 through 56: Heat exchanger surface temperatures
- Channels 57 through 60: Circuit board back plane temperatures
- Channels 61 through 70: DC power supply and all heating elements
- Channels 70 through 75: Circuit board back plane temperatures
- Channel 76: Ambient temperature

Components in the vertical orientation were numbered in the same way as in the horizontal orientation: bottom to top and right to left, viewed from the surface containing the components. The horizontal orientation was rotated 90° to arrive at the vertical orientation. The component faces were then numbered using the scheme described by Aytar (1991): center, top, right, left, bottom and back, beginning with component #1 and ending with component #9.

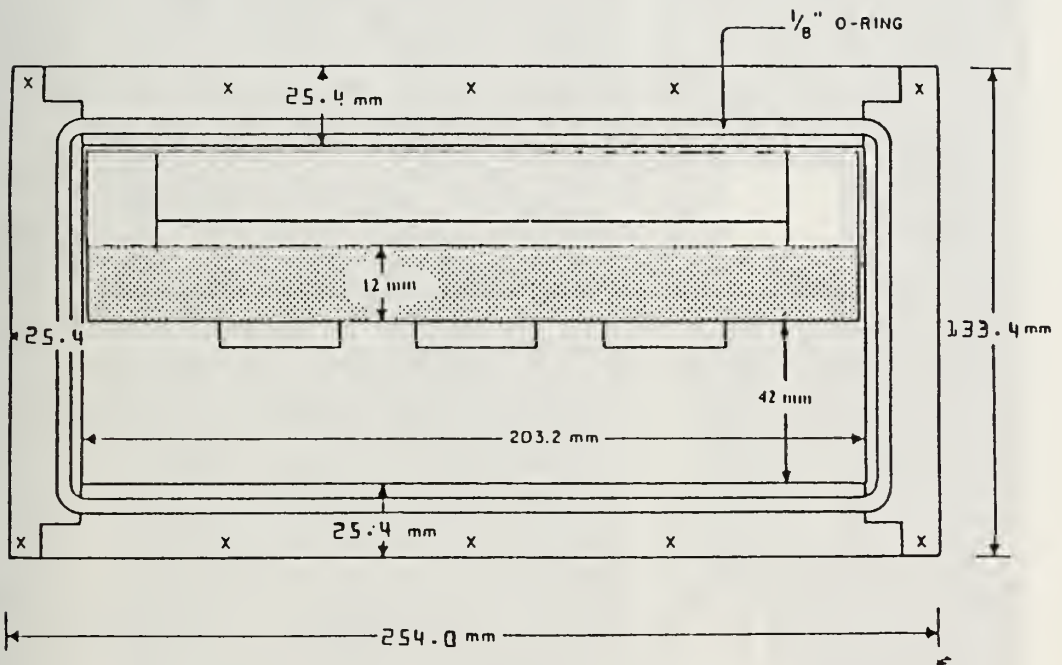


Figure 1. Top View of the Test Chamber and Circuit Board with Vertically Oriented Components.

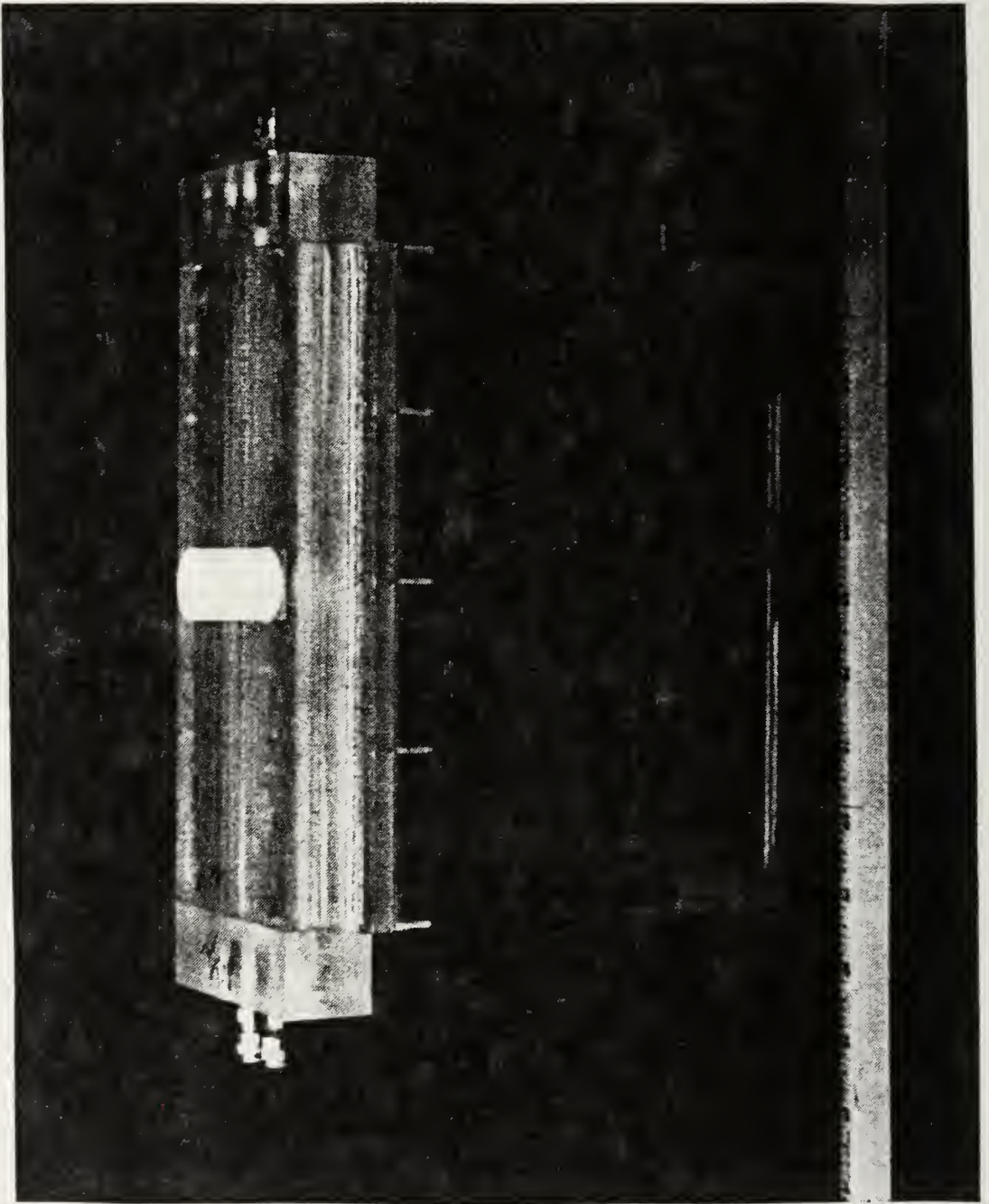


Figure 2. Plexiglass Enclosure with the Water Chilled Heat Exchanger Mounted in Place.

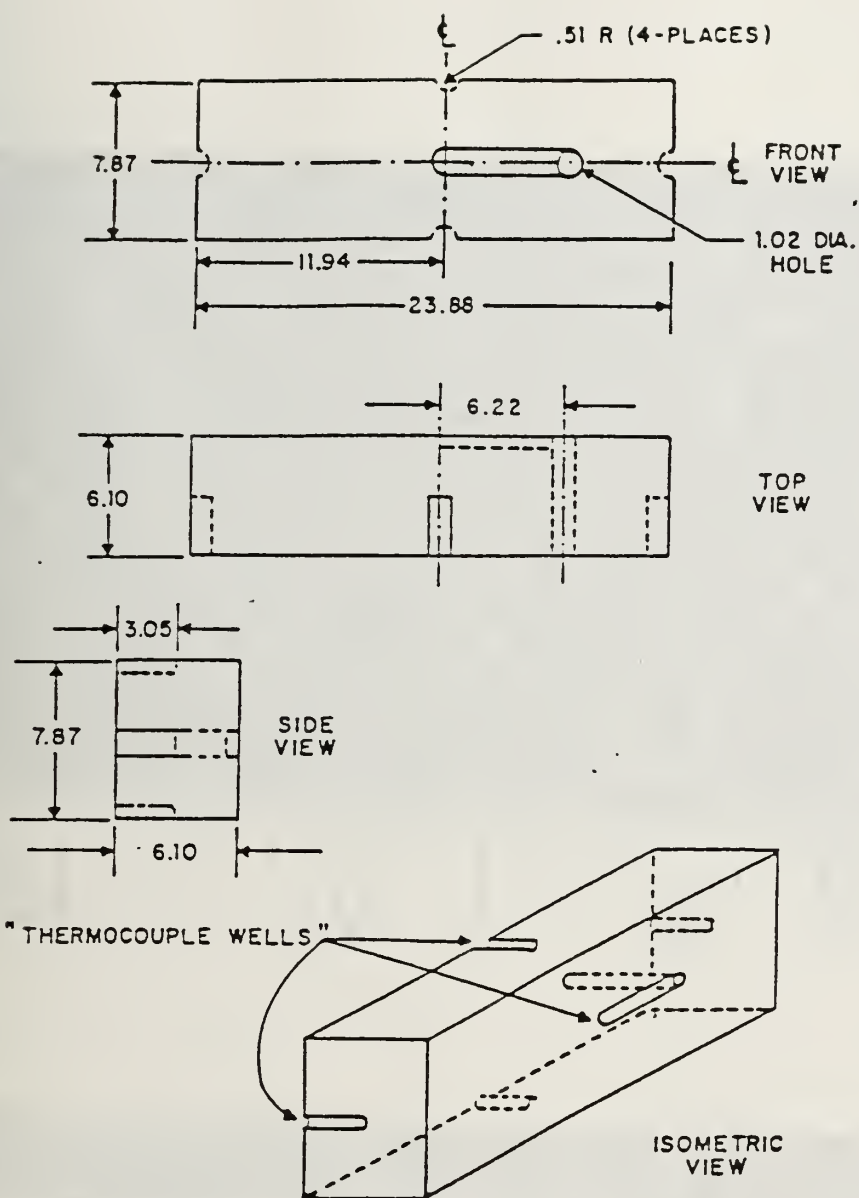


Figure 3. Aluminum Blocks and Thermocouple Wells.

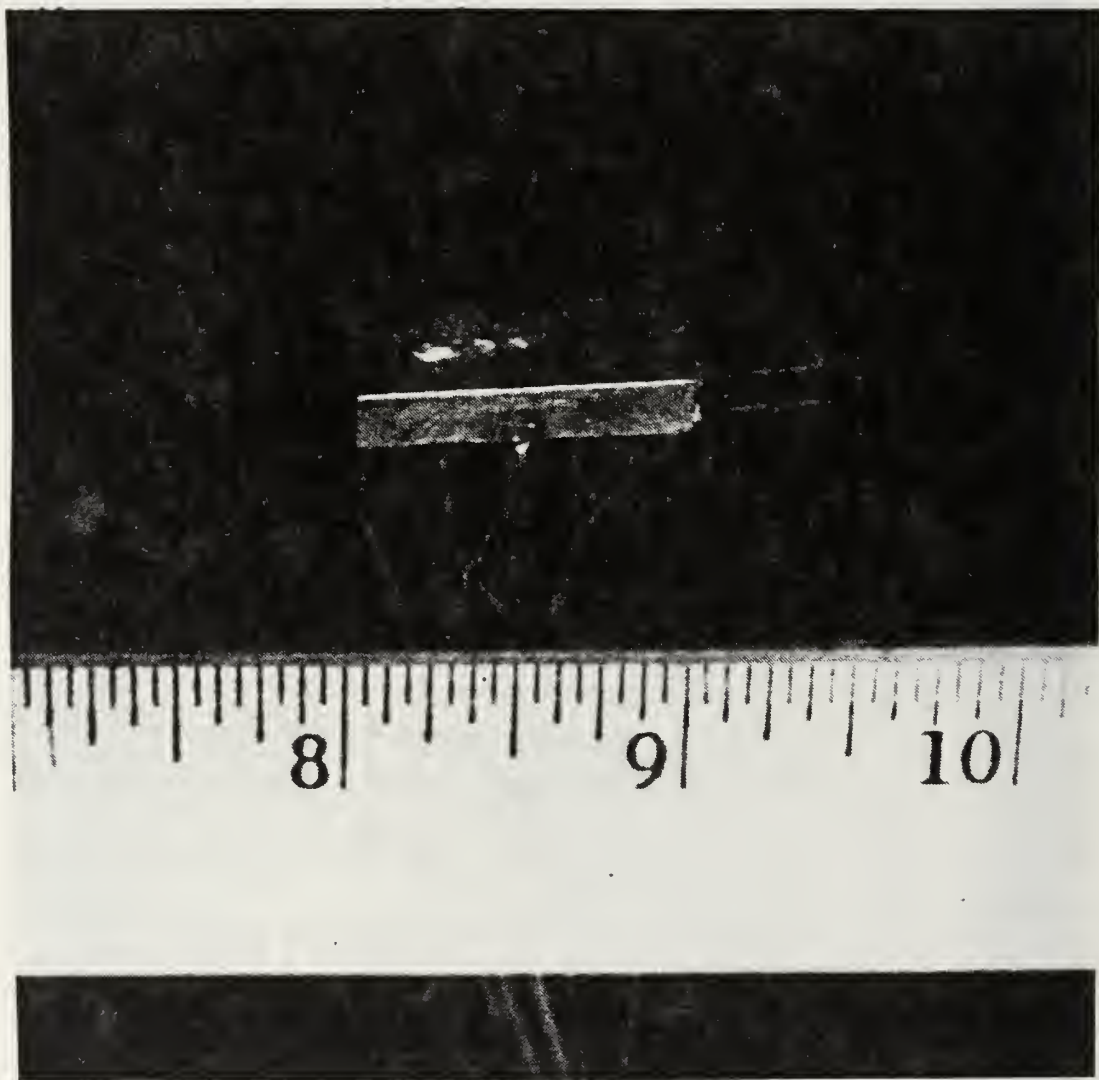


Figure 4. Aluminum Block Mounted with Copper-Constantan Thermocouples and an Inconel Foil Heating Element.

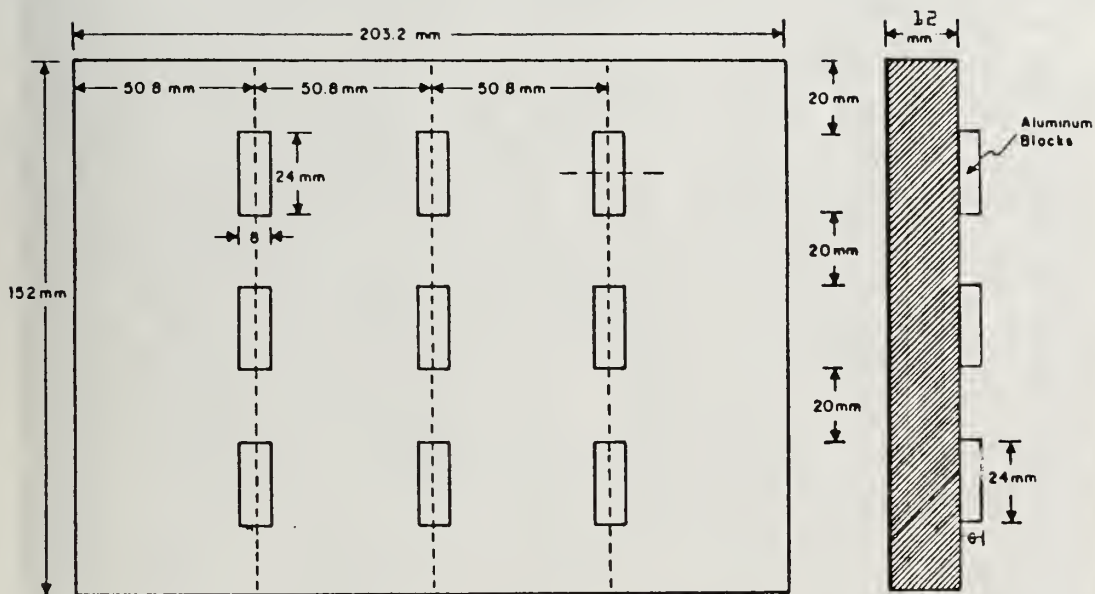


Figure 5. Front and Plan View of Circuit Board and Vertically Oriented Components.

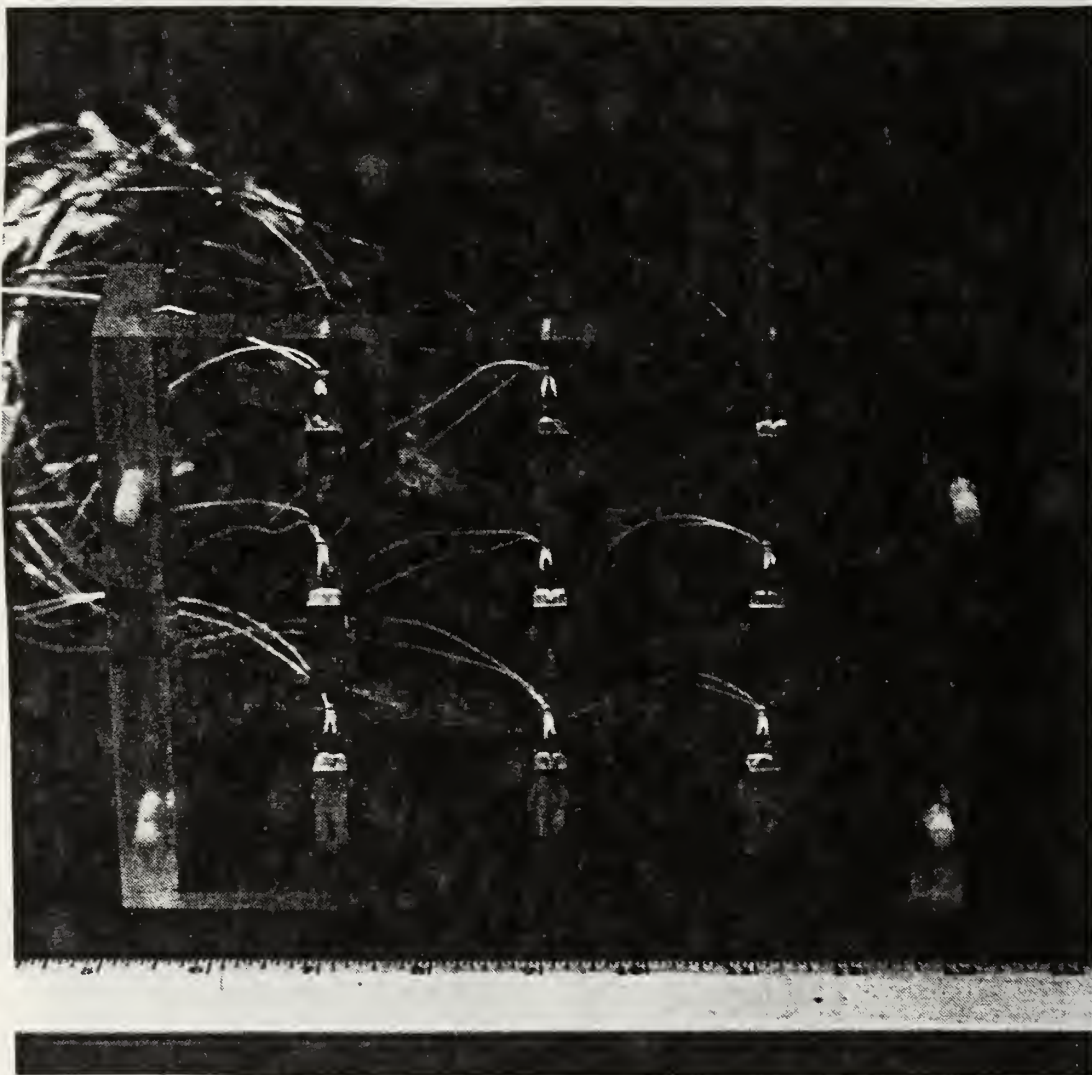


Figure 6. Circuit Board with Vertically Oriented Components.

III. EXPERIMENTAL PROCEDURE AND DATA ANALYSIS

A. SYSTEM PREPARATION

Prior to each experimental run, the following preparatory steps were completed.

1. The required spacer (if any) was inserted into the chamber. The heat exchanger was affixed to the chamber only enough to ensure that the circuit board and spacer were secure. Using a ruler graduated in millimeters, the chamber width was measured at various points along the height of the plexiglass substrate from the exterior of the chamber, to ensure that the distance from the circuit board to the spacer was consistent. These measurements were taken on both sides of the chamber. Once the chamber width was set at the proper distance, the heat exchanger was then completely affixed to the chamber.
2. The heat exchanger supply and return lines were attached, and the system tested for any interior or exterior leakage. This test was conducted with the flow setting at its maximum.
3. Upon a satisfactory heat exchanger seal test, the flow control was set to zero and the bath temperature control set to 10°C. The bath was allowed to reach test conditions while the remaining preparations were completed.
4. The chamber was filled with the appropriate dielectric liquid, ensuring that as much air as possible was removed from the chamber (this is especially important at smaller chamber widths). The chamber was observed for any visible sign of leakage.
5. Foam insulation padding was affixed to the bottom and vertical surfaces of the chamber.
6. The appropriate heat exchanger thermocouples were chosen based on the chamber width under investigation.
7. All thermocouples and heating elements were checked for continuity by stepping through each channel of the HP3497A data acquisition system and monitoring the digital voltmeter.

B. EXPERIMENTAL PROCEDURE

Once system preparations were complete, the following steps were followed to accomplish an experimental run, which consisted of a single chamber width at all power levels.

1. The voltage on the DC power supply was set to produce the required power level.
2. The refrigerated bath's flow control was opened to its maximum position.
3. The heat exchanger thermocouples (channels 54-56) were monitored, and the bath temperature control adjusted to attain the 10°C upper boundary condition.
4. Once the average heat exchanger temperature stabilized, an initial data set was taken to establish a system start time.

5. Steady state conditions were assumed when the temperature fluctuations from all thermocouples were less than 1°C in 10 minutes for FC-75 and 0.4°C in 10 minutes for FC-43. These conditions were the same as those used by Aytar (1991), and are based on steady state surface temperature fluctuation measurements. As reported by Aytar (1991), the time constant of the system was a function of chamber width and the dielectric fluid used. This also held true for the vertical component orientation. Typical time requirements to achieve steady state from ambient conditions were approximately $3\frac{1}{2}$ - 4 hours. For subsequent runs at the same chamber width, the time decreased to approximately 2 - $2\frac{1}{2}$ hours.

C. DATA ACQUISITION

Data acquisition and processing was accomplished using the software programs ACQUIRE and CALCDIEL. These programs were the same as those used by Pamuk (1987), Benedict (1988), Torres (1988), Powell (1989) and Aytar (1991), with the following modifications:

- A one point calibration was done for each card of the data acquisition system using an ice bath reference. Three random channels per card were tested against the ice bath reference, and the arithmetic average of the 3 emf readings was assumed to be a constant offset for that particular data acquisition system card.
- CALCDIEL was made completely general and interactive, so that any combination of power level, chamber width, dielectric liquid or component orientation could be used as an input.

IV. DATA ANALYSIS

The following analysis was used to reduce the raw data obtained by ACQUIRE into non-dimensional parameters (Nu_i , Ra_i , Ra_f). These non-dimensional parameters were determined for each component at the various power levels and chamber widths for both FC-75 and FC-43 using CALCDIEL. The assumptions used to arrive at the expressions in the following analysis are given below:

- Heat transfer from the heating elements to the plexiglass substrate occurred via 1-Dimensional conduction.
- A linear temperature profile existed across the thickness of the plexiglas substrate.
- The surface area of the plexiglass substrate not occupied by a component was adiabatic (i.e. there was no heat transfer between the dielectric liquid and the substrate).
- The thermophysical properties of the dielectric liquid near each component were uniform and constant, and were evaluated at the film temperature (T_{film}).
- The thermal conductivity of the plexiglass substrate was homogenous.
- There was negligible contact resistance between the aluminum blocks and the foil heaters.
- There was negligible contact resistance between the foil heaters and the plexiglass substrate.

A components average surface temperature was approximated as an area based average over the entire wetted surface area of the component:

$$T_{avg} = \frac{\sum_{i=1}^S A_i T_i}{A_{total}}$$

where,

A_i, T_i = area and temperature of the i^{th} surface

A_{total} = total wetted surface area of a component

The net power dissipated by a heating element was determined by measuring the voltage drop across the heating element, and multiplying it by the current passing through the precision resistor-heating element series combination:

$$POWER = V \cdot i = emf \cdot \frac{(volt - emf)}{R_p}$$

where,

emf = voltage drop across a resistive heating element

volt = DC power supply voltage

R_p = resistance of a precision resistor (2Ω)

The total heat loss from the array's heating elements to the plexiglass substrate was calculated as a sum of contributions from each independent heating element. The process was considered to occur via 1-D conduction across the thickness of the substrate, where a linear temperature profile was assumed.

$$Q_{loss} = \frac{\sum_{i=1}^9 \left(\frac{\Delta T_i}{R_c} \right)}{9}$$

$$R_c = \frac{t}{k_p A}$$

$$\Delta T = T_{cb} - T_{bp}$$

where,

T_{cb} = component back surface temperature

T_{bp} = the back circuit board temperature

R_c = conductive thermal resistance of the plexiglass

k_p = thermal conductivity of the plexiglass

A = rear face surface area of the component

t = thickness of the circuit board

The net heat transferred from a component to the surrounding dielectric liquid was determined by subtracting the total heat loss to the substrate via 1-D conduction from the net power dissipated by its heating element:

$$Q_{net} = POWER - Q_{loss}$$

The average heat transfer coefficient for a component, h , was determined from Newton's Law of Cooling for convective heat transfer:

$$h = \frac{Q_{net}}{A_{total}(T_{avg} - T_{sink})}$$

$$T_{sink} = \frac{T_{54} + T_{55} + T_{56}}{3}$$

where,

T_{sink} = average temperature of the heat exchanger

The non-dimensional Nusselt number (Nu_1), was defined as:

$$Nu_1 = \frac{hL}{k_f}$$

where,

L = vertical dimension of the component in the direction of the gravitational vector

k_f = thermal conductivity of the dielectric liquid

The non-dimensional Grashof number, which relates the effects of buoyant forces to viscous forces in a natural convection environment, was defined as:

$$Gr = \frac{g\beta L^3(T_{avg} - T_{sink})}{\nu^2}$$

The thermal diffusivity, α , which indicates the thermal diffusion characteristics of a fluid, was found from:

$$\alpha = \frac{k_f}{\rho C_p}$$

The Prandtl Number, which relates the relative rates of viscous to thermal diffusion for a fluid, was defined as:

$$Pr = \frac{\nu}{\alpha}$$

The temperature based Rayleigh number, which is the product of the non-dimensional Grashof and Prandtl numbers, is synonymous with the Reynolds number (Re) used in forced convection heat transfer. This parameter was defined as:

$$Ra_t = Gr \cdot Pr = \frac{g\beta L^3 \Delta T}{\nu \alpha}$$

$$\Delta T = T_{avg} - T_{sink}$$

The flux based Rayleigh number was defined as:

$$Ra_f = \frac{g\beta L^4 Q_{net}}{k_f \nu \alpha A_{total}}$$

The thermophysical properties of the dielectric liquids were determined from the following relations, and evaluated at the film temperature, T_{film} :

$$T_{film} = \frac{T_{avg} + T_{sink}}{2}$$

Thermal Conductivity, k_f

$$\text{for FC-75: } k_f = \frac{[0.65 - 7.8947 \times 10^{-4} \times T_{film}]}{10}$$

$$\text{for FC-43: } k_f = \frac{[0.666 - 9.864 \times 10^{-5} \times T_{film}]}{10}$$

Density, ρ

$$\text{for FC-75: } \rho = [1.825 - 0.00246 \times T_{film}] \times 10^3$$

$$\text{for FC-43: } \rho = [1.913 - 0.00218 \times T_{film}] \times 10^3$$

Specific Heat, C_p

$$\text{for FC-75 and FC-43: } C_p = [0.241111 + 3.7037 \times 10^{-4} \times T_{film}] \times 4.18 \times 10^3$$

Kinematic Viscosity, ν

FC-75:

$$\nu = [1.4074 - 2.964 \times 10^{-2} \times T_{film} + 3.8018 \times 10^{-4} \times T_{film}^2 - 2.7308 \times 10^{-6} \times T_{film}^3 + 8.1679 \times 10^{-9} \times T_{film}^4] \times 10^{-6}$$

FC-43:

$$\nu = [8.8750 - 0.47007 \times T_{film} + 1.387 \times 10^{-2} \times T_{film}^2 - 2.1469 \times 10^{-4} \times T_{film}^3 + 1.3139 \times 10^{-6} \times T_{film}^4] \times 10^{-6}$$

Thermal Expansion Coefficient, β

$$\text{for FC-75: } \beta = \left[\frac{0.00246}{(1.825 - 0.00246 \times T_{film})} \right]$$

$$\text{for FC-43: } \beta = \left[\frac{0.00218}{(1.913 - 0.00218 \times T_{film})} \right]$$

V. RESULTS

A. GENERAL

Dimensional and non-dimensional data output was used to study the heat transfer characteristics of a 3x3 array of vertically oriented simulated electronic components using two dielectric fluids: FC-75 and FC-43, at chamber widths of 42, 30, 18, 11, and 7 mm and power levels from 0.114-2.9W. The non-dimensional data from this study was combined with data obtained by Aytar (1991), to produce an empirical correlation which accounted for variations in:

- Rayleigh number
- Chamber Width
- Prandtl number
- Component orientation

Each of these effects were addressed separately and then subsequently combined to develop a relation of the form:

$$Nu_1 = aRa_l^{b_1}X^{b_2}Pr^{b_3}$$

where Nu_1 is the Nusselt number based on the components dimension in the direction of the gravitational vector, X is a non-dimensional chamber width based on the maximum chamber width attainable and a , b_1 , b_2 and b_3 are constants.

B. DIMENSIONAL RESULTS

Figure 7 and Figure 8 show the average array temperature as a function of both the net power dissipated by the array and chamber width, for both the vertical and horizontal orientations. For both orientations, average array temperatures are seen to be independent of chamber width at power levels less than 0.1W, and nearly independent of chamber width at all power levels for chamber widths of 30mm or greater. At power levels greater than 0.5W, the data form straight lines with slopes that increase as the wall spacing decreases from 42mm. This trend was also observed for FC-43. As mentioned previously, two data sets were taken for FC-75 at chamber widths of 42, 30, 18 and 11mm. When the data for the 2 test chambers were plotted as in Figure 7, the two data sets fell within the maximum uncertainty range of the thermocouples. The uncertainty was specified as 1% of the temperature value or $\pm 0.5^\circ\text{C}$, whichever was greater. The

increase in wall thickness therefore had no effect on the data. The two data sets were averaged to produce one data set for those chamber widths. The averaged data set was used to produce all quantitative results, whereas all qualitative results were based on the data taken using the second chamber.

The maximum increase in the average array temperature for the vertical orientation, for all chamber widths and power levels, was 34.9°C for FC-75 and 48.3°C for FC-43. For the horizontal orientation, the maximum temperature increase was 42.5°C for FC-75 and 44.5°C for FC-43. Maximum average component temperatures for the vertical orientation were 52°C for FC-75 and 68°C for FC-43, whereas for the horizontal orientation maximum average component temperatures were 59.8°C for FC-75 and 68.3°C for FC-43. These maximum temperatures occurred at a power level of approximately 2.8W and a chamber width of 7mm for both orientations and dielectric liquids.

The average component temperatures for FC-75 and a vertical component orientation were nearly uniform throughout the array for power levels less than 1.70W and chamber widths of 42, 30, and 18mm. As the chamber width was decreased to 11mm, the power level below which component average temperatures remained uniform, decreased to 0.80W. At 7mm, this power level decreased to 0.34W. For each chamber width, temperature differences between rows developed above those power levels where the average component temperatures remained uniform. These temperature differences became more pronounced as the power level increased, with noticable patterns forming between the rows. However, average component temperatures within each row remained nearly uniform. In order to make comparisons between the rows, an average row temperature was determined from the 3 components within each row. For FC-75 and a vertical component orientation, the order of average row temperatures was: middle > top > bottom. This pattern occurred at all chamber widths, but at the different power levels where the average component temperatures ceased to be uniform. This pattern may be attributed to the dominance of the buoyancy forces over viscous forces. A strong upward flow induced by the buoyancy forces retards the development of the ascending boundary layer. The decrease in the average row temperature from the middle to top row was attributed to the close proximity of the components in the top row to the upper isothermal boundary. The maximum temperature difference between the middle and bottom rows was 6.8°C, and occurred at a power level of 2.86W and a chamber width of 11mm. There was no component, at any power level or wall spacing, which was consistently at either the maximum or minimum average temperature. The only conclusion that could be made was that the maximum temperature occurred on a

component in the middle row, and the minimum on a component in either the top or bottom row.

For FC-43 and a vertical component orientation, average component temperatures remained nearly uniform for all chamber widths at power levels of 0.34W or less. Again, temperature differences between rows developed at power levels greater than 0.34W, with average component temperatures within each row remaining nearly uniform. The order of average row temperatures for FC-43 and a vertical component orientation was: top > middle > bottom. This pattern occurred at all chamber widths and power levels, with the exception of a 7mm chamber width and power levels of 2.24W and 2.86W, where it was: middle > top > bottom. For the pattern mentioned first, viscous forces dominate buoyancy forces and the circuit board acts like a vertical, flat plate with a constant, uniform heat flux (Blasius flow). Here, the maximum temperature difference between the top and bottom average row temperatures was 3.5°C, and occurred at a chamber width of 7mm and a power level of 1.70W. The maximum average component temperature in the array occurred almost exclusively at chip 6, and was always in the upper row. For the second pattern mentioned above, which was the same as observed for FC-75 and a vertical component orientation, buoyancy forces appear to have overcome viscous forces. The relatively small distance from the center front face of the components to the wall (1mm) may have also affected the development of the ascending boundary layer, as well as the upward flow induced by the buoyancy forces. The maximum temperature difference between the middle and bottom row average temperatures was 6.4°C and occurred at a power level of 2.86W. The maximum average component temperatures for these two power levels at a 7mm chamber width, occurred at chip 2. The minimum average component temperature occurred at chip 7 for all cases described above.

C. NON-DIMENSIONAL RESULTS

1. FC-75

The maximum deviation in the flux based Rayleigh (Ra_f) number and Nusselt number (Nu_l), for a vertical component orientation, was 9.6% and 18.8% respectively. Both occurred at a chamber width of 7mm and a power setting of 2.87W. The average deviation in Ra_f and Nu_l , among all the data points for the vertical orientation, was 4.5% and 10.8% respectively. For the horizontal component orientation, Aytar (1991) reported a maximum deviation of 7% in both Ra_f and Nu_l for chamber widths of 42 and 30mm, and less than 3% deviation in Nu_l for all other chamber widths. These maximum

deviations corresponded to a temperature difference between components having maximum and minimum average temperatures of 7.7°C for the vertical component orientation, and 6°C for the horizontal component orientation.

Aytar (1991) found that array averaged Nusselt (Nu_1) and flux based Rayleigh (Ra_f) numbers plotted as straight lines of nearly constant slope, independent of chamber width, provided that Ra_f numbers corresponding to 0.115W were omitted. He reported a range of slopes between 0.296 and 0.340. Using a similar analysis, Nu_1 was plotted as a function of the temperature based Rayleigh number (Ra_t) and chamber width for both the horizontal component orientation ($1 \times 10^6 < Ra_t < 2 \times 10^7$) and the vertical component orientation ($3 \times 10^7 < 3 \times 10^8$). These data are presented in Figure 9. From Figure 9, the combined data set forms straight lines of constant slope, independent of chamber width. The effect of chamber width on the Nusselt number is more pronounced at 18, 11 and 7mm, whereas at 42 and 30mm, the effect is almost negligible.

a. Effect of Rayleigh Number

In a study conducted by Aytar (1991) using a horizontal component orientation, Rayleigh number dependence was determined using a flux based Rayleigh number. Prior to the correlation of any data, Nusselt number was plotted as a function of both the temperature and flux based Rayleigh numbers, using the data sets from both the horizontal and vertical orientations. Single straight line behavior was observed for both data sets when the temperature based Rayleigh number was used (Figure 9). Based on this observation, it was determined that the temperature based Rayleigh number was more appropriate than the flux based Rayleigh number. The relationship between the Nusselt number (Nu_1) and the temperature based Rayleigh number (Ra_t) was assumed to be of the simple form:

$$Nu_1 = c_1 Ra_t^{b_1}$$

where c_1 and b_1 are constants.

Because of the similar behavior of components within a row, row averaged as well as array averaged values were determined. These values were plotted for each spacing and dielectric liquid using a curve fit software program entitled "TABLECURVE" which fits the data using a least squares regression algorithm. Curve fit equations for array averaged values of Nu_1 and Ra_t for each width are presented in Figure 10 through Figure 14. Curve fit equations for bottom, middle and top row averaged values of Nu_1 and Ra_t for each chamber width are presented in Figure 15 through

averaged values, since presenting correlations for all of the rows, as well as the array, would be lengthy and cumbersome. However, all the pertinent data is contained within to produce a row averaged correlation, should the need exist.

The range of values for the exponent b_1 from the array averaged data for the vertical orientation was: $0.352 < b_1 < 0.409$, with an average value of 0.381. A value of 0.35 was chosen to represent the effect of Ra_t for the entire array at all chamber widths. Aytar (1991) reported using a value of $b_1 = 0.30$.

b. Effect of Chamber Width

The effect of chamber width was also assumed to be of the form:

$$Nu_1 = c_2 X^{b_2}$$

where $X \left(\frac{x}{W} \right)$ is the non-dimensional chamber width and W is the maximum chamber width attainable (42mm). The constant c_2 reflects the Rayleigh number dependence. Using the curve fit equations developed for each chamber width, and an arbitrary value of $Ra_t = 2 \times 10^7$, the Nusselt number was plotted as a function of the non-dimensional chamber width (see Figure 30), resulting in the following:

$$Nu_1 = 25.778 X^{0.23}$$

and therefore the following general correlation for FC-75:

$$Nu_1 = 0.07176 Ra_t^{0.35} X^{0.23}$$

which is valid over the ranges:

$$1 \times 10^6 < Ra_t < 3 \times 10^8$$

$$23.04 < Pr < 30.73$$

This correlation is valid for low values of Ra_t (i.e. 1×10^6) but not for power levels less than 0.2W, since those points did not follow the trend of the data in Figure 9, and were omitted from the analysis. This correlation is accurate to within 6% of the curve fit equations developed by TABLECURVE from the original array averaged data.

2. FC-43

The maximum deviation in the flux based Rayleigh number (Ra_t) and the Nusselt number (Nu_1) for the vertical orientation was 13.9% and 16.9% respectively.

Both occurred at a spacing of 11mm and a power setting of 2.85W. The average deviation in Ra_f and Nu_1 for the vertical orientation was 7.2% and 12.2% respectively. Aytar (1991) reported an approximate deviation of 12% for both Ra_f and Nu_1 at a 7mm spacing. These maximum deviations corresponded to a temperature difference between the components having the maximum and minimum average temperatures, of 7.4°C for the vertical orientation, and 8°C for the horizontal orientation.

Similar to the analysis of FC-75, Nu_1 was plotted as a function of Ra_f and chamber width for both the horizontal component orientation ($3 \times 10^5 < Ra_f < 5 \times 10^6$) and the vertical component orientation ($8 \times 10^6 < Ra_f < 2 \times 10^8$). These are shown in Figure 31. Again, data points corresponding to 0.115W were omitted. As observed for FC-75, the data at each chamber width follows a straight line, with nearly constant slope, independent of chamber width. Again, the effect of chamber width is almost negligible between the 42 and 30mm widths. This was also observed by Aytar (1991).

a. Effect of Rayleigh Number

Similar to the analysis for FC-75, the relationship between the Nusselt number (Nu_1) and the temperature based Rayleigh number (Ra_f) was assumed to be of the form:

$$Nu_1 = c_1 Ra_f^{b_1}$$

where b_1 and c_1 are constants. Again, because of the similar behavior of components in the same row, row averaged as well as array averaged values of Ra_f and Nu_1 were determined. Curve fit equations for array averaged values of Nu_1 and Ra_f are presented in Figure 32 through Figure 36. Curve fit equations for bottom, middle and top row averaged values of Nu_1 and Ra_f are presented in Figure 37 through Figure 51. For the same reasons given previously, only array averaged values were used after this point.

The range of values for the exponent b_1 from the array averaged data for the vertical orientation was: $0.354 < m < 0.387$, with an average value of 0.371. A value of $b_1 = 0.35$ was chosen to correspond with the value selected for FC-75.

b. Effect of Chamber Width

The relationship between the non-dimensional chamber width and Nusselt number was again assumed to be of the form:

$$Nu_1 = c_2 X^{b_2}$$

Using the curve fit equations developed for each chamber width, and an arbitrary value of $Ra_t = 2 \times 10^7$, the Nusselt number was plotted as a function of the non-dimensional chamber width, which resulted in the following relation (see Figure 30):

$$Nu_1 = 0.0803 Ra_t^{0.35} X^{0.28}$$

which is valid over the ranges:

$$3 \times 10^6 < Ra_t < 1 \times 10^8$$

$$57.3 < Pr < 127.5$$

Similar to the correlation developed for FC-75, this correlation is valid for low values of Ra_t , but not for low power levels, since those data points were omitted from the analysis. This correlation is accurate to within 3% of the curve fit equations derived from the array averaged data using TABLECURVE.

3. Effect of Component Orientation

The effect of component orientation on the heat transfer characteristics of the array was found to be inherently accounted for within the Grashof number:

$$Gr = \frac{g\beta L^3 \Delta T}{\nu^2}$$

provided that the dimension of the component in the direction of the gravitational vector (\vec{g}) was used. This result was based on a straight line fit of the data from both orientations, when the length scale used in the temperature based Rayleigh number was chosen in the direction of \vec{g} .

4. Effect of Prandtl Number

As in the other cases, the relationship between the Nusselt number and the Prandtl number was assumed to be:

$$Nu_1 = c_3 Pr^{b_3}$$

where c_3 is a constant which reflects the dependence on the Rayleigh number and the non-dimensional chamber width. In this analysis, an average value of $b_2 = 0.25$, the non-dimensional chamber width exponent has been used. Because the Prandtl number for each dielectric varied significantly over the range of chamber widths and power levels investigated, an average value of Pr was used for each dielectric liquid. Assuming an

for each dielectric varied significantly over the range of chamber widths and power levels investigated, an average value of Pr was used for each dielectric liquid. Assuming an arbitrary value of $Ra_t = 2 \times 10^7$, the Nusselt number was calculated for each non-dimensional chamber width and average Prandtl number using the general correlations found for each dielectric liquid. The Nusselt number was then plotted as a function of average Prandtl number for the various non-dimensional chamber widths (Figure 52). From the 5 curves, average values of a and b_3 were determined. This led to the overall correlation:

$$Nu_1 = 0.0717 Ra_t^{0.35} X^{0.25} Pr^{0.025}$$

which is valid over the ranges:

$$3 \times 10^6 < Ra_t < 3 \times 10^8$$

$$23.04 < Pr < 127.5$$

This correlation is accurate to within 11% of the curve fit equations developed from the original array averaged data for FC-75 and FC-43. This accuracy has been determined using the full range of Prandtl numbers for both dielectrics, rather than simply the average values used to determine the correlation.

It is important to note that although the Prandtl number dependence in the overall correlation is an order of magnitude less than either the Rayleigh number or chamber width effects, only 2 data points for the Prandtl number were used to determine this dependence. Additional experimental analysis may prove that this dependence is something other than what was presented here.

An interesting result is obtained if b_1 , the exponent of Ra_t , is chosen as 0.33 or $1/3$. The motivation for this choice is that the heat transfer coefficient becomes independent of the components length scale, as seen for turbulent flows. If the analysis used to arrive at the overall correlation presented above is repeated with $b_1 = 0.33$, the accuracy of the the resulting correlation is essentially the same as the initial correlation derived using $b_1 = 0.35$. The correlation which resulted from this analysis was:

$$Nu_1 = 0.1005 Ra_t^{0.33} X^{0.25} Pr^{0.026}$$

5. Uncertainty Analysis

Using the method of Kline and McClintock (1956), a zeroth order uncertainty analysis was carried out for all chamber widths and power levels, to determine the uncertainty in the Nusselt number (Nu_1) and temperature based Rayleigh number (Ra_1). The calculations were done on a component basis. The expressions used in this analysis are presented in Appendix A. Any uncertainty in calculating the thermophysical properties of the dielectrics has been neglected. Upon reviewing the data, the following observations were made:

1. The maximum uncertainty in both Nu_1 and Ra_1 was 2.5% for FC-75 and 1.9% for FC-43.
2. The maximum uncertainty in Ra_1 and Nu_1 occurred at the lowest power level, 0.115W. This held true for both dielectric liquids. This result was expected since the maximum uncertainty in the temperature measurements occurred at this power level.
3. The uncertainty in Nu_1 and Ra_1 decreased slightly as the chamber width decreased or the power level increased.

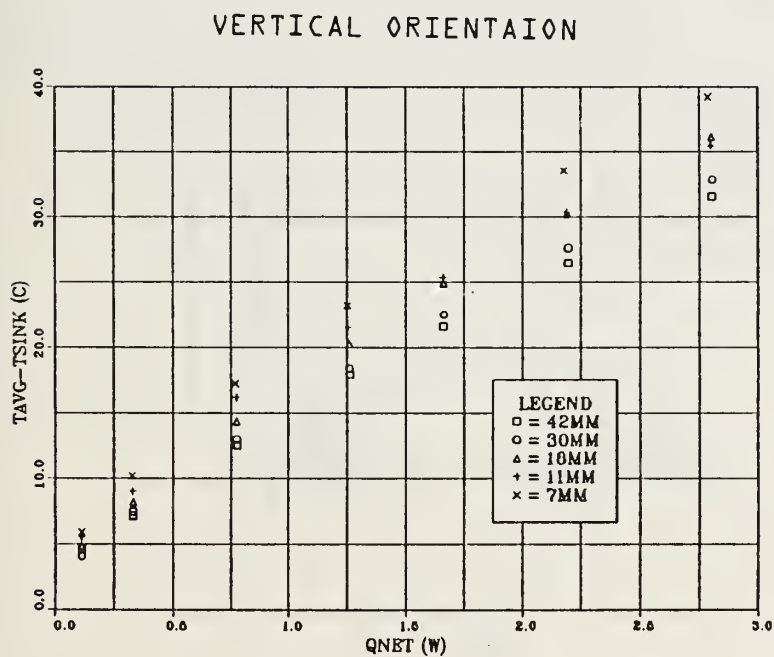
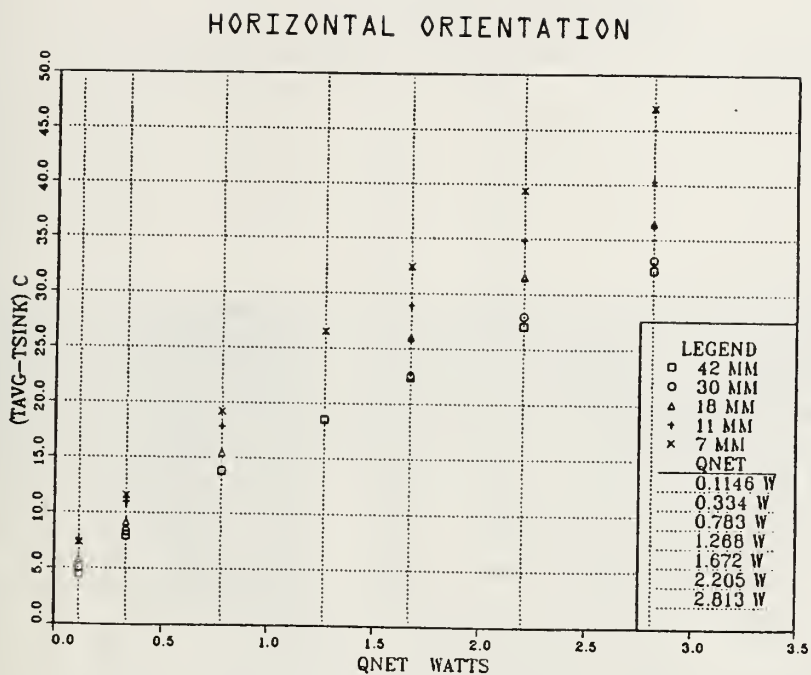


Figure 7. Average Array Temperature as a function of Net Power and Chamber Width for FC-75.

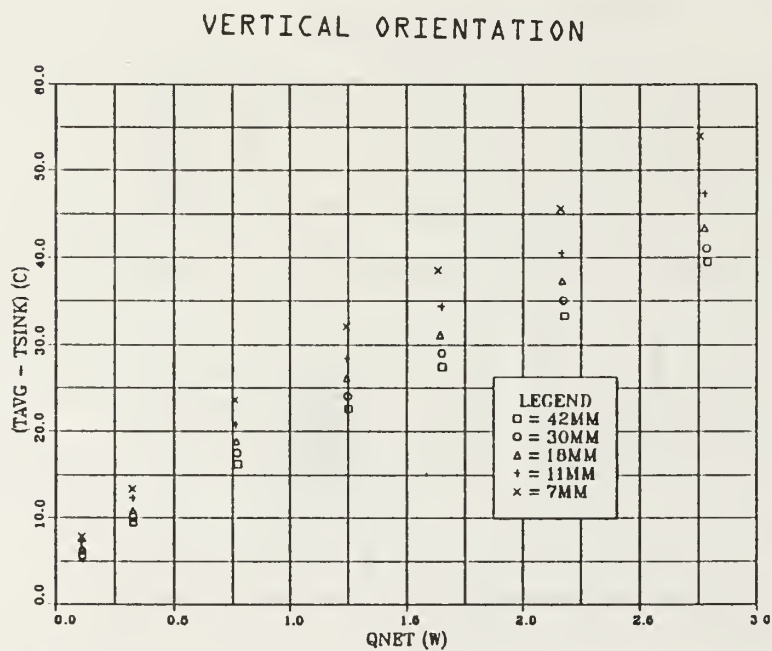
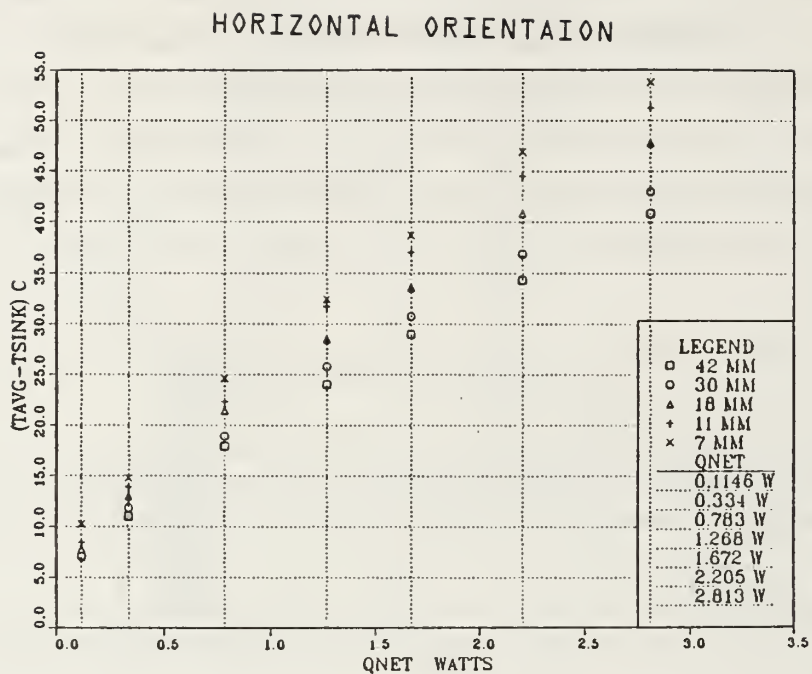


Figure 8. Average Array Temperature as a function of Net Power and Chamber Width for FC-43.

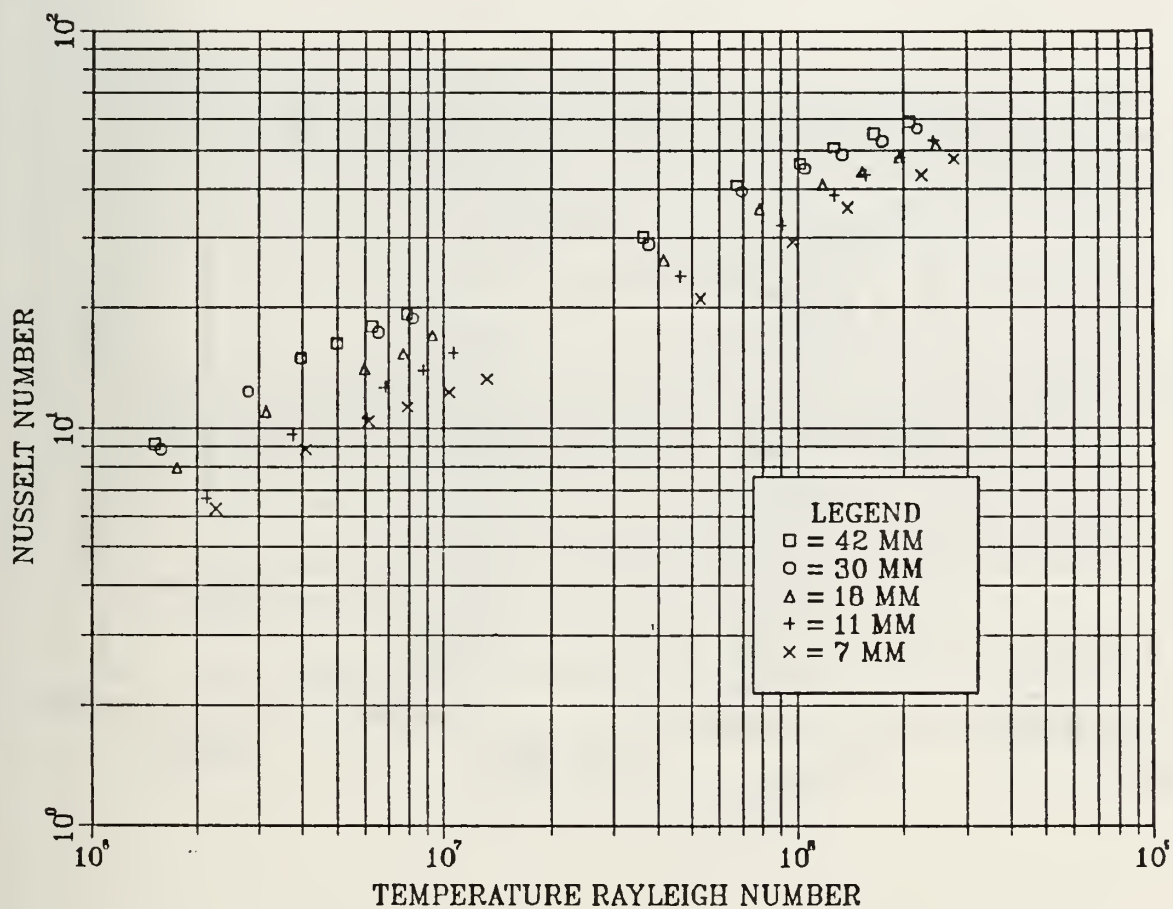


Figure 9. Nu_1 vs Ra , for a Vertical Component Orientation, FC-75 and all Chamber Widths.

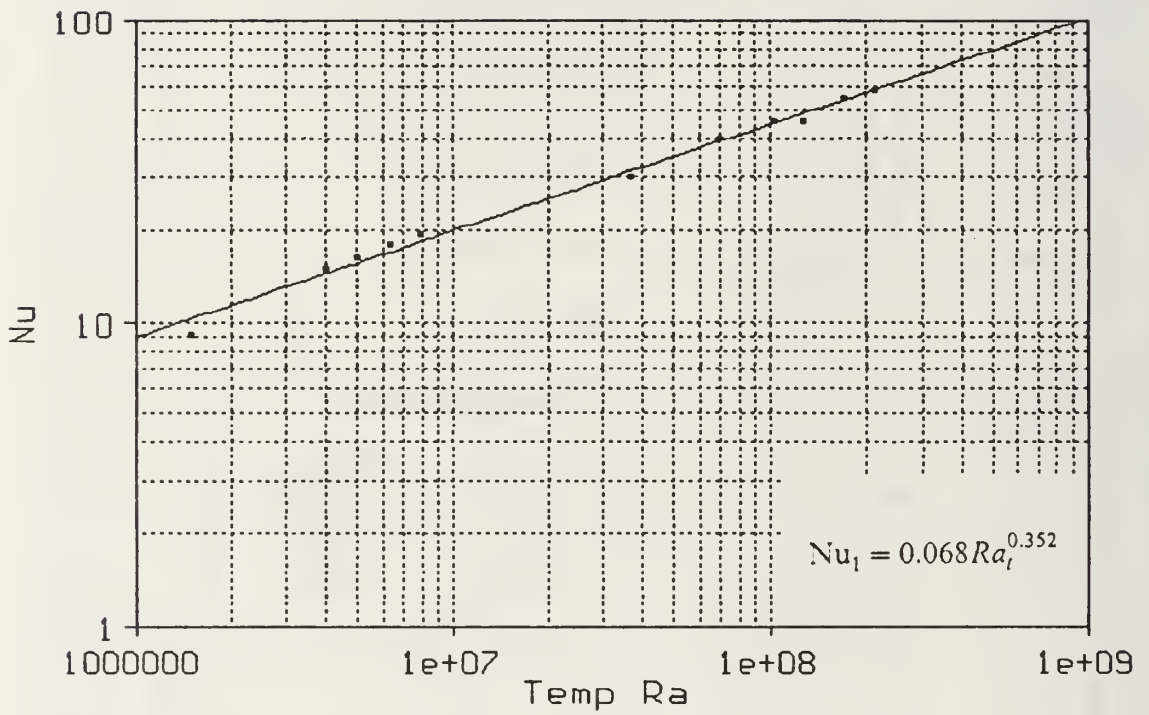


Figure 10. Nu_1 vs Ra_l for a Vertical Component Orientation, FC-75 and a 42mm Chamber Width using Array Averaged Values.

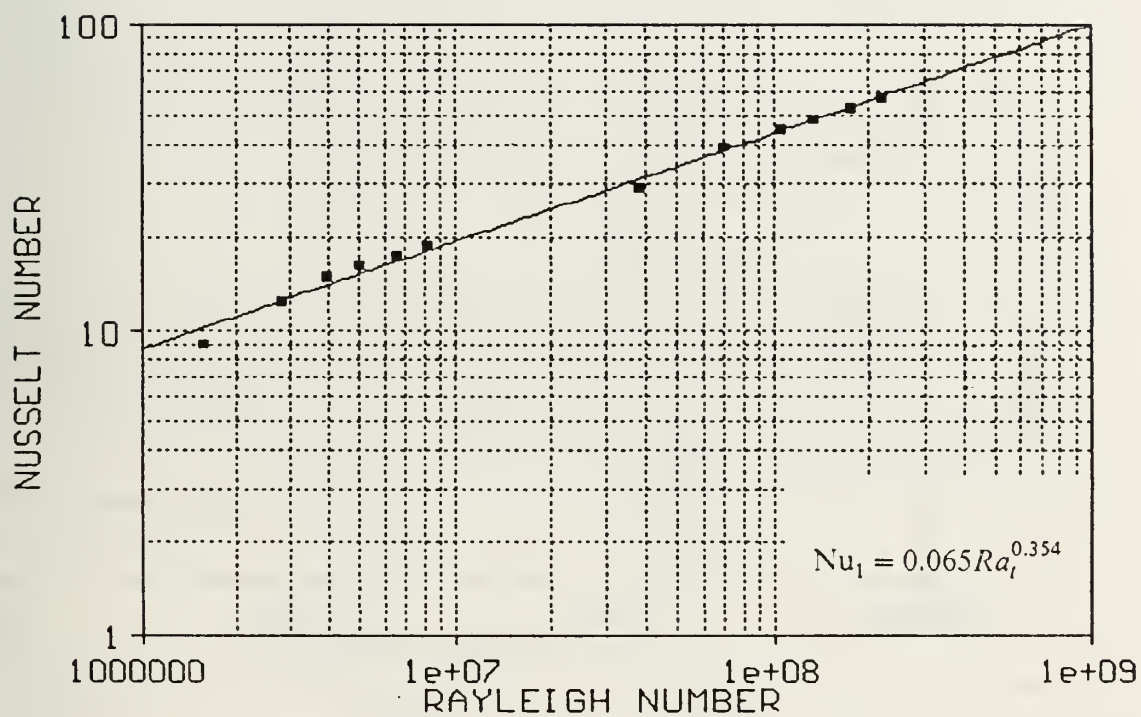


Figure 11. Nu_1 vs Ra_1 for a Vertical Component Orientation, FC-75 and a 30mm Chamber Width using Array Averaged Values.

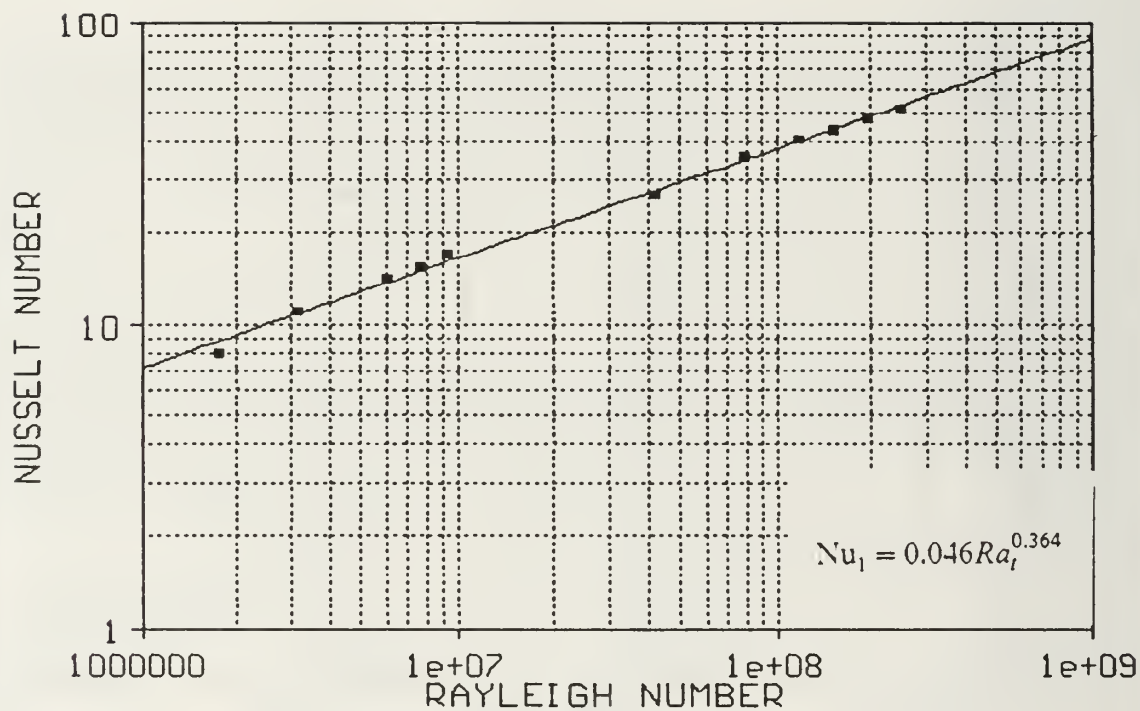


Figure 12. Nu_l vs Ra_l for a Vertical Component Orientation, FC-75 and an 18mm Chamber Width using Array Averaged Values.

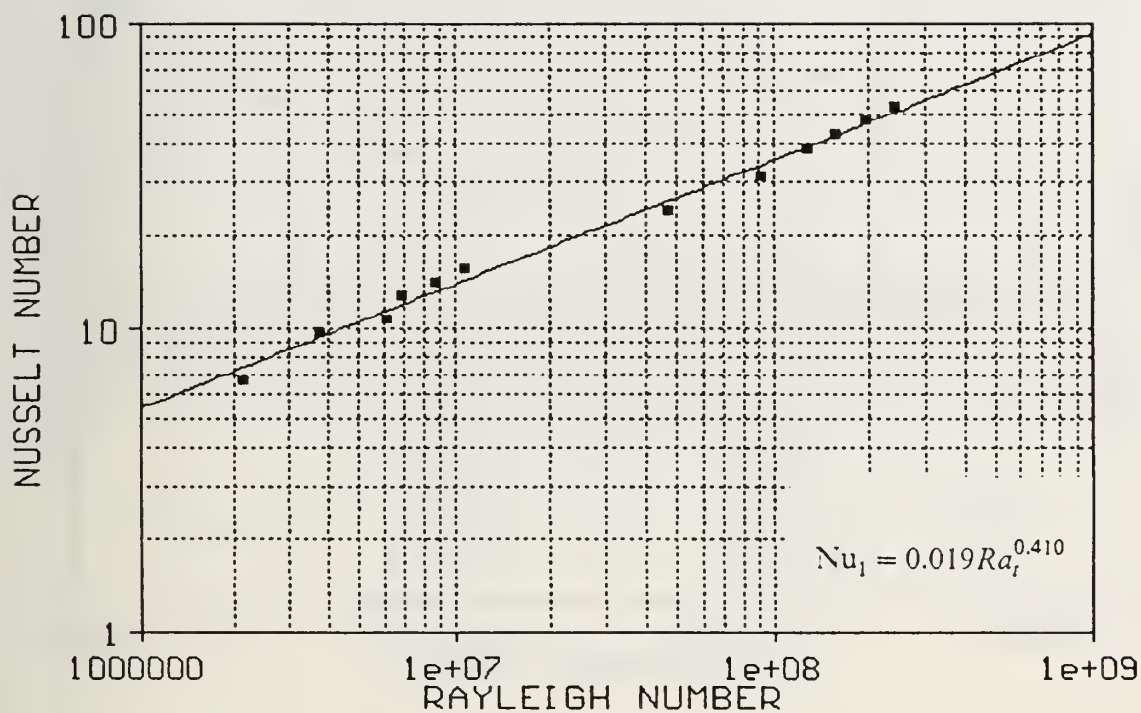


Figure 13. Nu_1 vs Ra_t for a Vertical Component Orientation, FC-75 and an 11mm Chamber Width using Array Averaged Values.

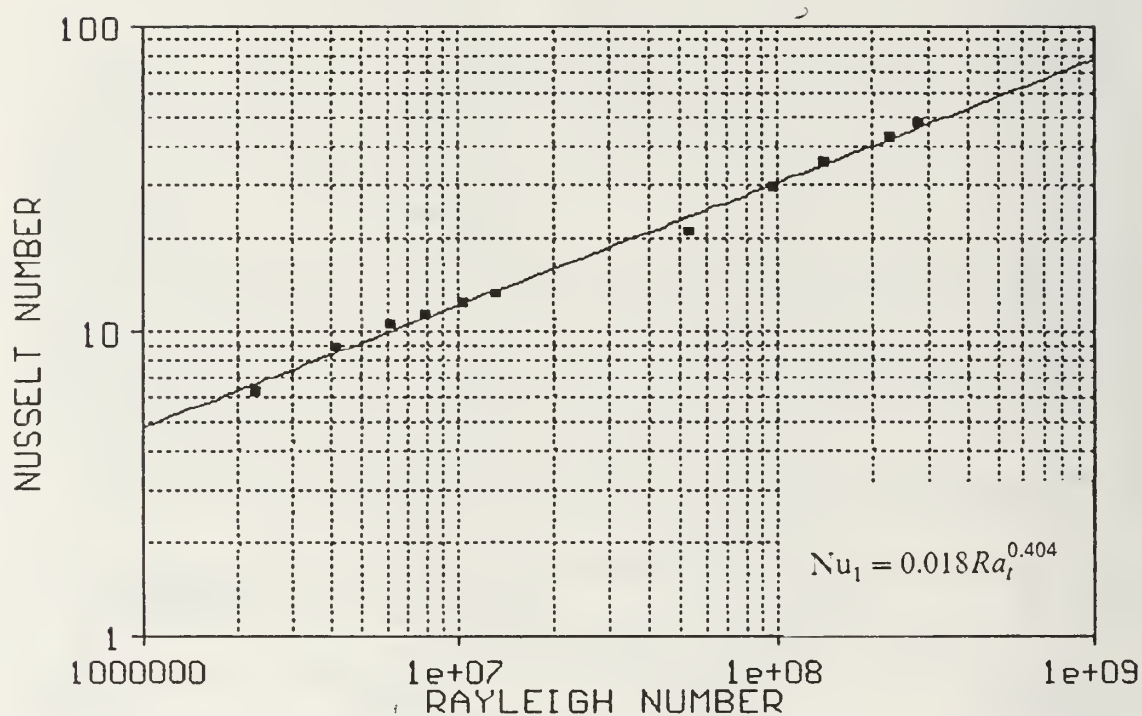


Figure 14. Nu_1 vs Ra_t for a Vertical Component Orientation, FC-75 and a 7mm Chamber Width using Array Averaged Values.

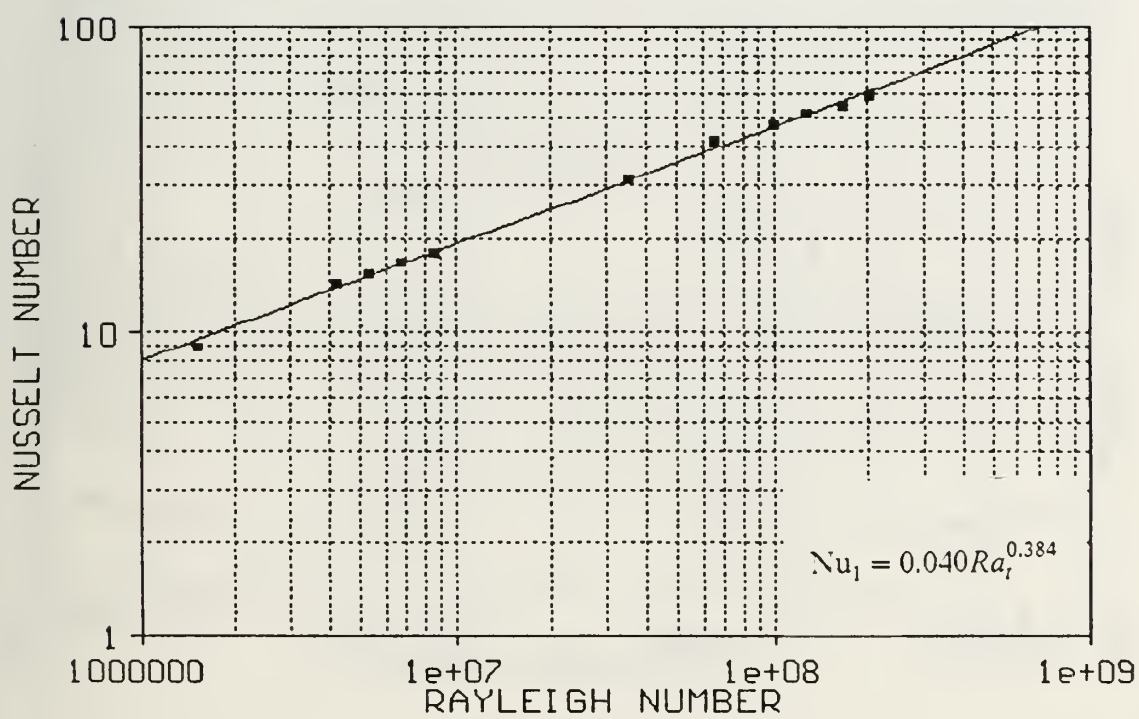


Figure 15. Nu_1 vs Ra_1 for a Vertical Component Orientation, FC-75 and a 42mm Chamber Width using Bottom Row Averaged Values.

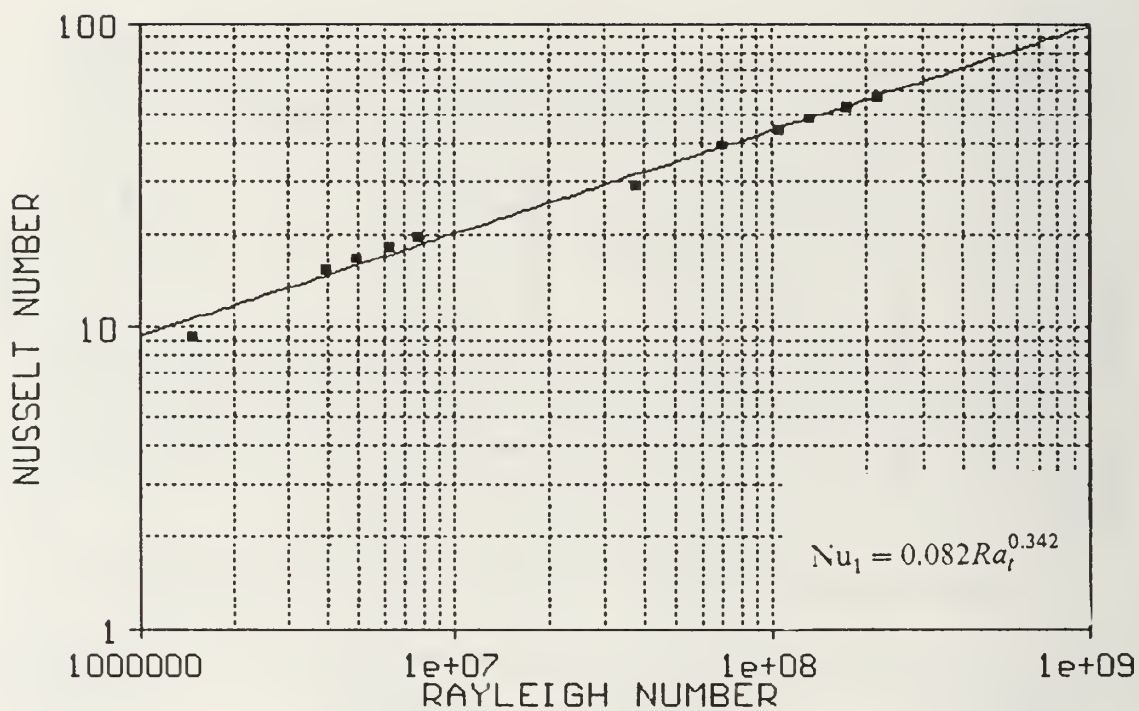


Figure 16. Nu_l vs Ra_l for a Vertical Component Orientation, FC-75 and a 42mm Chamber Width using Middle Row Averaged Values.

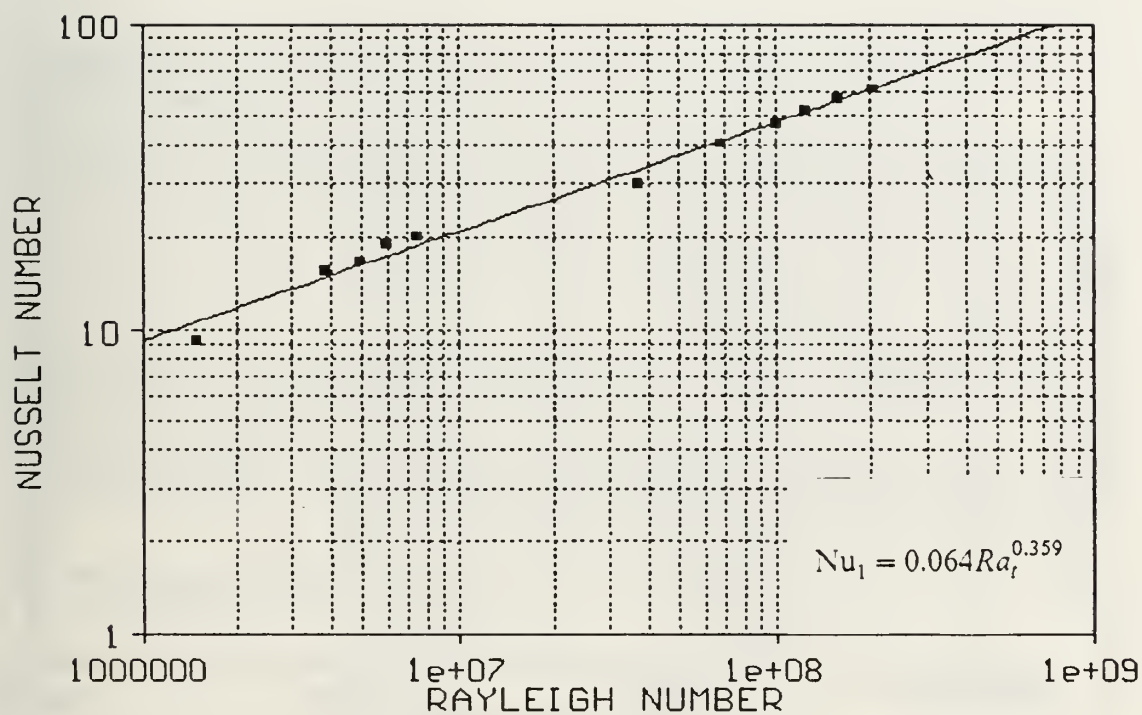


Figure 17. Nu_1 vs Ra_1 for a Vertical Component Orientation, FC-75 and a 42mm Chamber Width using Top Row Averaged Values.

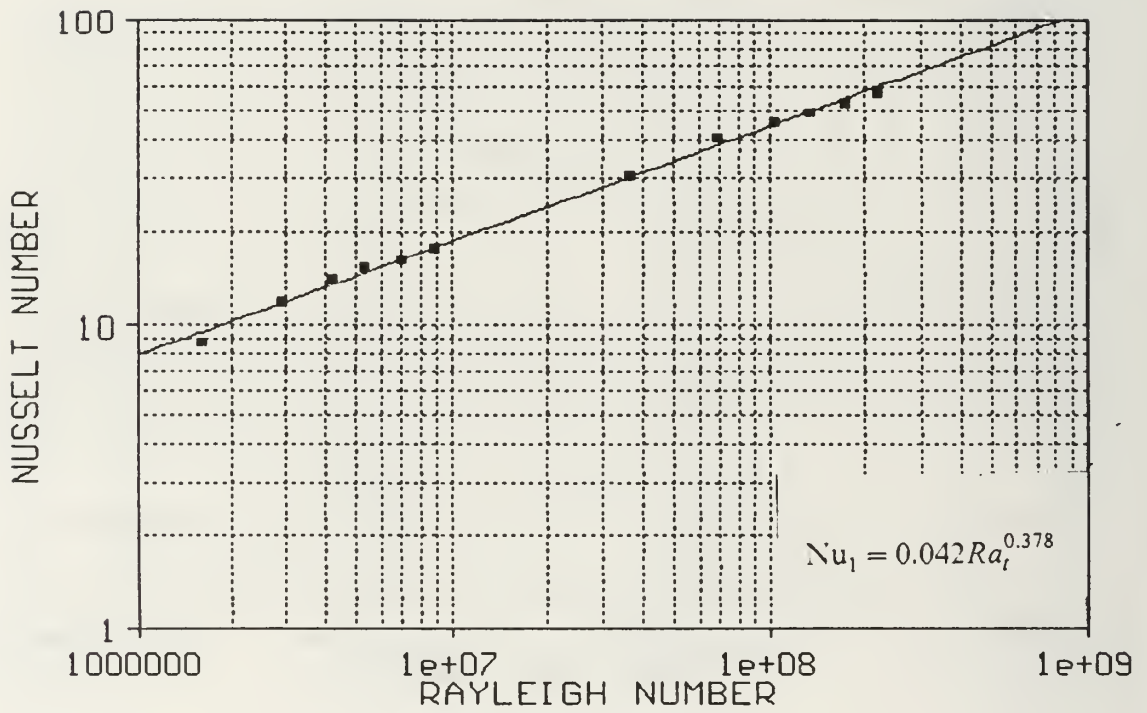


Figure 18. Nu_1 vs Ra_1 for a Vertical Component Orientation, FC-75 and a 30mm Chamber Width using Bottom Row Averaged Values.

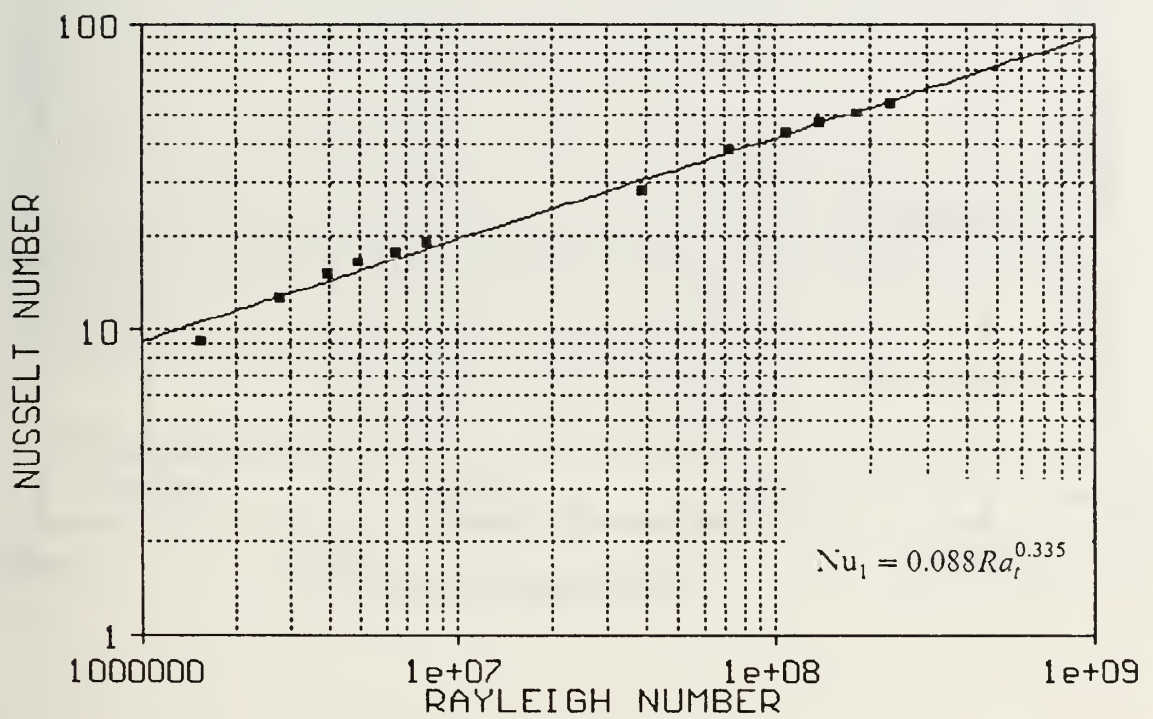


Figure 19. Nu_1 vs Ra_1 for a Vertical Component Orientation, FC-75 and a 30mm Chamber Width using Middle Row Averaged Values.

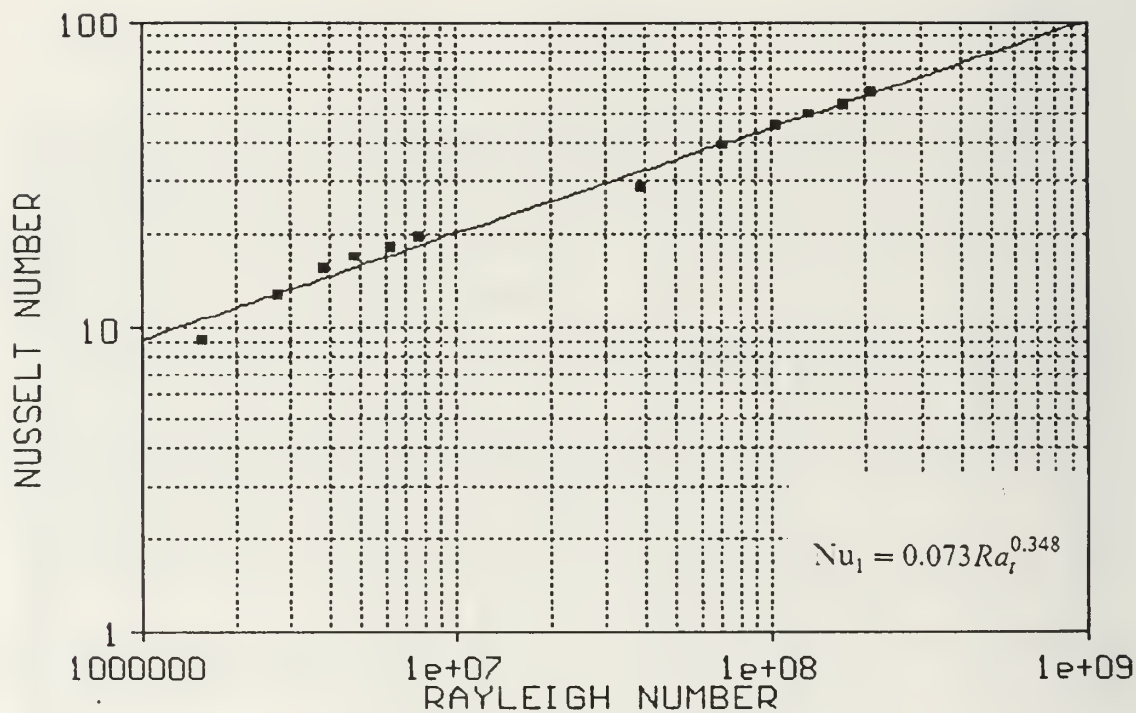


Figure 20. Nu_l vs Ra_l for a Vertical Component Orientation, FC-75 and a 30mm Chamber Width using Top Row Averaged Values.

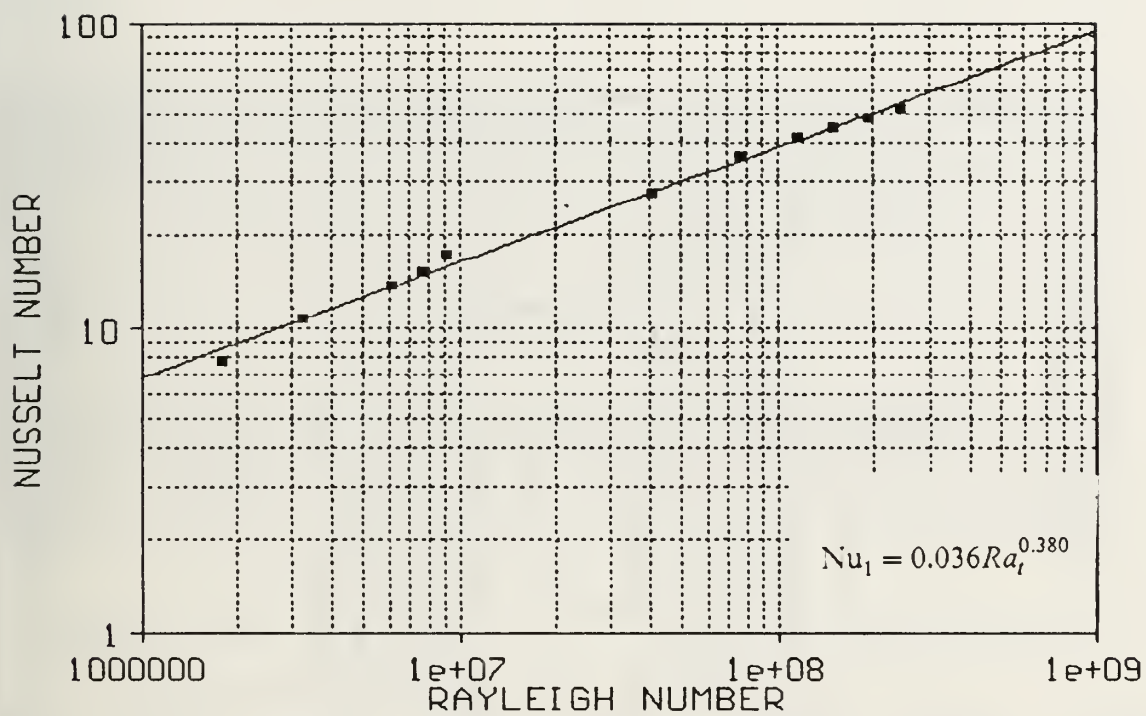


Figure 21. Nu_1 vs Ra_1 for a Vertical Component Orientation, FC-75 and an 18mm Chamber Width using Bottom Row Averaged Values.

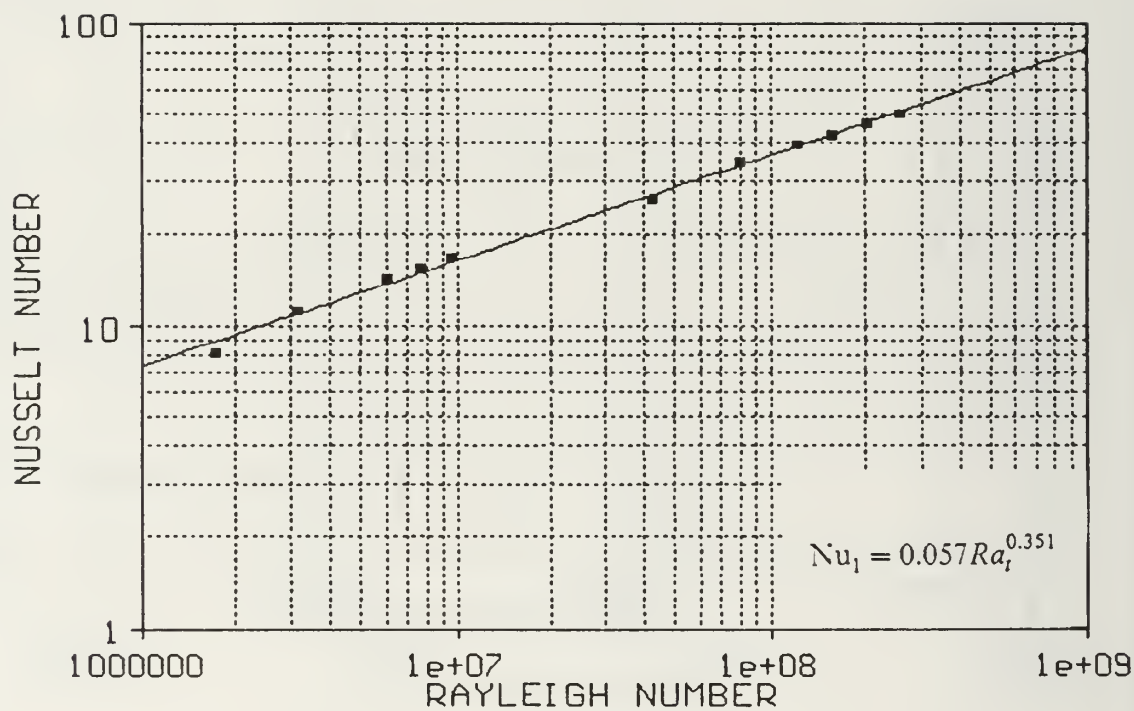


Figure 22. Nu_1 vs Ra_1 for a Vertical Component Orientation, FC-75 and an 18mm Chamber Width using Middle Row Averaged Values.

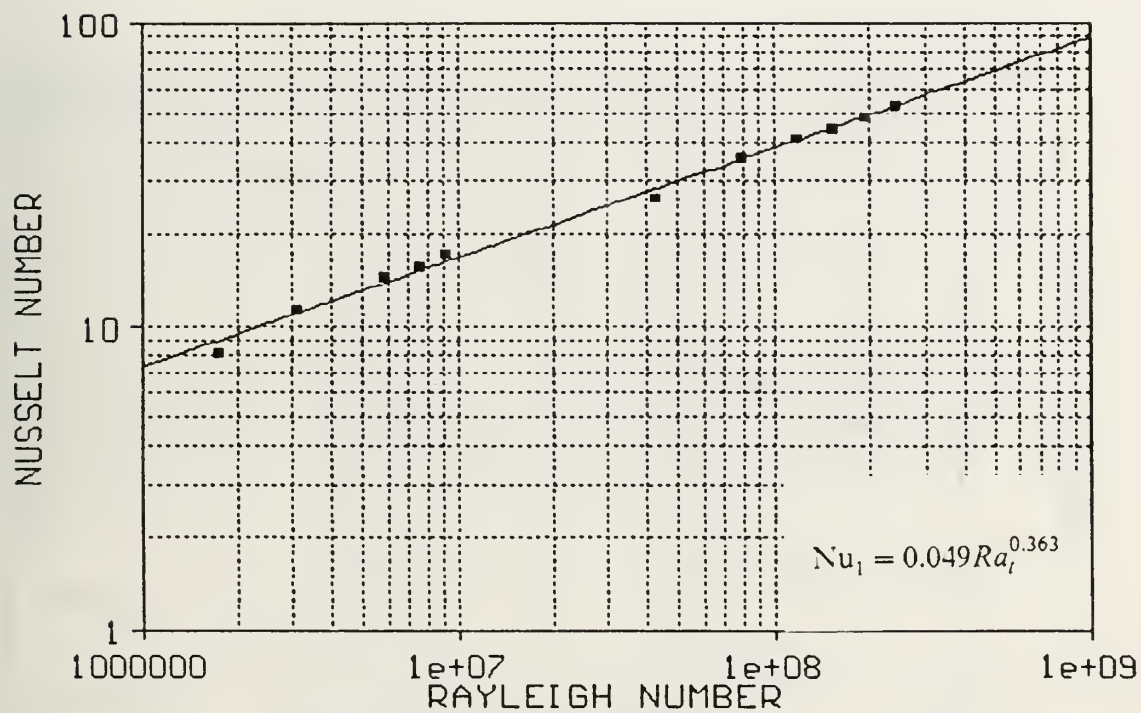


Figure 23. Nu_l vs Ra_l for a Vertical Component Orientation, FC-75 and an 18mm Chamber Width using Top Row Averaged Values.

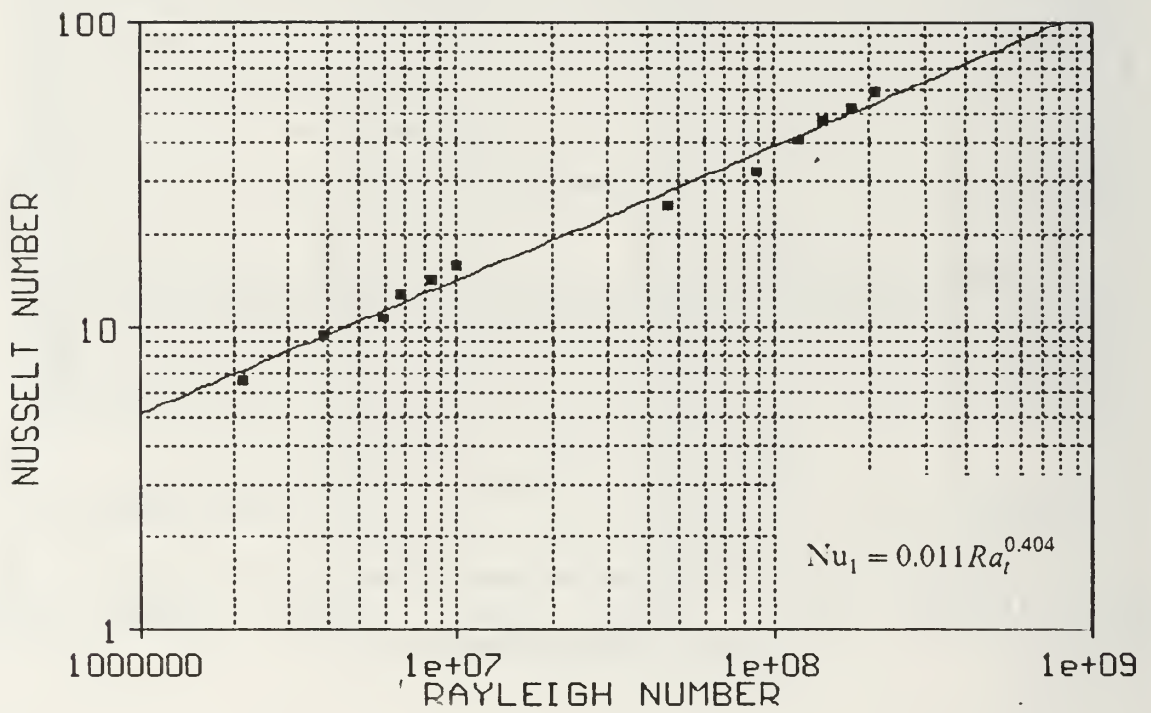


Figure 24. Nu_1 vs Ra_1 for a Vertical Component Orientation, FC-75 and an 11mm Chamber Width using Bottom Row Averaged Values.

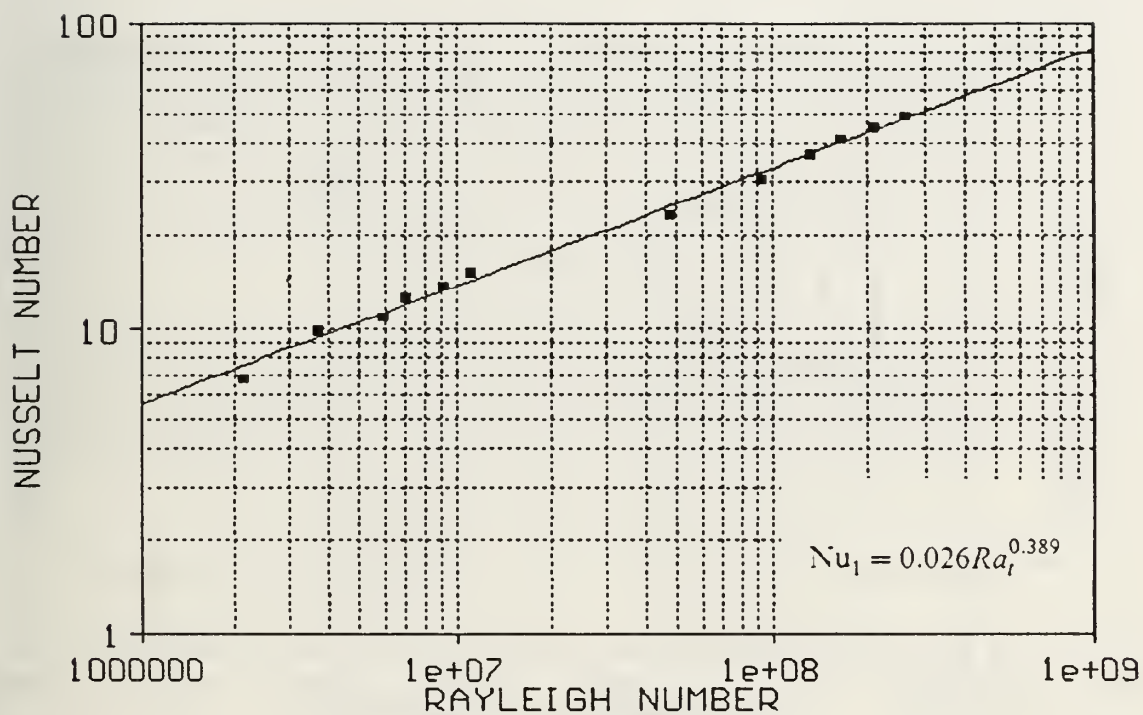


Figure 25. Nu_1 vs Ra_1 for a Vertical Component Orientation, FC-75 and an 11mm Chamber Width using Middle Row Averaged Values.

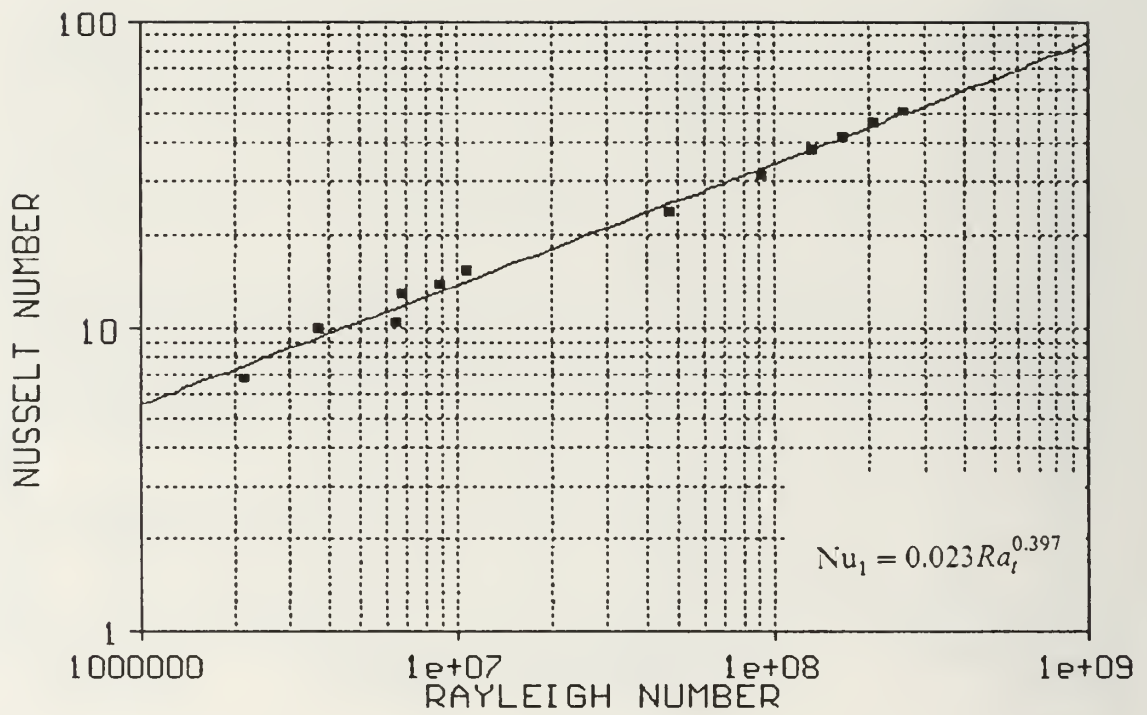


Figure 26. Nu_l vs Ra_l for a Vertical Component Orientation, FC-75 and an 11mm Chamber Width using Top Row Averaged Values.

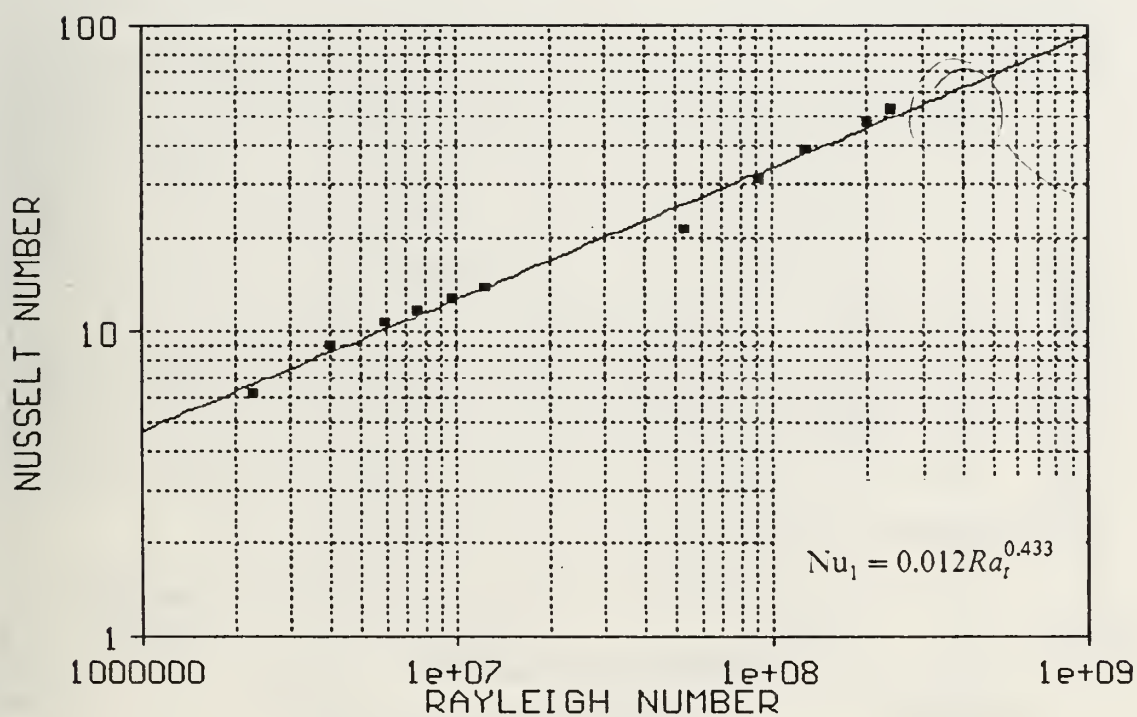


Figure 27. Nu_1 vs Ra_t for a Vertical Component Orientation, FC-75 and a 7mm Chamber Width using Bottom Row Averaged Values.

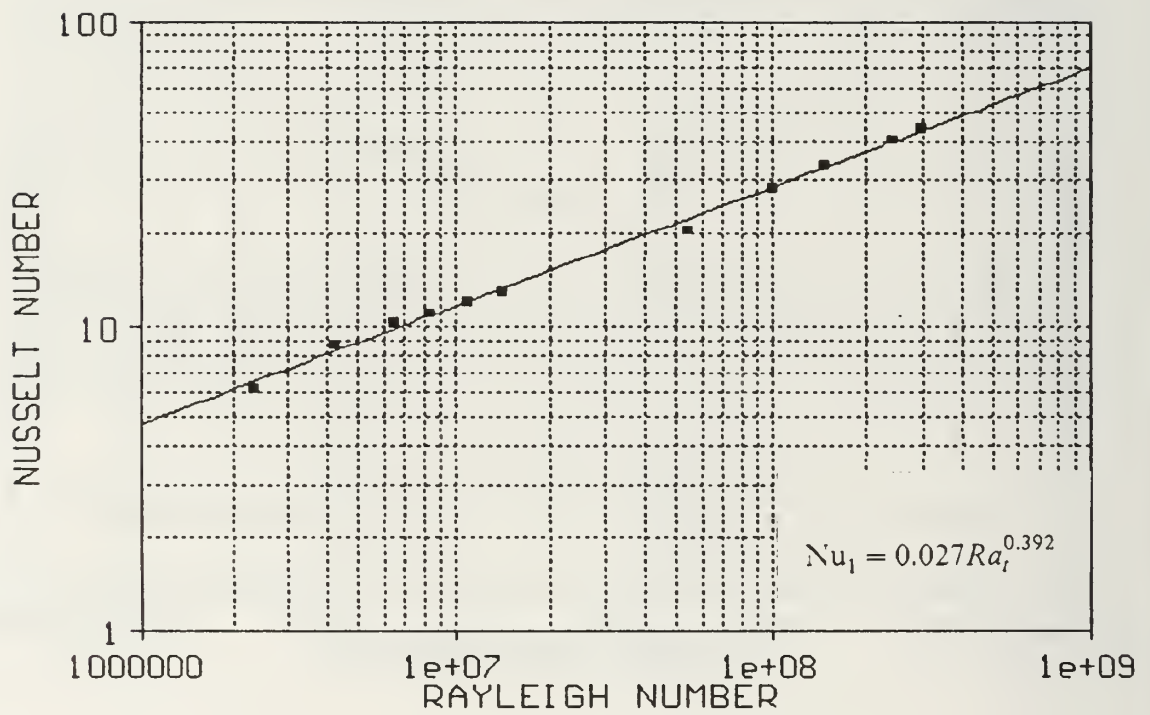


Figure 28. Nu_1 vs Ra_1 for a Vertical Component Orientation, FC-75 and a 7mm Chamber Width using Middle Row Averaged Values.

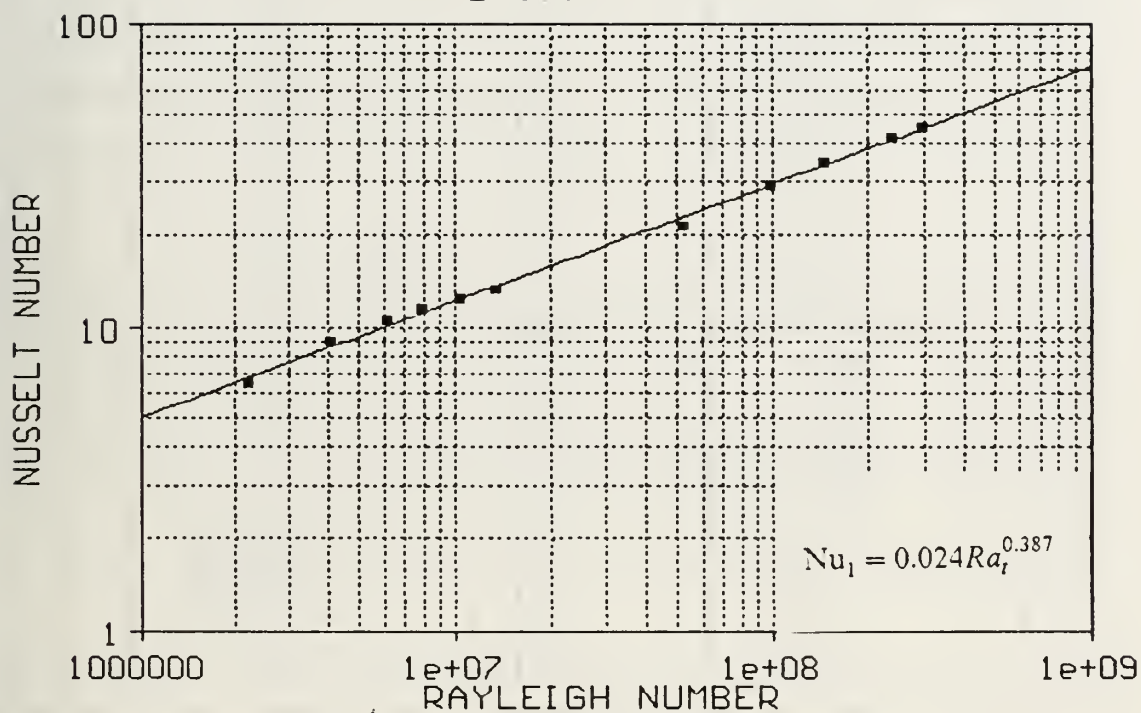


Figure 29. Nu_1 vs Ra_1 for a Vertical Component Orientation, FC-75 and a 7mm Chamber Width using Top Row Averaged Values.

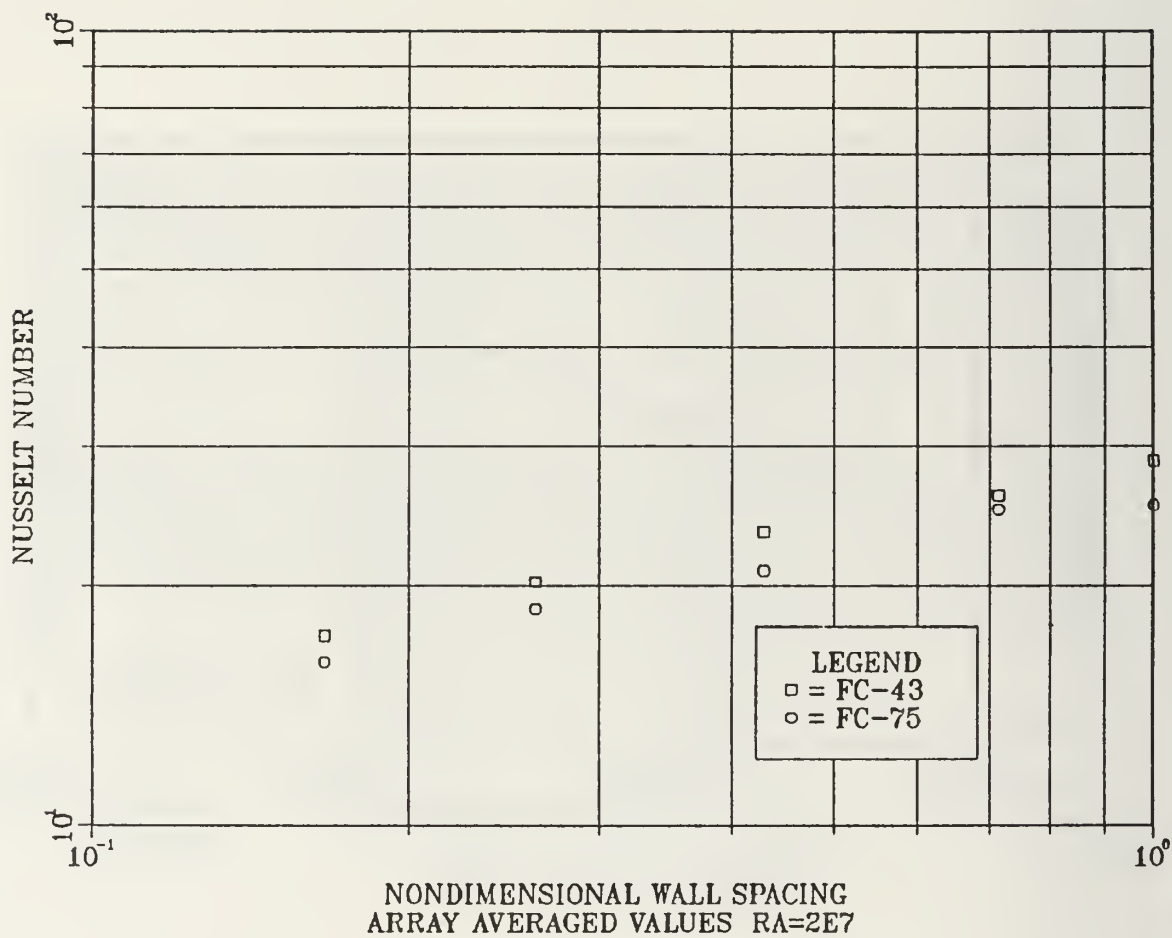


Figure 30. Nu_l vs X for a Vertical Component Orientation and both Dielectric Liquids.

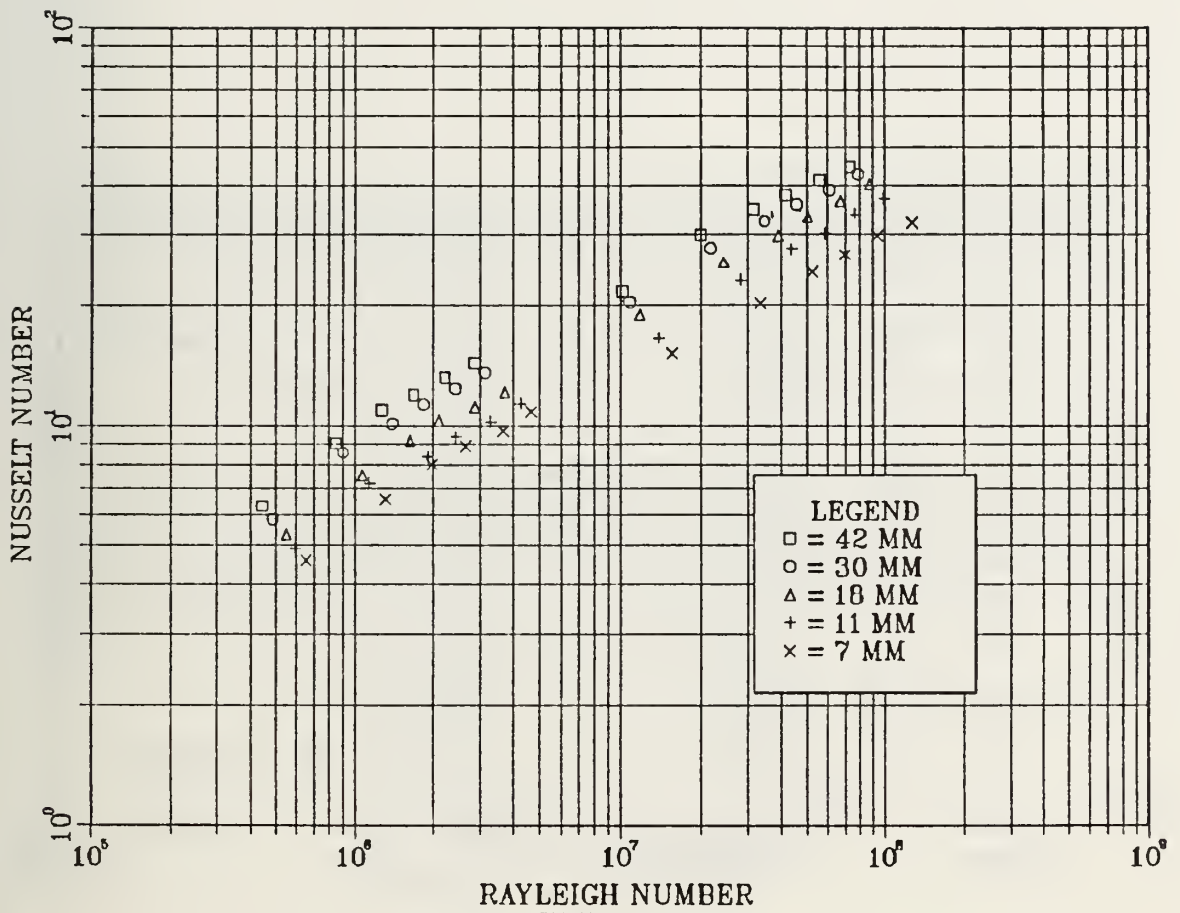


Figure 31. Nu_1 vs Ra_1 for a Vertical Component Orientation, FC-43 and all Chamber Widths.

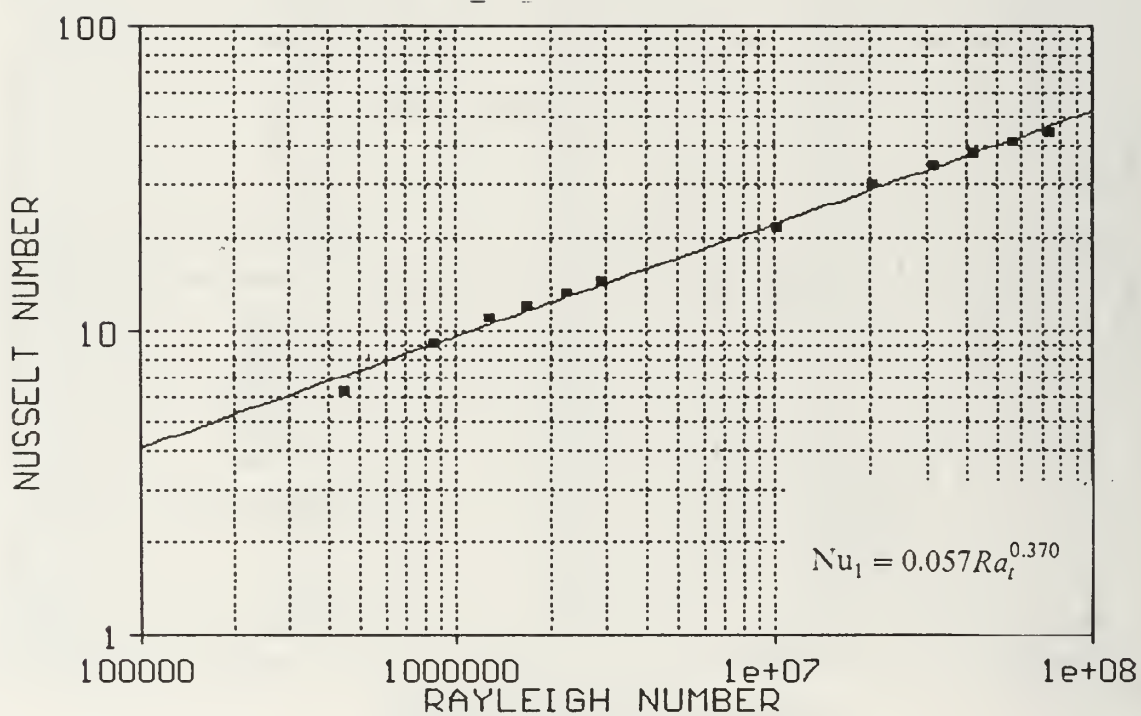


Figure 32. Nu_1 vs Ra_t for a Vertical Component Orientation, FC-43 and a 42mm Chamber Width using Array Averaged Values.

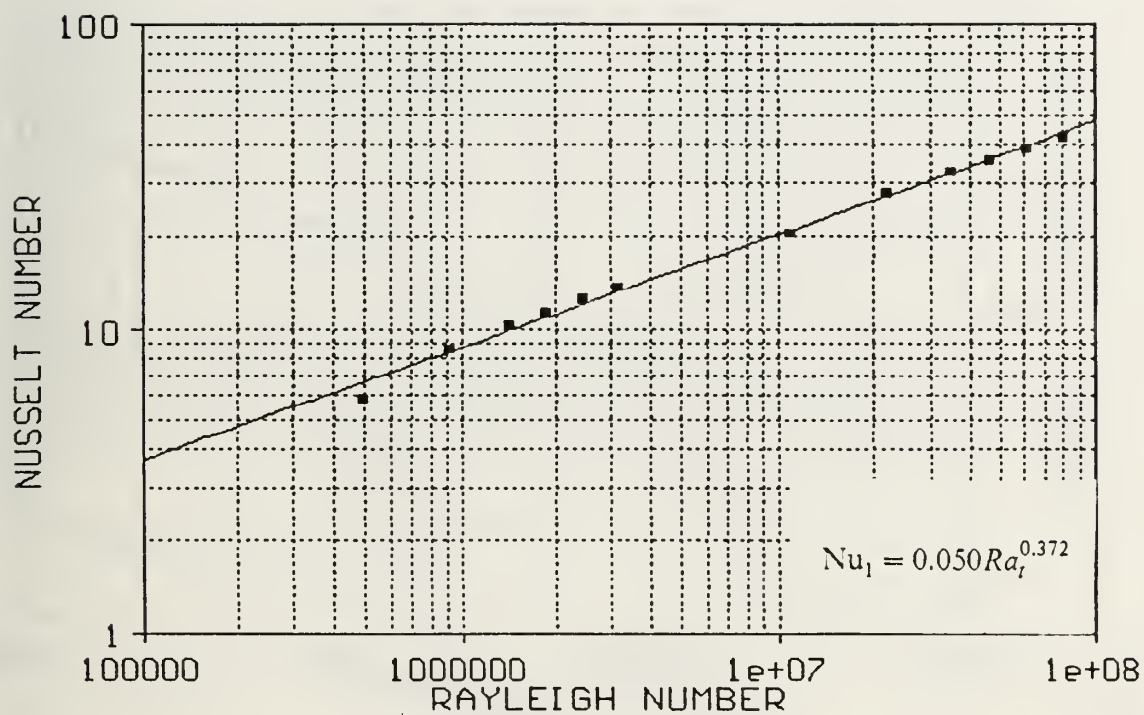


Figure 33. Nu_1 vs Ra_1 for a Vertical Component Orientation, FC-43 and a 30mm Chamber Width using Array Averaged Values.

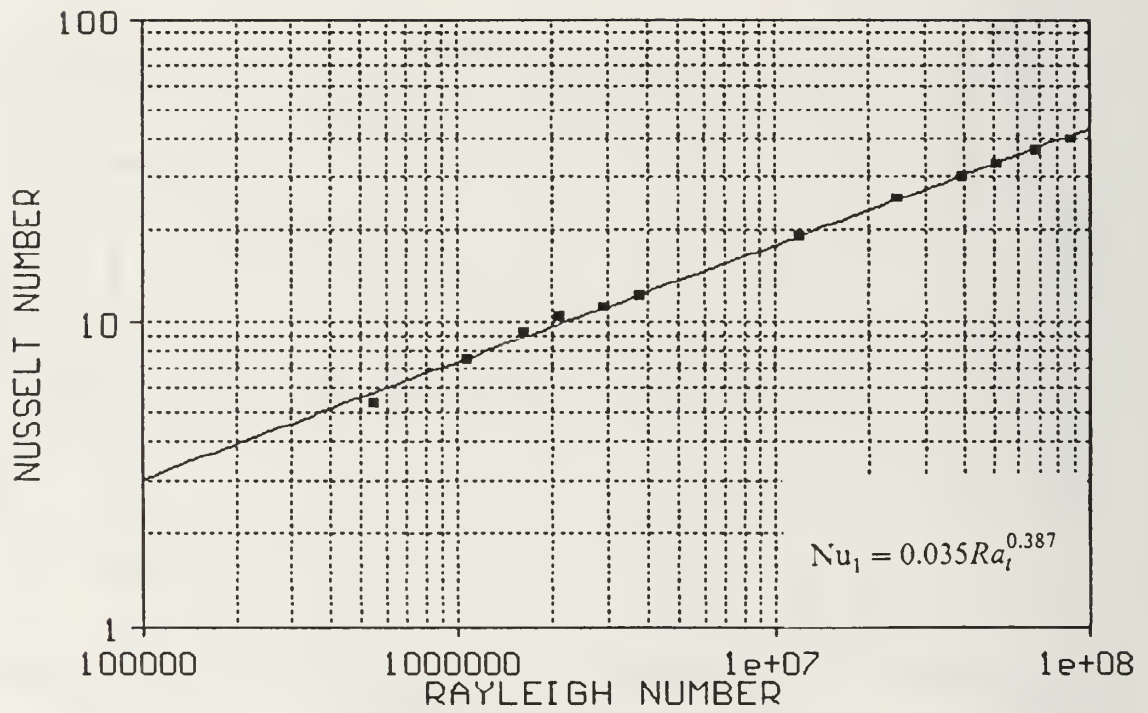


Figure 34. Nu_1 vs Ra_1 for a Vertical Component Orientation, FC-43 and an 18mm Chamber Width using Array Averaged Values.

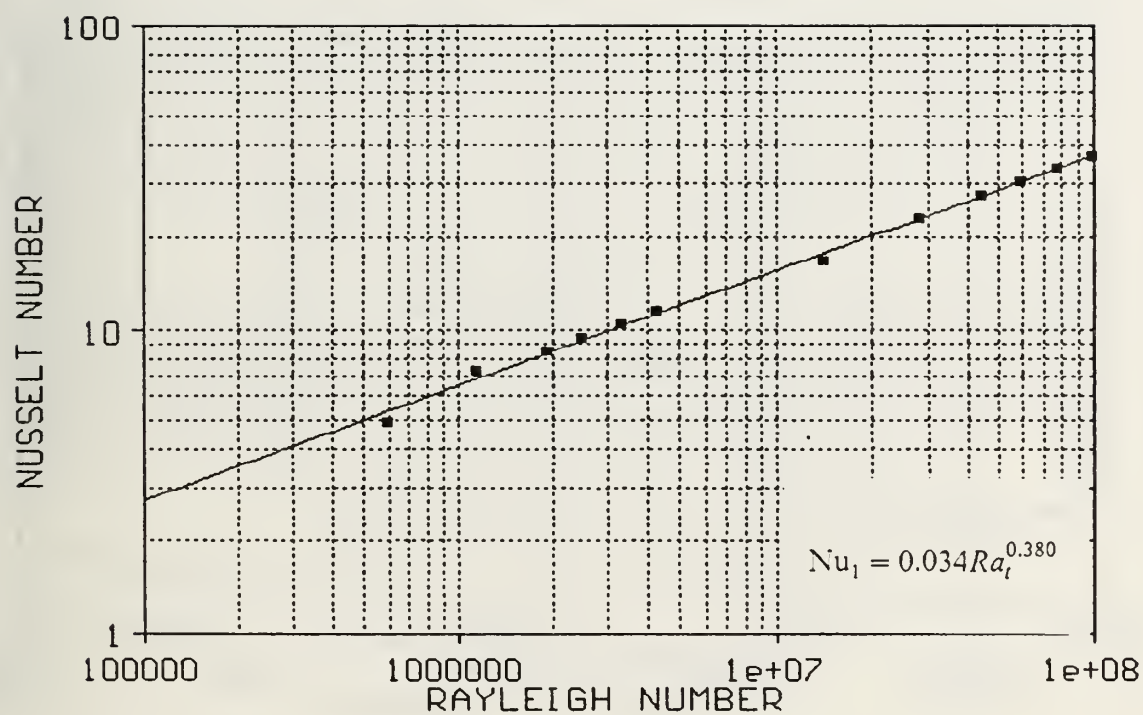


Figure 35. Nu_l vs Ra_l for a Vertical Component Orientation, FC-43 and an 11mm Chamber Width using Array Averaged Values.

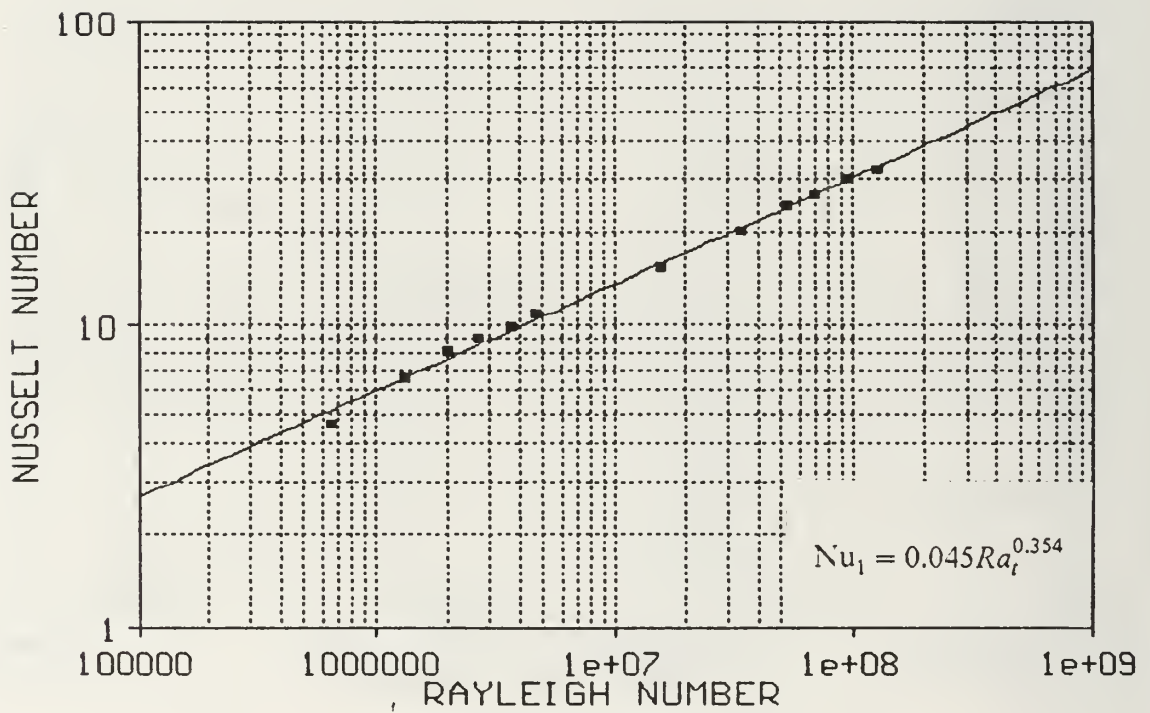


Figure 36. Nu_l vs Ra_l for a Vertical Component Orientation, FC-43 and a 7mm Chamber Width using Array Averaged Values.

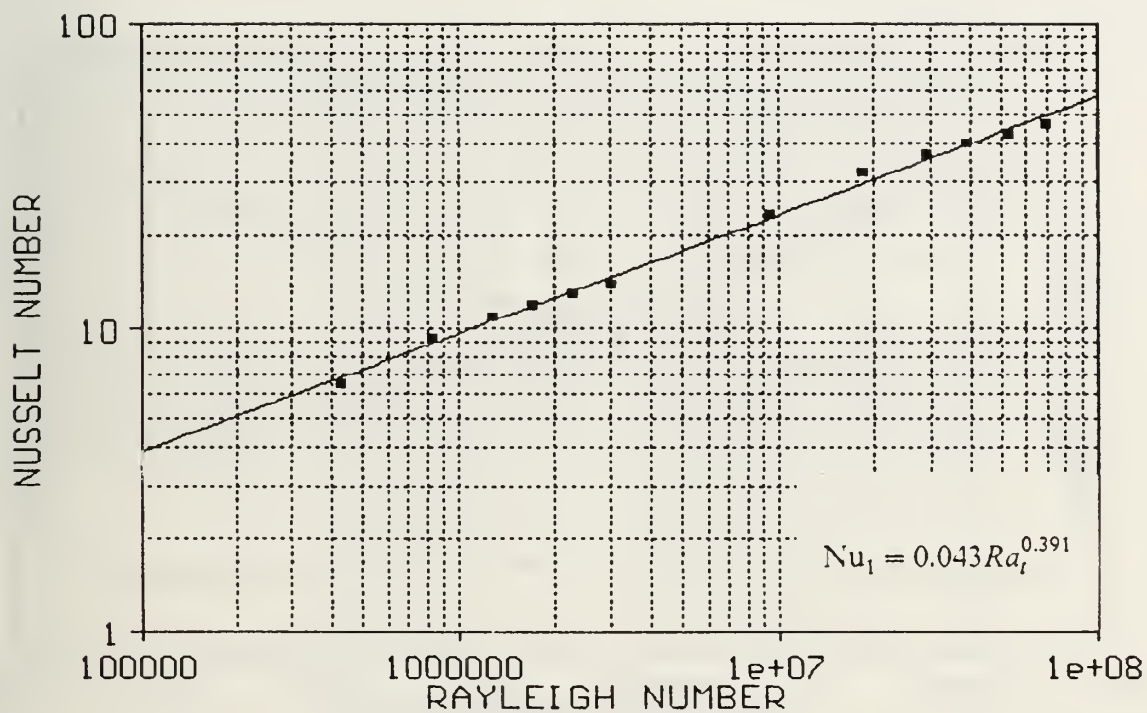


Figure 37. Nu_1 vs Ra_1 for a Vertical Component Orientation, FC-43 and a 42mm Chamber Width using Bottom Row Averaged Values.

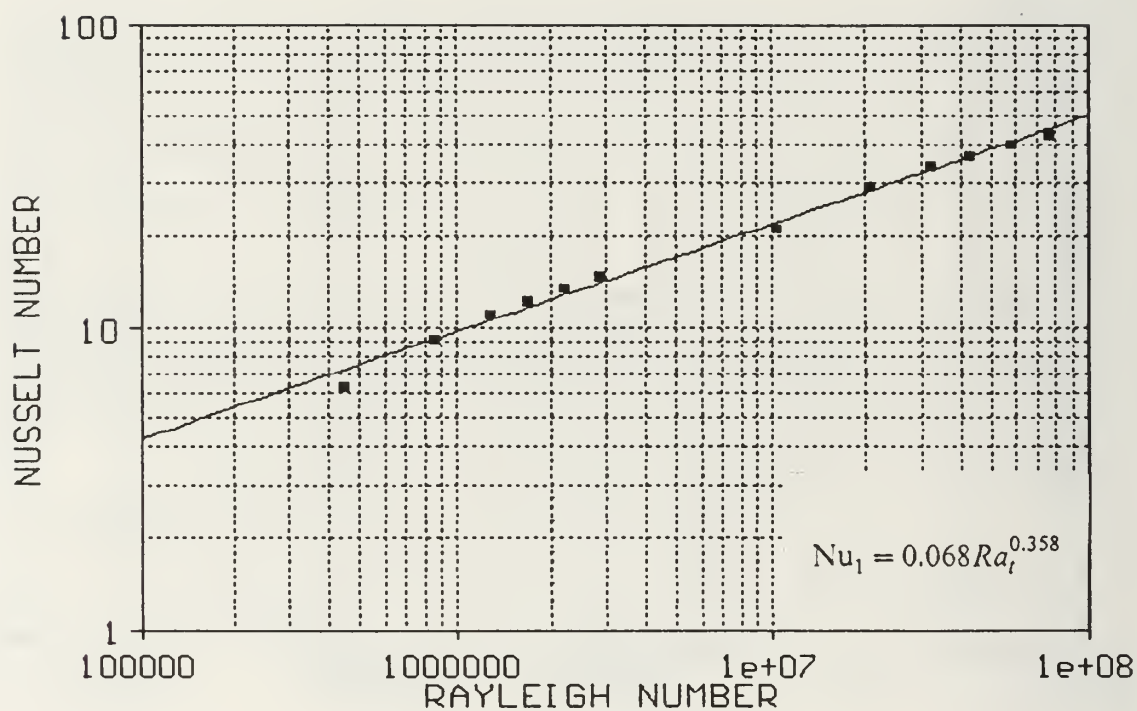


Figure 38. Nu_1 vs Ra_t for a Vertical Component Orientation, FC-43 and a 42mm Chamber Width using Middle Row Averaged Values.

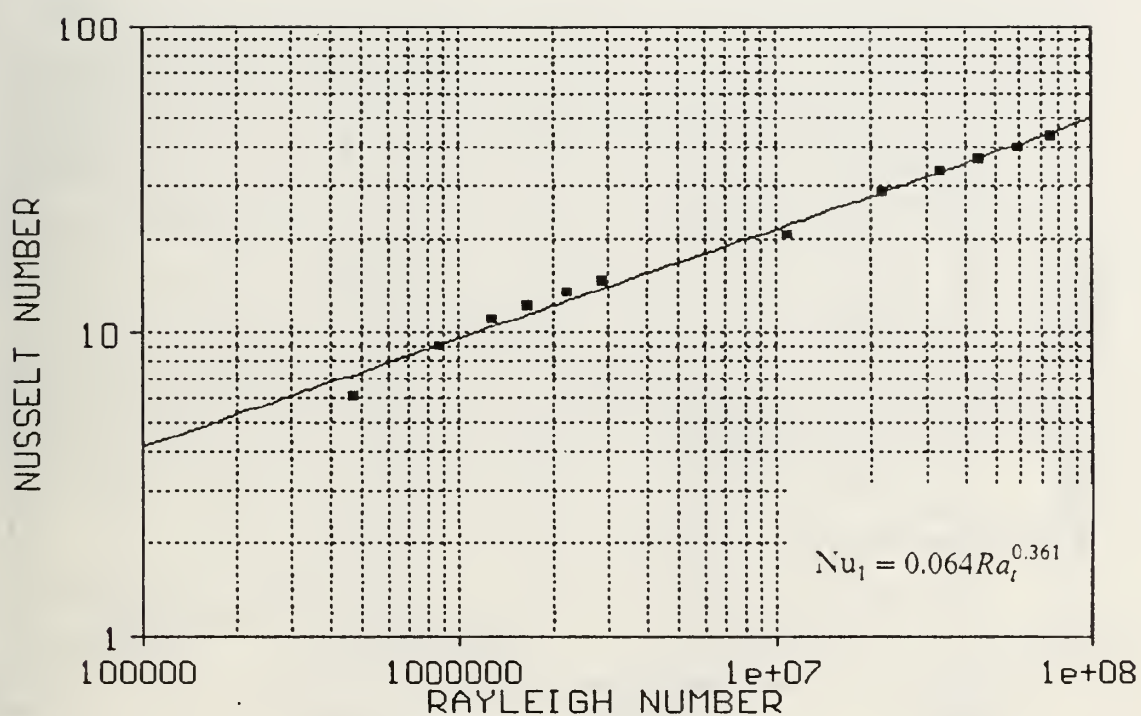


Figure 39. Nu_l vs Ra_l for a Vertical Component Orientation, FC-43 and a 42mm Chamber Width using Top Row Averaged Values.

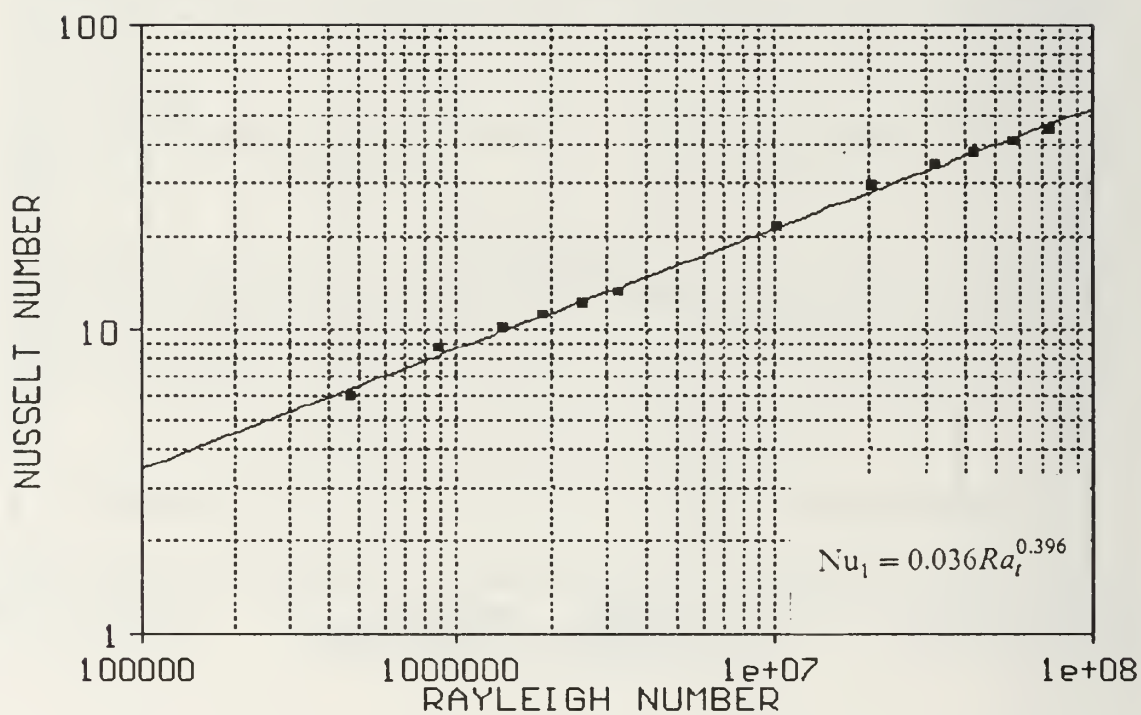


Figure 40. Nu_l vs Ra_l for a Vertical Component Orientation, FC-43 and a 30mm Chamber Width using Bottom Row Averaged Values.

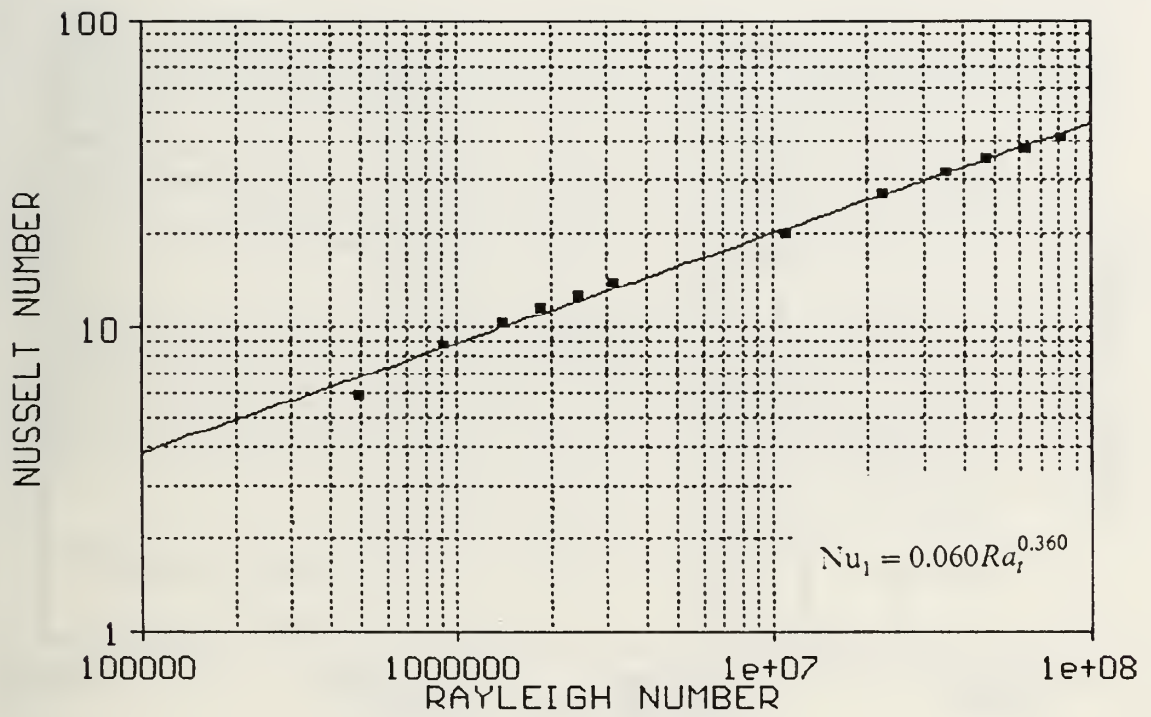


Figure 41. Nu_1 vs Ra_1 for a Vertical Component Orientation, FC-43 and a 30mm Chamber Width using Middle Row Averaged Values.

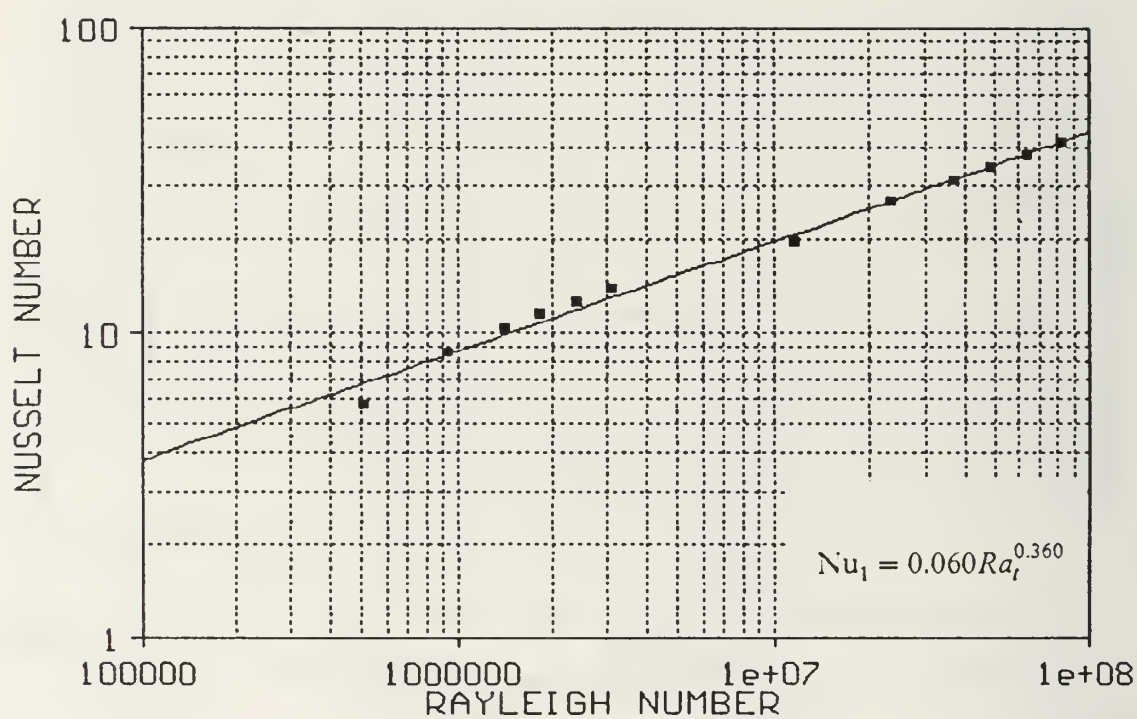


Figure 42. Nu_1 vs Ra_1 for a Vertical Component Orientation, FC-43 and a 30mm Chamber Width using Top Row Averaged Values.

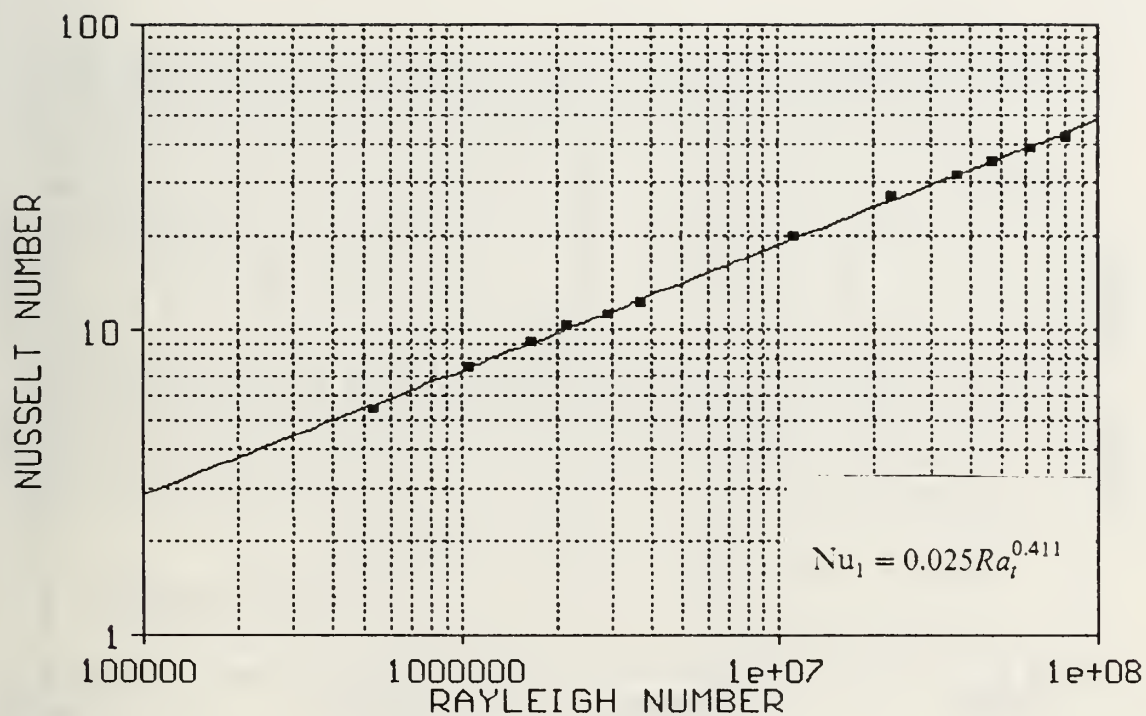


Figure 43. Nu_l vs Ra_l for a Vertical Component Orientation, FC-43 and an 18mm Chamber Width using Bottom Row Averaged Values.

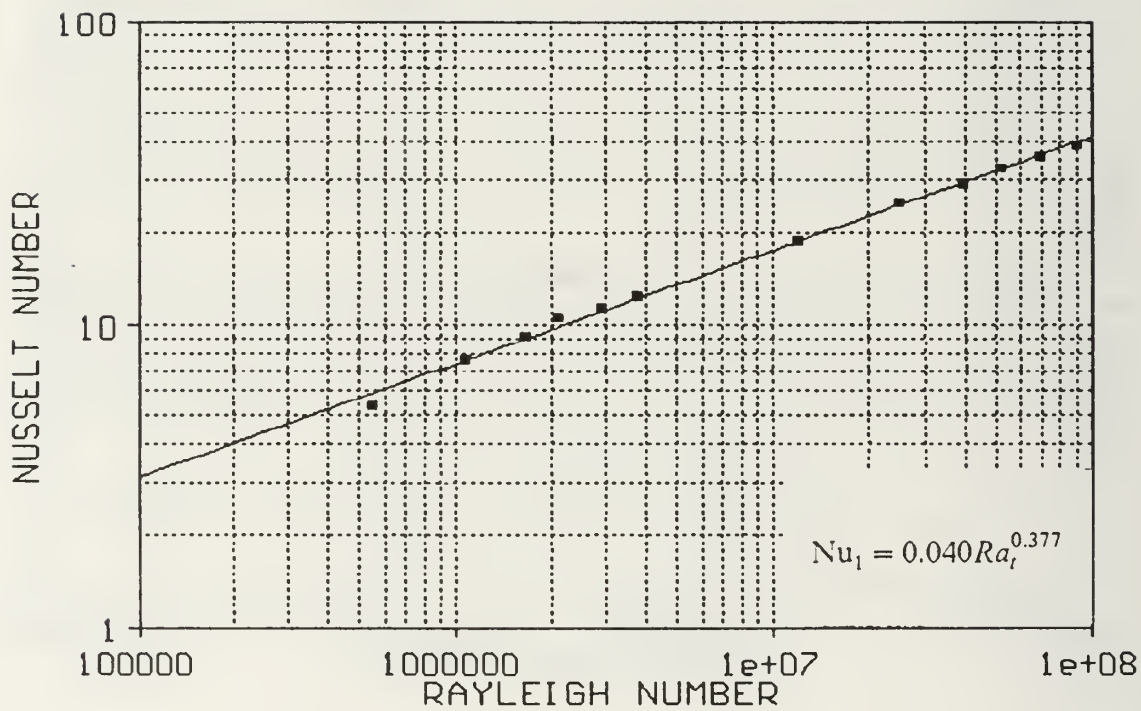


Figure 44. Nu_1 vs Ra_i for a Vertical Component Orientation, FC-43 and an 18mm Chamber Width using Middle Row Averaged Values.

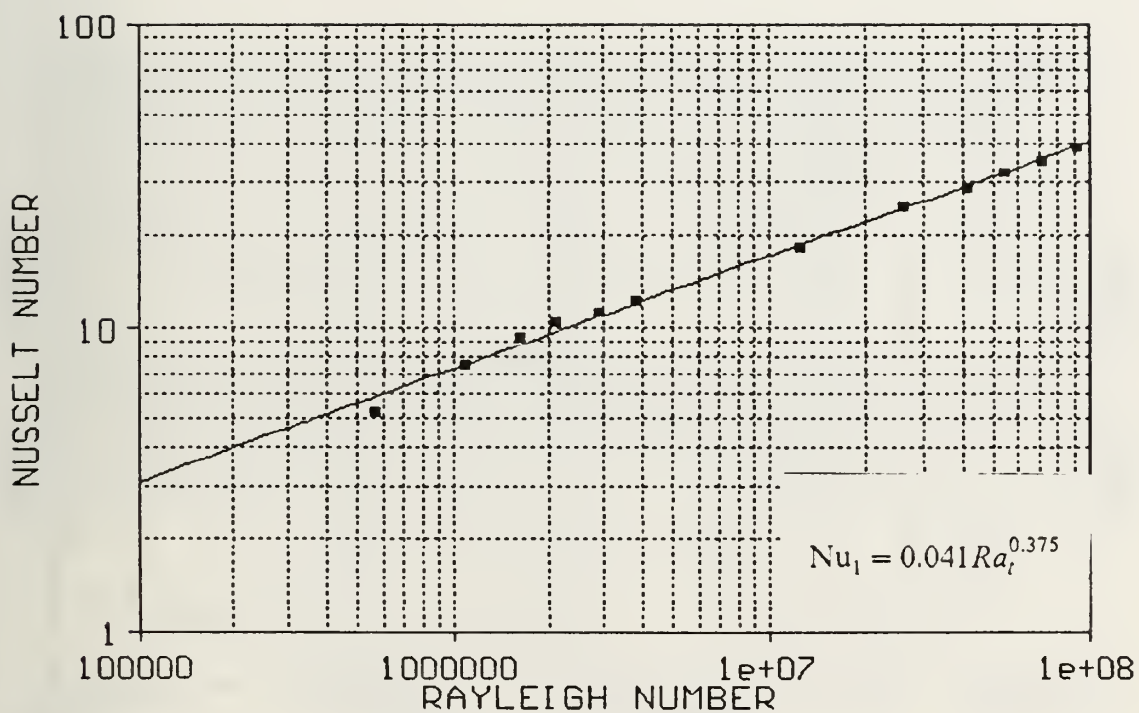


Figure 45. Nu_l vs Ra_l for a Vertical Component Orientation, FC-43 and an 18mm Chamber Width using Top Row Averaged Values.

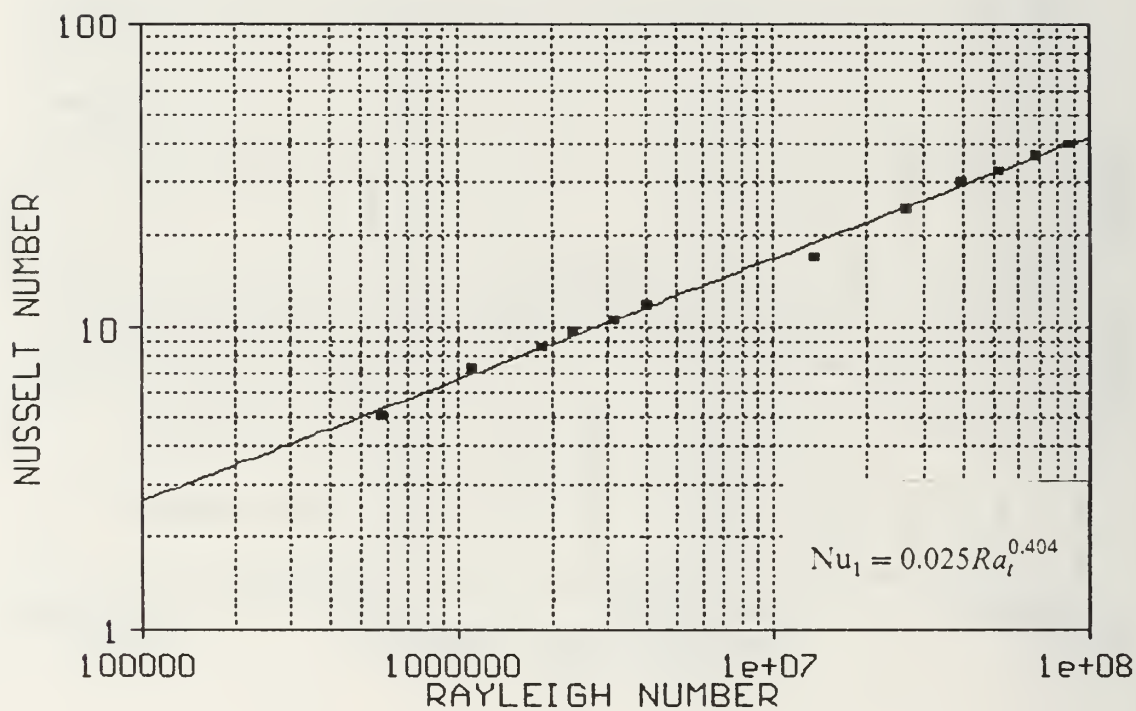


Figure 46. Nu_1 vs Ra_t for a Vertical Component Orientation, FC-43 and an 11mm Chamber Width using Bottom Row Averaged Values.

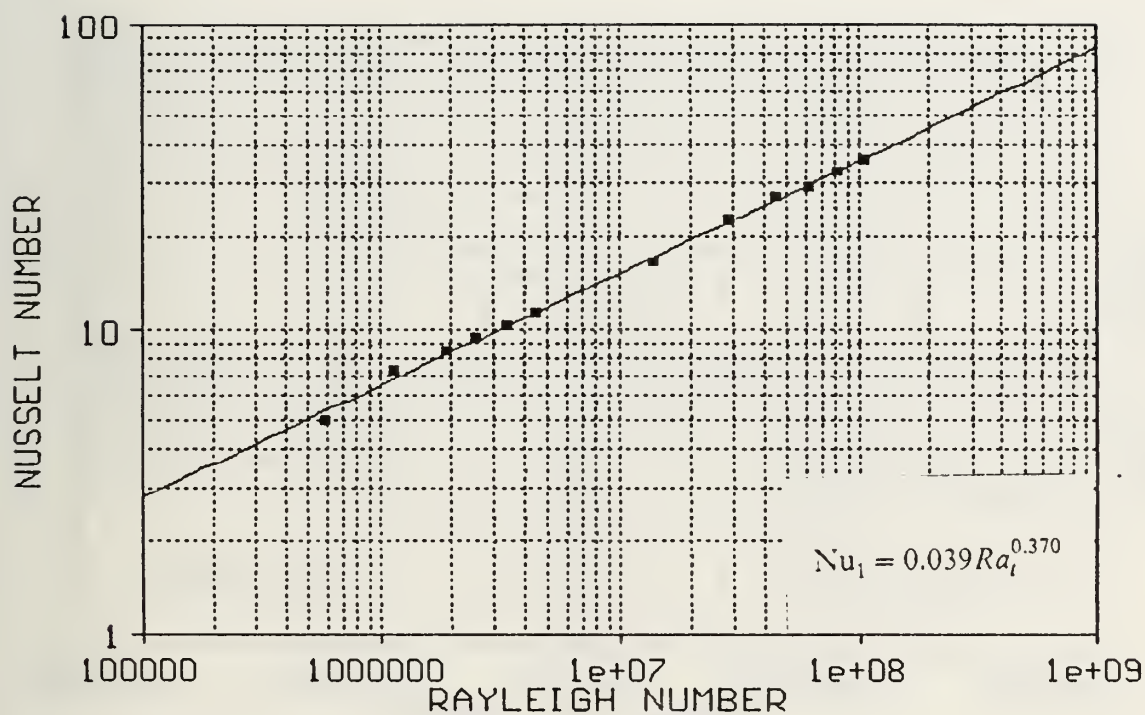


Figure 47. Nu_l vs Ra_l for a Vertical Component Orientation, FC-43 and an 11mm Chamber Width using Middle Row Averaged Values.

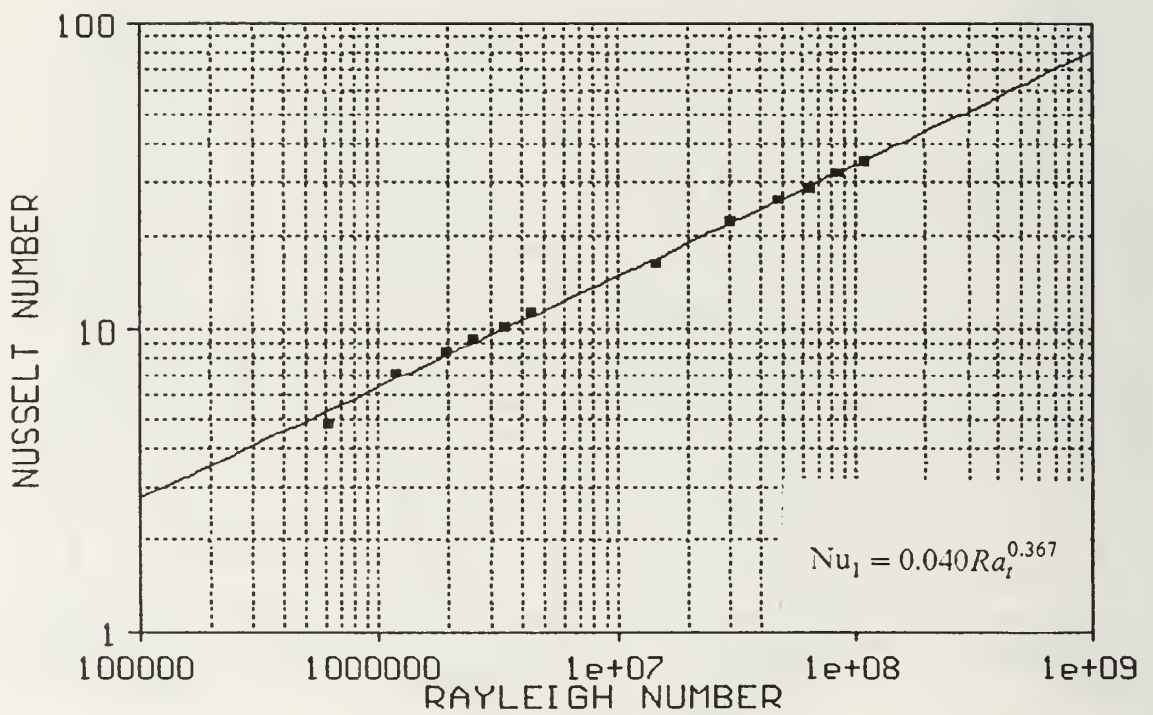


Figure 48. Nu_1 vs Ra_1 for a Vertical Component Orientation, FC-43 and an 11mm Chamber Width using Top Row Averaged Values.

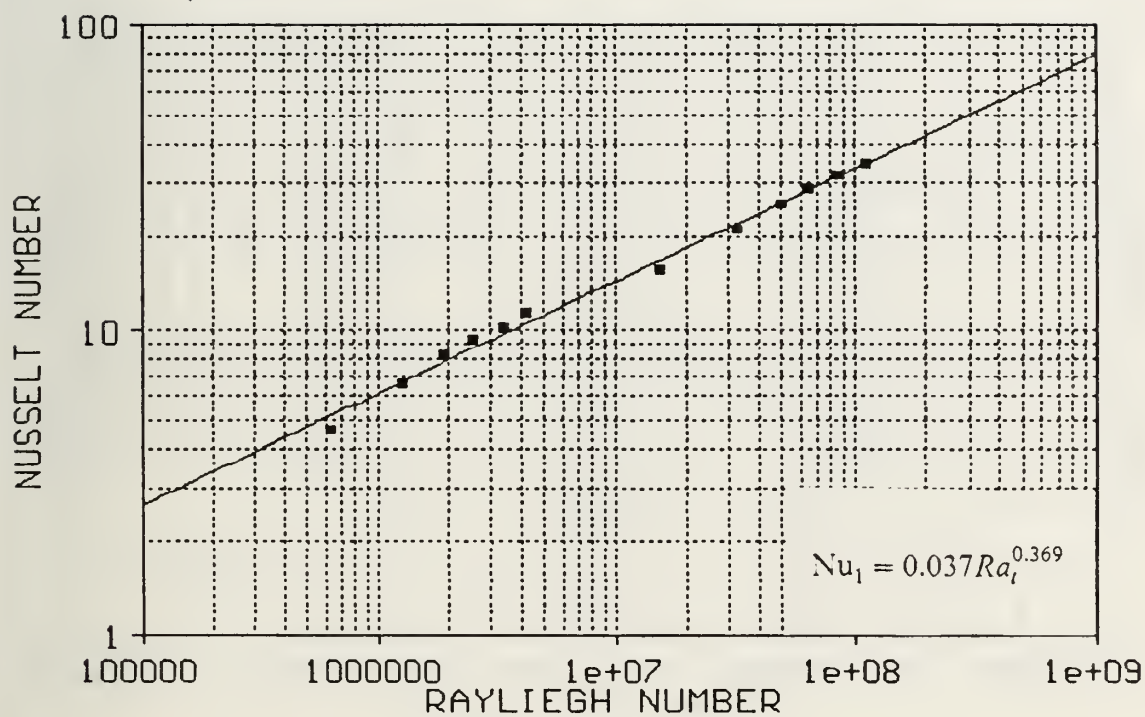


Figure 49. Nu_1 vs Ra_1 for a Vertical Component Orientation, FC-43 and a 7mm Chamber Width using Bottom Row Averaged Values.

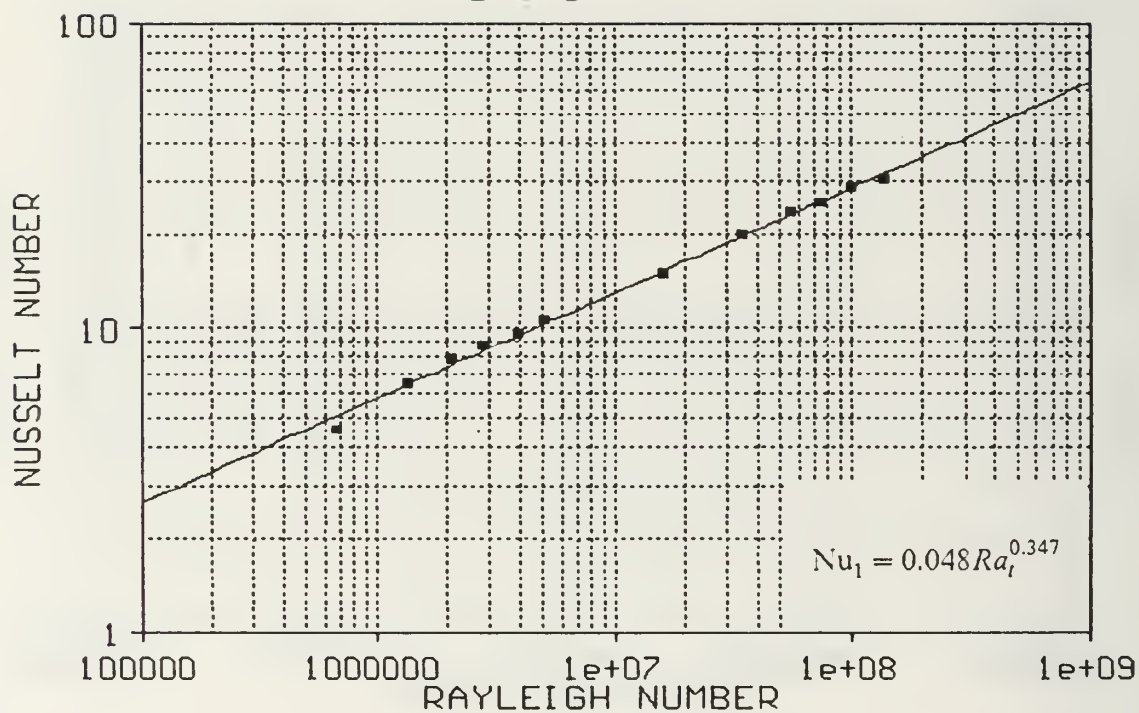


Figure 50. Nu_1 vs Ra_l for a Vertical Component Orientation, FC-43 and a 7mm Chamber Width using Middle Row Averaged Values.

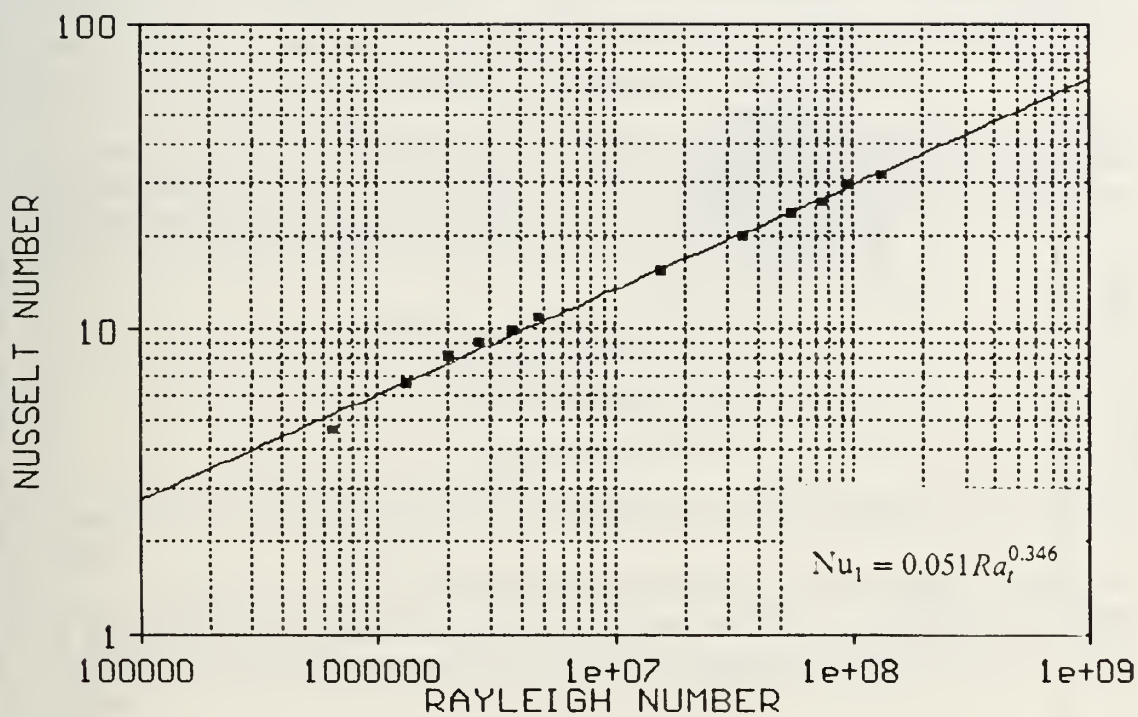


Figure 51. Nu_1 vs Ra_1 for a Vertical Component Orientation, FC-43 and a 7mm Chamber Width using Top Row Averaged Values.

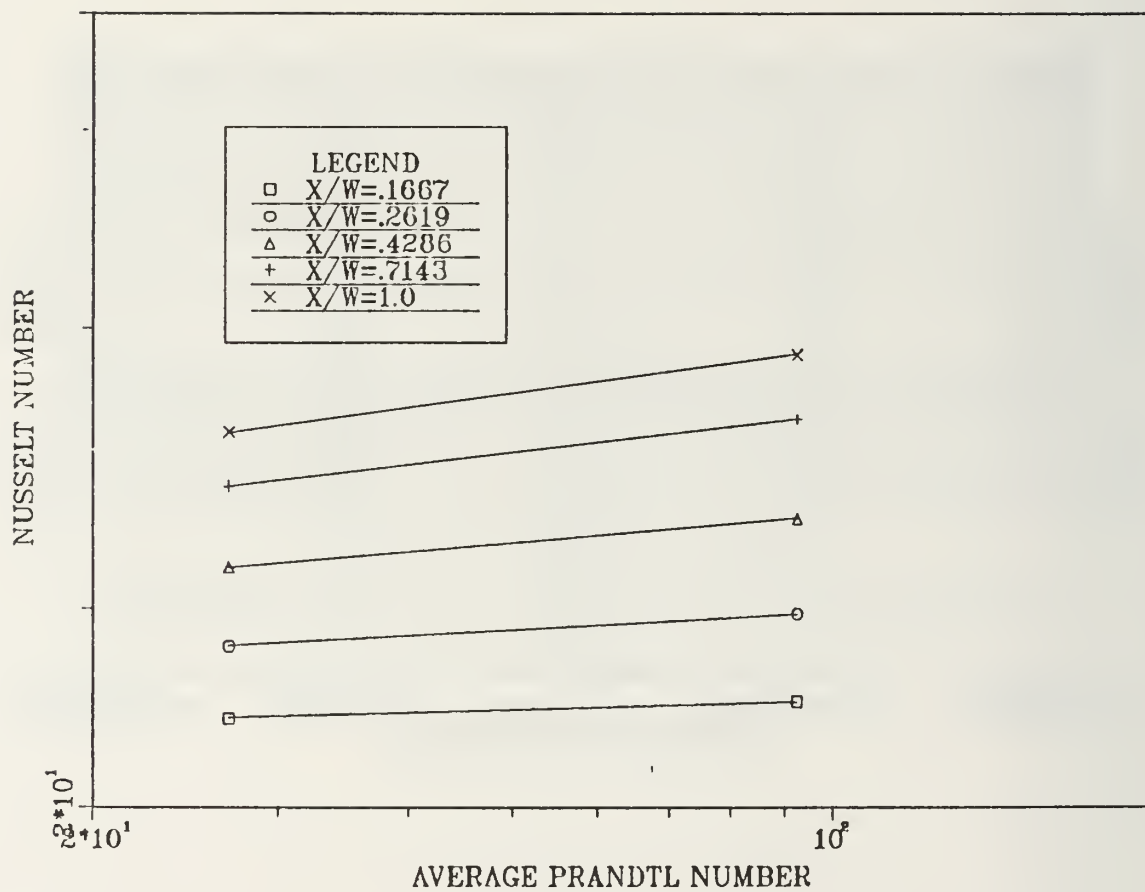


Figure 52. Nu_1 vs $Pr_{a,1}$ and Non-Dimensional Chamber Width for a Vertical Component Orientation.

VI. CONCLUSIONS

The natural convection heat transfer characteristics of a 3x3 array of vertically oriented simulated electronic components were studied. The components were mounted to a vertical plate affixed within a rectangular enclosure filled with a dielectric liquid (FC-75 or FC-43). Power was supplied to the components using Inconel foil heaters, and varied from 0.115W to 2.90W per component. The chamber width, measured from the surface of the circuit board to the opposite enclosure wall, varied from 42mm to 7mm. This was accomplished using plexiglass spacers. Data from this study was correlated with the data obtained from a horizontal component orientation, which was investigated by Aytar (1991). The following conclusions are made:

1. A general empirical correlation which predicts the Nusselt number as a function of temperature based Rayleigh number, non-dimensional chamber width, Prandtl number and component orientation was determined. This correlation was based on array averaged values for the Nusselt and Rayleigh numbers.

$$Nu_1 = 0.0717 Ra_t^{0.35} X^{0.25} Pr^{0.025}$$

$$3 \times 10^6 < Ra_t < 3 \times 10^8$$

$$23.04 < Pr < 127.5$$

The accuracy of this correlation was within 11% of the original array averaged data.

2. The average heat transfer coefficient is independent of the component length scale if b_1 , the Rayleigh number exponent, is chosen as 0.33. A correlation was determined that provided results with nearly the same accuracy as the correlation given above.
3. The effect of component orientation was found to be inherently accounted for within the temperature based Rayleigh number (Ra_t), provided the dimension of the component in the direction of the gravitational vector (\vec{g}) was used as the length scale in Ra_t .
4. The effect of chamber width on the Nusselt number was almost negligible between the 42mm and 30mm chamber widths. However, as chamber width varied from 18mm to 7mm, its effect on the Nusselt number became more pronounced.
5. Heat transfer in FC-75 was largely due to convection resulting from buoyancy forces, regardless of chamber width.
6. Heat transfer in FC-43 at chamber widths of 11mm or greater was mostly due to molecular diffusion.

7. Heat transfer in FC-43 at a chamber width of 7mm, in contrast to the results for the other chamber widths, was due mostly to convection resulting from buoyancy forces.
8. The maximum average component temperature for the horizontal orientation was 7°C higher than the vertical orientation, when FC-75 was used. For FC-43, the maximum average component temperatures were nearly identical for both orientations.
9. At a maximum heat flux of approximately 17 Watts/cm², the highest average component temperature for the vertical orientation was more than 20°C below the typical maximum allowable component temperature of 85°C.
10. The maximum uncertainty in the Nusselt and Rayleigh numbers was 2.5% and occurred at the lowest power level investigated (0.115W per component).

VII. RECOMMENDATIONS

Based on the findings of this study, the following recommendations are made:

1. Investigate additional dielectric liquids with range of Prandtl numbers wide enough to determine a more accurate Prandtl number dependence.
2. Mount thermocouples to the substrate in order to account for heat loss from the substrate to the dielectric liquid.
3. Correlate the horizontal and vertical orientation data using a more elaborate form, in order to improve the accuracy of the Nusselt number prediction.
4. Investigate a variable geometry, non-uniform component orientation.

APPENDIX A. UNCERTAINTY ANALYSIS

Using the method of Kline and McClintock (1956), a zeroth order uncertainty analysis was carried out to determine the uncertainties in the Nusselt number (Nu_i) and the temperature based Rayleigh number (Ra_i), for each of the chamber widths and power levels investigated. The uncertainties in Nu_i and Ra_i were calculated on a component basis. Any uncertainty in calculating the thermophysical properties of the dielectric liquids has been neglected. The expressions used in this analysis are presented below. Numerical values have been omitted to maintain generality.

1. Uncertainty in the power supplied to the heating elements

$$POWER = emf \frac{(volt - emf)}{R_p} = f(emf, volt, R_p)$$

$$\delta POWER = \sqrt{\left(\frac{\partial POWER}{\partial emf} \cdot \delta emf \right)^2 + \left(\frac{\partial POWER}{\partial volt} \cdot \delta volt \right)^2 + \left(\frac{\partial POWER}{\partial R_p} \cdot \delta R_p \right)^2}$$

where:

$$\frac{\delta POWER}{\delta emf} = \frac{(volt - 2emf)}{R_p}$$

$$\frac{\delta POWER}{\delta volt} = \frac{emf}{R_p}$$

$$\frac{\delta power}{\delta R_p} = -emf \frac{(volt - emf)}{R_p^2}$$

2. Uncertainty in the heat loss through the plexiglass substrate

$$Q_{loss} = \frac{\Delta T}{R_c} = f(\Delta T, R_c)$$

$$\delta Q_{loss} = \sqrt{\left(\frac{\partial Q_{loss}}{\partial \Delta T} \cdot \delta \Delta T \right)^2 + \left(\frac{\partial Q_{loss}}{\partial R_c} \cdot \delta R_c \right)^2}$$

$$\delta emf = \delta volt = \pm 0.001 V$$

$$\delta R_p = \pm 0.05 \Omega$$

where:

$$\frac{\delta Q_{loss}}{\delta \Delta T} = \frac{1}{R_c}$$

$$\frac{\delta Q_{loss}}{\delta R_c} = -\frac{\Delta T}{R_c^2}$$

$$\delta \Delta T = 10$$

$$\delta R_c = 10$$

3. Uncertainty in the net heat dissipated by the heaters

$$Q_{net} = POWER - Q_{loss} = f(POWER, Q_{loss})$$

$$\delta Q_{net} = \sqrt{(\delta POWER)^2 + (\delta Q_{loss})^2}$$

4. Uncertainty in the average heat transfer coefficient

$$h = \frac{Q_{net}}{A_{total} \Delta T} = f(Q_{net}, A_{total}, \Delta T)$$

$$\delta h = \sqrt{\left(\frac{\partial h}{\partial Q_{net}} \cdot \delta Q_{net} \right)^2 + \left(\frac{\partial h}{\partial A_{total}} \cdot \delta A_{total} \right)^2 + \left(\frac{\partial h}{\partial \Delta T} \cdot \delta \Delta T \right)^2}$$

$$\frac{\partial h}{\partial Q_{net}} = \frac{1}{A_{total} \Delta T}$$

$$\frac{\partial h}{\partial A_{total}} = -\frac{Q_{net}}{A_{total}^2 \Delta T}$$

$$\frac{\partial h}{\partial \Delta T} = -\frac{Q_{net}}{A_{total} \Delta T^2}$$

$$\delta A_{total} = \sqrt{\left(\frac{\partial A_{total}}{\partial B} \cdot \delta B \right)^2 + \left(\frac{\partial A_{total}}{\partial H} \cdot \delta H \right)^2 + \left(\frac{\partial A_{total}}{\partial L} \cdot \delta L \right)^2}$$

$$A_{total} = 2BH + 2LH + B$$

$$\frac{\partial A_{total}}{\partial B} = 2H + L$$

$$\frac{\partial A_{total}}{\partial H} = 2H + B$$

$$\frac{\partial A_{total}}{\partial L} = 2H + B$$

$$\delta \Delta T = 1$$

$$\delta B = \delta H = \delta L = 1 \times 10^{-4} m$$

5. Uncertainty in the Nusselt number

$$Nu = \frac{hL}{k_f}$$

$$\delta \text{Nu} = \sqrt{\left(\frac{\partial \text{Nu}}{\partial h} \cdot \delta h \right)^2 + \left(\frac{\partial \text{Nu}}{\partial L} \cdot \delta L \right)^2}$$

where:

$$\frac{\partial \text{Nu}}{\partial h} = \frac{L}{k_f}$$

$$\frac{\partial \text{Nu}}{\partial L} = \frac{h}{k_f}$$

6. Uncertainty in the Temperature based Rayleigh number

$$Ra_t = \frac{g\beta L^3 \Delta T}{\nu \alpha} = f(L, \Delta T)$$

$$\delta Ra_t = \sqrt{\left(\frac{\partial Ra_t}{\partial L} \cdot \delta L \right)^2 + \left(\frac{\partial Ra_t}{\partial \Delta T} \cdot \delta \Delta T \right)^2}$$

where:

$$\frac{\partial Ra_t}{\partial L} = \frac{3g\beta L^2 \Delta T}{\nu \alpha}$$

$$\frac{\partial Ra_t}{\partial \Delta T} = \frac{g\beta L^3}{\nu \alpha}$$

REFERENCES

- Aytar, E., "Natural Convection Immersion Cooling of an Array of Heated Protrusions in an Enclosure Filled with Dielectric Liquid: Effects of Enclosure Width and Fluid Prandtl Number," Master of Science Thesis, Naval Postgraduate School, Monterey, California, March 1991.
- Benedict, T.J., "An Advanced Study of Natural Convection Immersion Cooling of a 3x3 Array of Simulated Components in an Enclosure Filled with a Dielectric Liquid," Master of Science Thesis, Naval Postgraduate School, Monterey, California, June 1988.
- Incopera, F.P., "Convection Heat Transfer in Electronic Equipment Cooling," Transactions of the ASME, Journal of Heat Transfer, vol. 110, pp. 1097-1108, November 1988.
- Fujii, T., and Fujii, M., 1976, "The Dependence of Local Nusselt Number on Prandtl Number in the Case of Free Convection Along a Vertical Surface With Uniform Heat Flux," International Journal of Heat and Mass Transfer, Vol. 19, pp. 121-122.
- Kelleher, M.D., Knock, R.H., and Yang, K.T., "Laminar Natural Convection in a Rectangular Enclosure Due to a Heated Protrusion on One Vertical Wall - Part I: Experimental Investigation," Proceedings of 2nd ASME/JSME Thermal Engineering Joint Conference, Honolulu, Hawaii, pp. 169-177, 1987.
- Keyhani, M., Chen, L., Pitts, D.R., "The Aspect Ratio Effect on Natural Convection in an Enclosure With Protruding Heat Sources," ASME Journal of Heat Transfer, Vol. 113, pp.883-891, November 1991.
- Lee, J.J., Liu, K.V., Yang, K.T., and Kelleher, M.D., "Laminar Natural Convection in a Rectangular Enclosure Due to a Heated Protrusion on One Vertical Wall - Part II: Numerical Solutions," Proceedings of 2nd ASME/JSME Thermal Engineering Joint Conference, Honolulu, Hawaii, pp. 179-185, 1987.
- Oktay, S., "High Heat From a Small Package," Mechanical Engineering, vol. 108, March 1986.
- Pamuk, T., "Natural Convection Immersion Cooling of an Array of Simulated Components in an Enclosure Filled with Discrete Fluid," Master of Science Thesis, Naval Postgraduate School, Monterey, California, December 1987.
- Park, K.A., and Bergles, A.E., "Natural Convection Heat Transfer Characteristics of Simulated Microelectronic Chips," Transactions of the ASME, Journal of Heat Transfer, vol. 109, pp. 90-96, February 1987.
- Powell, M.E., "Natural Convection From an Array of Rectangular Protrusions in an Enclosure Filled with Dielectric Fluid: Effects of Boundary Conditions, Fluid Prandtl Number, and Selective Powering," Master of Science Thesis, Naval Postgraduate

School, Monterey, California, September 1989.

Torres, E., "Natural Convection Cooling of a 3 by 3 Array of Rectangular Protrusions in an Enclosure Filled with Dielectric Liquid: Effects of Boundary Conditions and Component Orientation," Master of Science Thesis, Naval Postgraduate School, Monterey, California, December 1988.

INITIAL DISTRIBUTION LIST

	No. Copies
1. Defense Technical Information Center Cameron Station Alexandria, VA 22304-6145	2
2. Library, Code 52 Naval Postgraduate School Monterey, CA 93943-5002	2
3. Department Chairman, Code 69 Department of Mechanical Engineering Naval Postgraduate School Monterey, California 93943-5000	1
4. Prof. M.D. Kelleher, Code ME/Kk Department of Mechanical Engineering Naval Postgraduate School Monterey, California 93943-5000	2
5. Prof. Y. Joshi, Code ME/Ji Department of Mechanical Engineering Naval Postgraduate School Monterey, California 93943-5000	1
6. Curricular Officer, Code 34 Department of Mechanical Engineering Naval Postgraduate School Monterey, California 93943-5000	1
7. Naval Weapons Support Center Code 6042 Crane, Indiana 47522	1
8. LT Scott Matthews 805 Larkspur Lane Chesapeake, Virginia 23323	1

DUDLEY KNOX LIBRARY
NAVAL POSTGRADUATE SCHOOL
MONTEREY CA 93943-5101

DUDLEY KNOX LIBRARY



3 2768 00307924 5